THE UNIVERSITY OF CHICAGO

THE NEURAL BASIS OF TACTILE TEXTURE PERCEPTION

A DISSERTATION SUBMITTED TO

THE FACULTY OF THE DIVISION OF THE BIOLOGICAL SCIENCES

AND THE PRITZKER SCHOOL OF MEDICINE

IN CANDIDACY FOR THE DEGREE OF

DOCTOR OF PHILOSOPHY

COMMITTEE ON COMPUTATIONAL NEUROSCIENCE

BY

JUSTIN LIEBER

CHICAGO, ILLINOIS

JUNE 2018

TABLE OF CONTENTS

LIST OF FIGURES

LIST OF TABLES

ACKNOWLEDGEMENTS

Advisor:

Sliman J. Bensmaia

Thesis Committee:

David J. Freedman

Daniel Margoliash

Stephanie E. Palmer

Bensmaia Lab:

Frank Dammann

Benoit Delhaye

Michael A. Harvey

Oksana Lakowsky

Katie Long

Louise R. Manfredi

Kristine Mclellan

Molly O'Donnell

Julia Ran

Hannes P. Saal

Erik Schluter

Alison I. Weber

Jeremy Winberry

Xinyue Xia

ARC

Alyssa Brown

Maggie Bruner

Jennifer McGrath

Marek Niekrasz

Allison Ostdiek

Karin Peterson

ABSTRACT

The objective of my program of research is to shed light on how texture is encoded in the nerve, to investigate texture representations in somatosensory cortex – including Brodmann's areas 3b, 1 and 2 –, and to assess how these neural representations give rise to percepts of texture. To this end, we combine psychophysical experiments with human observers and neurophysiological recordings, both from first-order somatosensory afferents and from somatosensory cortical neurons of Rhesus macaques. First, we show that, in the peripheral nerve, the neural code for roughness – the dominant perceptual dimension of texture – relies on the integration of signals from all three major classes of tactile fibers, and that roughness information is encoded in spatial patterns of activation in one population of nerve fibers and in temporal patterns of activation in two others. Second, we show that these two streams of information – spatial and temporal – are integrated in somatosensory cortex resulting in a representation of texture that is distributed over a large population of cells with heterogeneous response properties. Combining data from our peripheral and cortical recordings, we determine which tactile submodalities drive the responses of individual cortical neurons, and show that neurons driven by afferents that specialize in spatial signaling more effectively encode coarse textural features, and neurons driven by afferents that specialize in temporal signaling more effectively encode fine textural features. Third, we show that, while texture signals at the periphery are highly dependent on the speed at which the surface moves across the finger, texture signals in cortex are nearly independent of speed and can account for the documented speed-invariance of texture perception.

INTRODUCTION

We can identify objects by the way they feel. As we move our fingers over objects in our pocket or purse, we can easily pick out our keys or our phone from an assortment of other items. When we manipulate an object, the skin is deformed, which in turn results in stresses and strains in the tissue, ultimately driving electrical activity in several populations of mechanoreceptors (Sripati et al., 2006a; Saal et al., 2017). Tactile nerve fibers then carry the resulting signals to the brain, where they are integrated and transformed through successive stages of neural processing to ultimately culminate in a tactile percept. Like its visual and auditory counterparts, the somatosensory neuraxis works to extract object-specific, behaviorally relevant information about objects, a process about which much remains to be discovered.

The study of tactile texture perception – the sensory experience associated with surface microstructure – is a fruitful paradigm to interrogate these neural mechanisms for several reasons. First, texture perception is a domain in which touch is the most sensitive sensory modality, far surpassing vision and hearing (Lederman, 1979; Heller, 1989; Klatzky et al., 1993; Guest and Spence, 2003; Klatzky and Lederman, 2010). Second, texture perception operates over six orders of magnitude of spatial scales, ranging from tens of nanometers to tens to millimeters (Skedung et al., 2013). Third, the sensory space of texture is complex, comprising at least four main perceptual axes – roughness, hardness, stickiness, and warmth –, which only partially define it (Hollins et al., 2000a). Fourth, texture exploration typically involves movement between skin and surface (Katz, 1925; Lederman and Klatzky, 1987; Callier et al., 2015). As a result, instantaneous spatial patterns of skin deformation engage spatial encoding mechanisms that draw compelling analogies with vision (Pack and Bensmaia, 2015), and texture-elicited vibrations engage temporal encoding mechanisms that draw analogies to audition (Hollins and Risner, 2000; Bensmaia and Hollins, 2003; Bensmaïa and Hollins, 2005; Yau et al., 2009; Saal et al., 2016). Fifth,

stimulation paradigms have been developed and honed to achieve precise experimental control on the speed and force of texture presentation (Johnson and Phillips, 1988; Weber et al., 2013), a necessary precondition to understand tactile processing given the exquisite sensitivity of this sense to submicron skin deformations.

Much of the early work on texture perception was carried out using Braille-like dot patterns which have the merit of being defined by a small set of parameters (dot height, dot width, inter-dot distance, dot configuration). Studies using these stimuli arrived at the conclusion that information about tactile texture is mediated entirely by one population of tactile fibers (Blake et al., 1997). Later studies, however, showed that this conclusion was partially an artifact of the stimulus set, which only spanned a narrow range of spatial scales, measured in the millimeters. The processing and perception of more naturalistic textures, like fabrics or sandpapers, which comprise textural elements over a wider range of spatial scales, rely on the integration of signals from all three main afferent classes (Weber et al., 2013). Interestingly, texture information at different scales is encoded in different ways: Coarse textural features are encoded in spatial patterns of afferent activation and fine features are encoded in temporal patterns evoked as the skin moves across the surface.

In this chapter, we first discuss the phenomenology of texture perception with a review of the psychophysical literature. We then discuss what is known about the neural basis of texture perception, first in the nerve then in cortex. This prior knowledge forms the basis for my dissertation project. In our discussion of the neural basis of texture processing, we omit two interposed neural structures – the cuneate nucleus and thalamus – as the texture responses in these structures have not been explored.

WHAT IS TEXTURE?

Classically, the term “texture” refers to the feel or appearance of an object’s surface. And yet, not every aspect of a surface is necessarily considered texture – for example, buttons on a video game console are

shapes rather than features. So what are the qualities that separate a shape from a texture? One distinction is that textural features are generally distributed across the extent of a surface, and their precise pattern is meaningless, while shape features tend to be more discrete and their configuration is typically meaningful. In touch, another distinction is the relevant spatial scale: a feature that extends beyond a fingerpad is likely not a textural one.

One way to define a distribution of textural features is to characterize what aspects of this distribution vary between samples and which do not. In other words, we are looking for a set of "generative" statistics that produce non-identical stimuli that are perceptually equivalent, known as metamers (Julesz, 1962, 1981). This approach has been quite successful for visual textures: a generative model can compute a small set of statistics based on early visual representations of natural images, and use those statistics to produce new images that appear to have the same texture (Portilla and Simoncelli, 2000). A similar approach has been fruitfully applied to generate auditory textures, such as the sound of a burbling stream or crackling fire (McDermott and Simoncelli, 2011). This approach cannot straightforwardly be applied to tactile texture, however, because early processing – well established for vision and audition and crucial for the generation of metamers – has not been established for touch. Furthermore, biomechanical interactions between skin and surface complicate the relationship between stimulus and neural response and thus further thwart the application of the generative approach to tactile texture.

TACTILE TEXTURE PERCEPTION

Texture is a key component of our ability to quickly identify everyday objects through touch (Klatzky et al., 1985) and provides information beyond that available visually (Fishkin et al., 1975; Lederman and Abbott, 1981; Heller, 1982; Lederman et al., 1986). However, because perceived texture is determined in part by complex biomechanical interactions between skin and surface, the link between physical

features of a surface and the evoked percept has been elusive except for highly contrived stimuli, such as gratings and embossed dot patterns.

Nonetheless, examination of the perceptual space of texture has revealed distinct structure. For example, multidimensional scaling based texture dissimilarity judgments consistently yields a space with a few well defined dimensions that approximately map onto qualitative textural continua, including rough/smooth, hard/soft, sticky/slippery, and warm/cool (Figure I.1) (Hollins et al., 2000a; Picard et al., 2003; Okamoto et al., 2013).

The dominant and most studied perceptual dimension of texture is roughness (Hollins et al., 2000a). Perceived roughness maps systematically onto surface microstructure as evidenced by the fact that human observers overwhelmingly agree on the relative roughness of textured surfaces (Stevens and Harris, 1962; Lederman, 1983; Sathian et al., 1989; Connor et al., 1990; Connor and Johnson, 1992; Blake et al., 1997). However, this relationship is not always straightforward. For example, while the roughness of sandpaper increases systematically with decreases in grit, the roughness of embossed dot patterns increases then decreases as inter-dot spacing increases (Connor et al., 1990), except for tall dots (Sutu et al., 2013). In fact, unlike most other sensory continua, there is no established physical determinant of

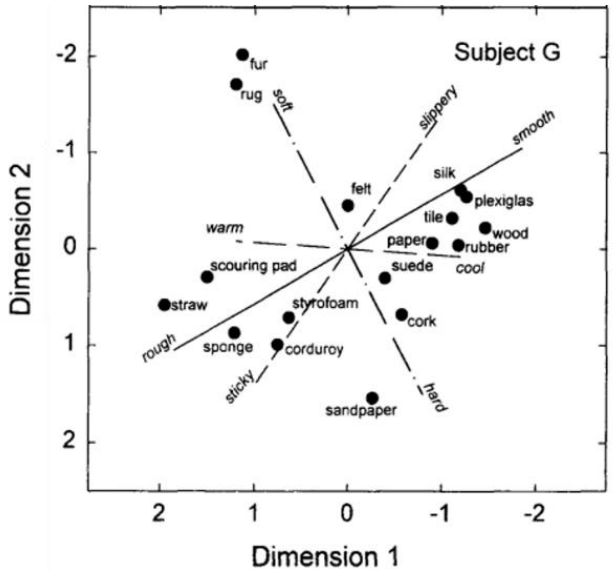

Figure I.1. **The sensory space of texture is multidimensional.** Projection of the multidimensional space of texture, estimated from ratings of dissimilarity, onto two dimensions for an example subject. Textures are further apart to the extent that they are perceived as more dissimilar. The axes of the space map approximately onto subjective dimensions, including rough/smooth and hard/soft. Adapted from Hollins et. al. 2000.

perceived roughness. In contrast, the neural basis of roughness in the nerve has been well established (see below), suggesting that the subjective experience of roughness is largely shaped by our peripheral apparatus.

The second major axis of texture perception is hardness/softness (Klatzky et al., 1989; Hollins et al., 2000a), which closely tracks surface compliance (Harper and Stevens, 1964; Yoshioka et al., 2007; Friedman et al., 2008). When touching a surface, differences in surface compliance lead to different distributions of force across the surface of the finger, both during initial contact and static grip. These forces provide multiple cues – in their spatial distribution and temporal progression – which can be used to extract information about compliance. Indeed, we reliably perceive hardness during static grip, a mode that minimizes temporal cues, (though these are still present at the onset of grip)(Friedman et al., 2008) but we can also perceive the hardness of a surface explored through a rigid probe, an ability that relies on temporal cues from vibrations transmitted through the probe (LaMotte, 2000). When tactile cues are eliminated altogether through digital anesthesia, we can still under certain circumstances perceive hardness using only kinesthetic cues, signaling the movement of the fingers into the object (Srinivasan and LaMotte, 1995).

The third axis of texture is stickiness, which tracks the friction between skin and surface (Smith and Scott, 1996; Yoshioka et al., 2007). For natural textures, perceptual judgments of stickiness are often correlated with judgments of roughness (Hollins et al., 2000a), but this relationship can be broken if friction is controlled (Taylor and Lederman, 1975). While stickiness is a far weaker determinant of perceived texture, the perception of stickiness is critical to the determination of the force required to grasp an object (Cadoret and Smith, 1996).

A fourth, modest axis of texture is warmth (Hollins et al., 2000a), associated with the thermal conductivity of the surface material. Indeed, at room temperature, objects are colder than is the body,

Nerve fiber	End organ	RF size	Optimal Stimulus	Response Properties
Slowly adapting type 1 (SA1)	Merkel cell	Small	Indentation	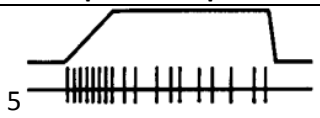
Rapidly adapting (RA)	Meissner corpuscle	Small	Flutter, slip	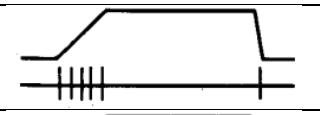
Pacinian corpuscle-associated (PC)	Pacinian corpuscle	Large	Vibration	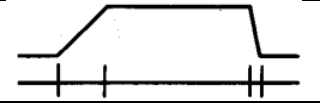

Table I.1. **Cutaneous Mechanoreceptors.** Typical response properties of the three main mechanoreceptors in the glabrous skin. While different afferent types respond differently to skin deformations, they are typically all activated during every day interactions with objects. Table adapted from Ginty et. al. 2013 and Johansson and Vallbo 1983.

so heat will tend to flow out of the skin and into the object. The rate of this heat transfer depends on the thermal conductivity of the material and determines the warmth of the surface, with higher heat transfer leading to cooler surfaces (Ho and Jones, 2006). The thermal properties of a surface are likely encoded by thermoreceptive afferents (Johnson et al., 1973, 1979, Darian-Smith et al., 1979a, 1979b).

Remarkably, the perception of texture is stable whether textures are actively explored or passively scanned over the finger (Lederman, 1981; Lamb, 1983; Friedman et al., 2008; Yoshioka et al., 2011). Furthermore, perceived texture is regardless of how fast the texture moves across the skin (Lederman, 1974, 1983; Yoshioka et al., 2011; Boundy-Singer et al., 2017). Texture invariance across scanning speeds is especially surprising given the strong dependence of skin responses (Manfredi et al., 2014) and afferent responses (Weber et al., 2013) on speed.

THE INNERVATION OF THE SKIN

Fine discriminative touch with the palmar surface of the hand relies on three main mechanoreceptors: slowly adapting type-1 (SA1) fibers, rapidly adapting (RA) afferents, and Pacinian-associated (PC) fibers (Table I.1). A fourth type of nerve fiber, slowly adapting type-2 fibers, which innervate Ruffini end-

organs, only sparsely innervate the glabrous skin of humans and are absent in non-human primates (Paré et al., 2002, 2003) so will not be further discussed here.

SA1 fibers

SA1 fibers are characterized by two main features: 1) small receptive fields (2-3 mm diameter, (Vega-Bermudez and Johnson, 1999)), and 2) a sustained response to a static indentation into the skin (Pei et al., 2009). SA1 afferents innervate Merkel cells (Abraira and Ginty, 2013) and densely innervate the skin,

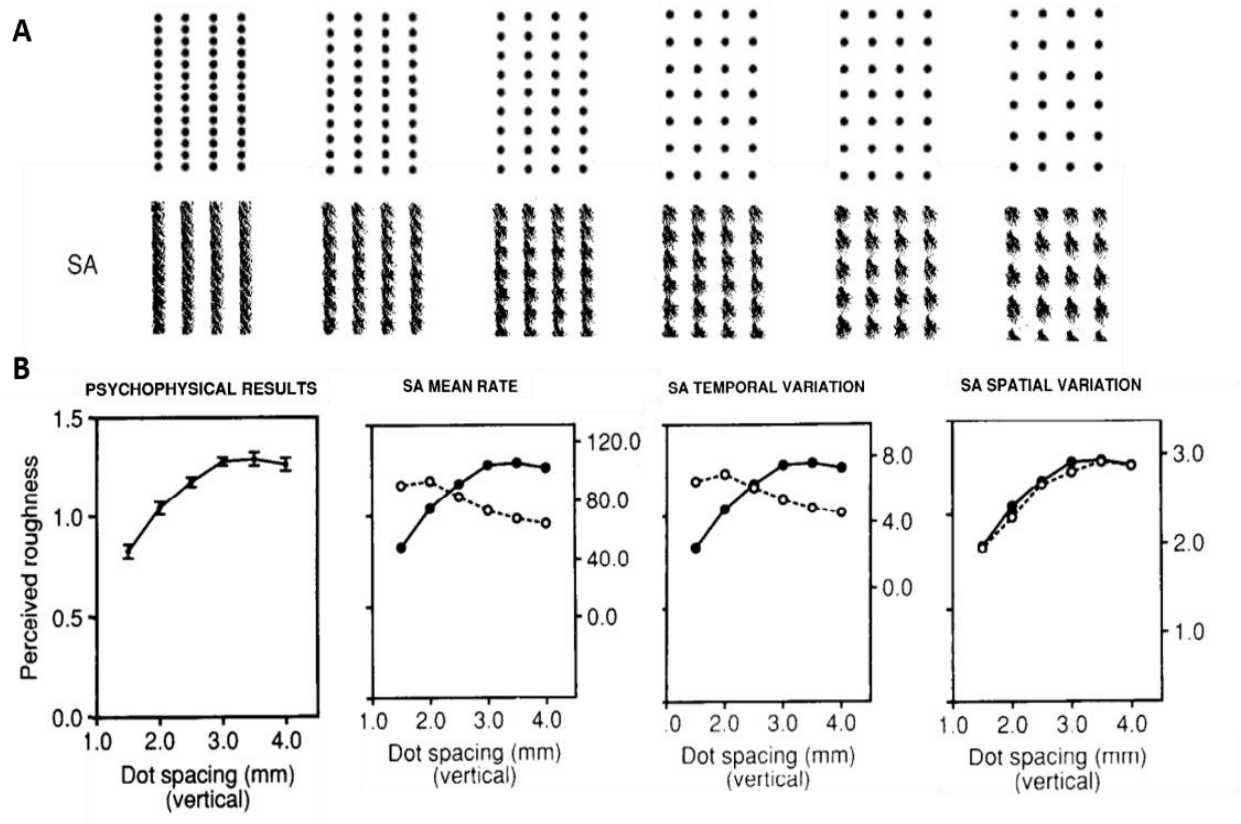

Figure I.2. **Spatial variation code for perceived roughness.** A| Reconstructed pattern of activation that would be elicited in a population of identical SA1 fibers (bottom row) by a series of dot patterns (shown above). Each line of action potentials corresponds to a single scan of the texture over the skin. Successive lines represent a 200 micron shift of the pattern, perpendicular to the scanning direction. B| Human subjects rated the roughness of each of the dot patterns (left). Neither the firing rate nor the temporal variation of SA1 responses can account how rough the surfaces feel. Rather, perceived roughness mirrors the spatial variability across the SA1 fibers. Adapted from Connor et. al. 1992.

with as many as 1.4 / mm^2 in the fingertip (Darian-Smith and Kenins, 1980). Populations of SA1 afferents faithfully reproduce the shape of objects that are statically indented into the skin (Phillips and Johnson, 1981) or scanned over the skin (Johnson and Lamb, 1981; Phillips et al., 1988; Connor et al., 1990; LaMotte et al., 1996). That is, SA1 afferents encode spatial patterns in a manner analogous to photoreceptors in the retina and their spatial resolution (around 0.5 - 1 mm, (Phillips and Johnson, 1981)) sets the limits of human tactile acuity (Johnson and Phillips, 1981). On the other hand, SA1 fibers resolve temporally varying stimuli only poorly: they respond best to slowly varying stimuli and the temporal precision of their spiking tends to be lower than that of other classes of tactile afferents (Talbot et al., 1968; Bensmaia et al., 2005; Mackevicius et al., 2012).

RA afferents

RA afferent fibers are characterized by two main features: 1) small receptive fields (3-5 mm diameter, (Vega-Bermudez and Johnson, 1999)), and 2) responses to the transient phases of a skin indentation (onset and offset) but not to the sustained phase (Pei et al., 2009). RA afferents innervate Meissner corpuscles located in dermal papillae densely (1.7 / mm^2 on the fingertips, (Darian-Smith and Kenins, 1980)). The neural image carried by RA fibers is blurrier than its SA1 counterparts (Phillips and Johnson, 1981) because each fiber branches widely to innervate multiple corpuscles (~30-80, (Paré et al., 2002)). RA fibers are sensitive to skin vibration over the so-called flutter range (5-40 Hz) and tend to produce entrained responses at these frequencies (Talbot et al., 1968). RA responses also tend to be highly precise in their temporal structure and RA spiking sequences can carry information about skin vibrations or textured surfaces (Mackevicius et al., 2012; Weber et al., 2013). An important role for RA fibers may be to signal slip events to trigger short-latency adjustments of grip force during grasp (Johansson and Westling, 1987; Macefield et al., 1996).

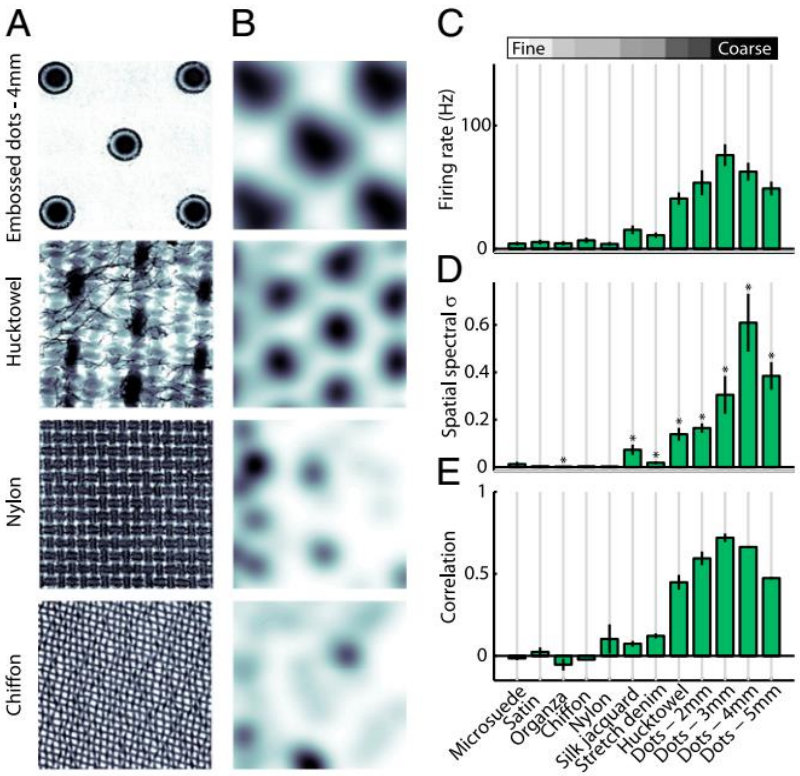

Figure I.3. Spatial coding cannot explain fine texture perception. A| Surface profiles of four different textures, two with coarse spatial features (dots and hucktowel) and two with fine spatial features (nylon and chiffon). B| Spatial patterns of activation (spatial event plots) averaged over 15 SA1 afferents, in response to the four textures. While the coarse textures evoke patterns of activity that preserve the spatial structure in the stimulus, the fine textures do not. C| Average firing rate evoked by twelve different textures, average across the SA1 afferent population. These textures are ordered from least rough (left) to most rough (right). Finer textures do not evoke significant spiking in SA1 afferents. D| Standard deviation across all frequencies the SEP spatial power spectrum (a measure of spatial patterning), plotted for all 12 textures. Responses to coarse textures show more spatial patterning than fine textures. E| Correlation between the surface profiles and the SEPs, plotted for all 12 textures. The structure of coarse textures are faithfully reconstructed in the SA1 population response, while features of fine textures are not. Adapted from Weber et. al .2013.

PC afferent

PC afferent fibers are characterized by three main features: 1) large receptive fields that sometimes encompass the entire hand (Johnson, 2001), 2) responses to the transient phases of a skin indentation but not to the sustained phase, and 3) sensitivity to high frequency vibrations. Due to their large receptive fields and low density in the glabrous skin (1/7.5 mm^2 (Darian-Smith and Kenins, 1980)), PC

afferents are poorly suited for spatial processing, failing to resolve features spaced 5 mm apart (Phillips and Johnson, 1981). On the other hand, PC fibers are exquisitely sensitive to high-frequency skin vibrations, peaking in sensitivity at around 250-300 Hz, which corresponds to the resonance frequency of the skin (Sherrick, 1953; Manfredi et al., 2012). Indeed, this population of tactile fibers primarily accounts for the perception of skin vibrations above 100-150 Hz (Talbot et al., 1968) and conveys information about fine surface microstructure and about distal contact events from vibrations transmitted through an object grasped in the hand (Brisben et al., 1999; Johnson, 2001).

TEXTURE SIGNALS IN THE NERVE

As we run our hand across a surface, spatiotemporal patterns of activation in all three populations of nerve fibers convey detailed information about the microstructure of that surface, ultimately giving rise to a rich textural percept. Information about surface texture is conveyed in different aspects of afferent responses, with spatial patterns of activation encoding coarse features and temporal patterns encoding fine features. The spatial code for coarse textures, originally hypothesized based on the results of psychophysical experiments with gratings (Taylor and Lederman, 1975; Lederman, 1983), was first established by comparing judgments of roughness of embossed dot patterns, obtained from human observers, to the responses evoked by these textures in the three populations of tactile fibers. In an elegant series of experiments, Johnson and colleagues tested a series of hypotheses as to the neural determinants for roughness and eliminated all but one (Connor et al., 1990; Connor and Johnson, 1992; Blake et al., 1997): Across all conditions tested, the variation (or degree of inhomogeneity) across the responses of SA1 fibers could account, with remarkable precision, for roughness judgments (Figure I.2). This roughness computation could be well approximated by a Gabor filter convolved across the spatial pattern of activation in this population of fibers. That SA1 fibers carry a faithful neural image of embossed dot patterns and that this image accounts for roughness judgments was taken as evidence that SA1 fibers mediates tactile perception of texture across the tangible range (Yoshioka et al., 2001).

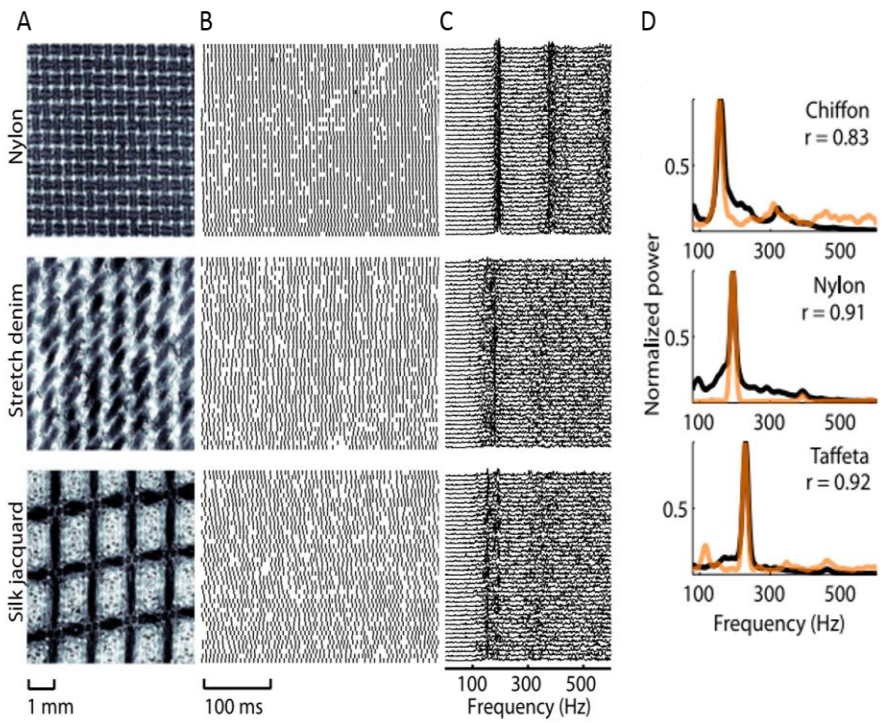

Figure I.4. **Fine textures evoke temporally patterned spiking responses.** A| Surface profiles for three finely textured materials. B| The spiking responses of a single PC afferent to 42 presentations of each of these three textures. Each texture evokes a consistent pattern of response. C| The power spectrum of each corresponding single trial neural response. PC responses are highly repeatable and afferent responses to texture exhibit consistent spectral signatures. D| The power spectral densities in response to a single texture (averaged across all trials and PC afferents) are plotted in orange, the densities of texture-elicited vibrations are shown in black. The frequency composition of the neural response matches that of the vibrations elicited in the skin (plotted in black). Adapted from Weber et. al. 2013.

However, the spatial image carried by SA1 fibers, while effectively relaying information about coarse textural features, lacks the resolution to encode fine features, given the filtering properties of the skin and its innervation density (Figure I.3) (Phillips and Johnson, 1981; Sripati et al., 2006a). Rather, the perception of finely textured surfaces features requires movement between skin and finger (Katz, 1925; Hollins and Risner, 2000). Indeed, scanning a surface results in the elicitation of characteristic vibrations in the skin whose properties depend on texture (Bensmaia and Hollins, 2003; Bensmaïa and Hollins, 2005; Delhaye et al., 2012; Manfredi et al., 2014): Differences in the texture-elicited vibrations predicts how dissimilar textures feel (Bensmaïa and Hollins, 2005), vibrations imposed onto textures make

textures feel rougher (Hollins et al., 2000b), and adaption of vibration-sensitive nerve fibers impairs subjects' ability to discriminate fine but not coarse textures (Lederman et al., 1982; Hollins et al., 2001). Texture elicited skin vibrations then drive highly precise and repeatable temporal spiking patterns in RA and PC afferents (Figure I.4) which are, in turn, highly texture specific and thus informative about texture, including its fine features (Figure I.5) (Weber et al., 2013). Furthermore, temporal spiking patterns dilate or contract systematically with decreases or increase in scanning speed, but texture information can be extracted from them regardless of speed if they are rescaled to space rather than time (Figure I.6).

In summary, then, coarse textural features are encoded in the spatial pattern of activity evoked in one population of afferents – SA1 fibers – while fine textural features are encoded in the temporal patterns of activity evoked in the other two, RA and PC fibers.

As discussed above, most work on texture coding has focused on roughness, the most dominant perceptual dimension of texture. However, the neural determinants of other textural continua have also been investigated. The consensus is that perceived hardness, like roughness, depends on both temporal and spatial codes. Surfaces of differing compliance will create different spatiotemporal patterns of activation when they make contact with the skin. For example, at equal contact force, the area of contact between skin and surface is wider for soft than for hard surfaces and forces drop off more

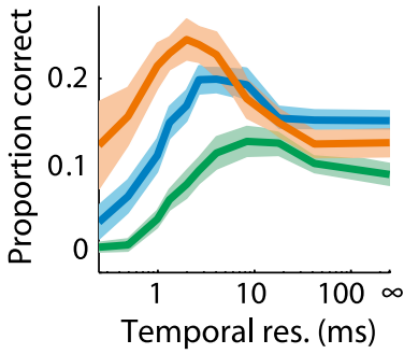

Figure I.5. **Temporal spiking patterns convey texture information.** The timing of afferent responses (ISI distributions) was used to identify texture identity (55 textures total). Classification performance is plotted for SA1 (green), RA (blue) and PC (orange) afferents against the temporal resolution at which the spike timing is read out. Spike timing in RA and PC responses is most informative about texture identity at a temporal resolution of ~5 and ~2 ms, respectively. Adapted from Weber et. al. 2013.

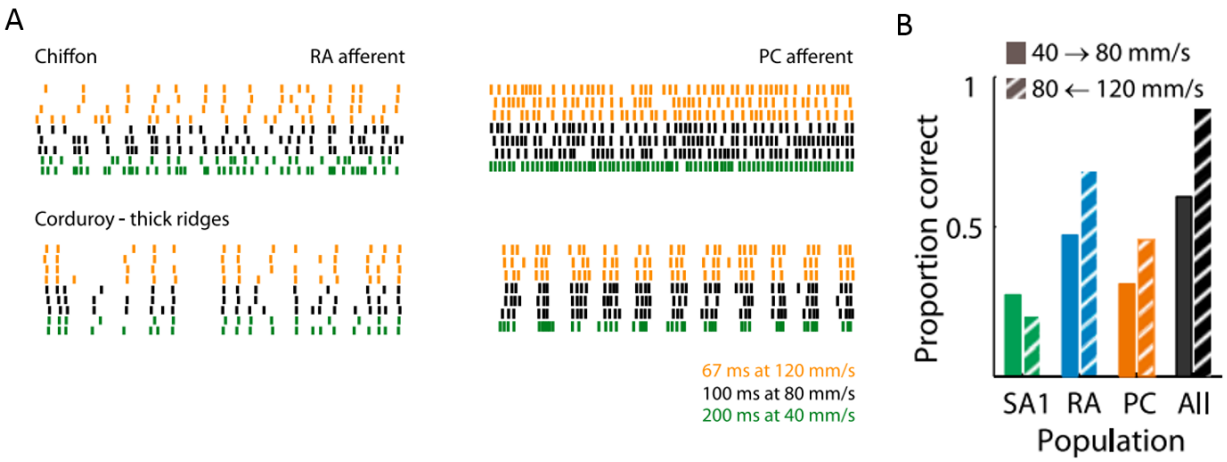

Figure I.6. **Temporal patterns scale proportionally with speed.** A| Spiking responses evoked in an example RA and PC afferent by two textures at three different speeds. Responses at 40 mm/s are compressed (twofold) and responses at 120 mm/s are expanded (by a factor of 1.5so that they are placed on a common spatial scale. B| Classification performance of small populations of afferents, based on the distance between warped spike trains (using a spike distance metric). The temporal structure of spike trains, when scaled appropriately for speed (to a common spatial frame of reference), contains texture-specific information. Adapted from Weber et. al. 2013.

progressively for soft than hard surfaces. As a result, the distribution of SA1 responses is thus shaped, in part, by surface compliance: SA1 fibers are activated over a wider area and the drop off in their activation is more progressive when contacting a compliant surface (Condon et al., 2014; Hudson et al., 2015). However, hardness can also be perceived through rapid tapping of surface with a probe (LaMotte, 2000), which elicits hardness-dependent vibrations in the probe which are transduced primarily by RA and PC fibers.

Finally, stickiness is correlated with tangential forces that stretch the skin; both SA1 and RA fibers respond to tangential forces (Birznieks et al., 2001, 2010) as do SA2 fibers, but little work has been done to quantitatively link stickiness perception to patterns of afferent activation.

Ascending Somatosensory Pathway

Touch signals from the hand are carried by the somatosensory nerves through the spinal cord and into the brainstem, where they synapse (ipsilaterally) onto neurons in the cuneate nucleus. Neurons from

this nucleus send axons across the midline to the contralateral ventral posterolateral nucleus of the thalamus (VPL). The few studies of tactile responses within these two nuclei suggest that their tactile responses look qualitatively similar to those of peripheral afferents (Douglas et al., 1978; Ghosh et al., 1992; Zhang et al., 2001) but texture representations have not been systematically investigated there.

SOMATOSENSORY CORTEX

Anterior parietal cortex (APC), located on the posterior bank of the central sulcus and on the postcentral gyrus, comprises four cortical modules, namely Brodmann's areas 3a, 3b, 1, and 2, progressing posteriorly (Geyer et al., 1999). All of these areas receive direct projections from thalamus (Jones, 1975, 1983; Jones and Burton, 1976; Jones and Friedman, 1982; Padberg et al., 2009), though cutaneous neurons in thalamus project to areas 3b, 1, and 2, while proprioceptive ones project to areas 3a and 2 (Friedman and Jones, 1981). Only area 3b receives thalamocortical input that is characteristic of primary sensory areas, and so this area is considered to be primary somatosensory cortex proper (Kaas, 1983).

Texture coding in APC

Little is known about the neural representation of texture in APC. In studies using dot patterns and gratings as stimuli, neurons in APC have been shown to depend on the spatial period of the stimulus as it is scanned across the skin (Darian-Smith et al., 1982; Sinclair and Burton, 1991; Burton and Sinclair, 1994; Tremblay et al., 1996). Furthermore, some APC neurons respond more strongly to textures that are perceived as rougher (Figure I.7) (Chapman et al., 2002; Bourgeon et al., 2016), however the stimulus space in these studies is very narrow and, as discussed above, yields an incomplete view of texture processing. Lesions to area 1 seem to lead to specific deficits in texture perception (Randolph and Semmes, 1974; Carlson, 1981) but results from aforementioned electrophysiological studies suggest that this area does not carry a more elaborate representation of texture than do its neighbors.

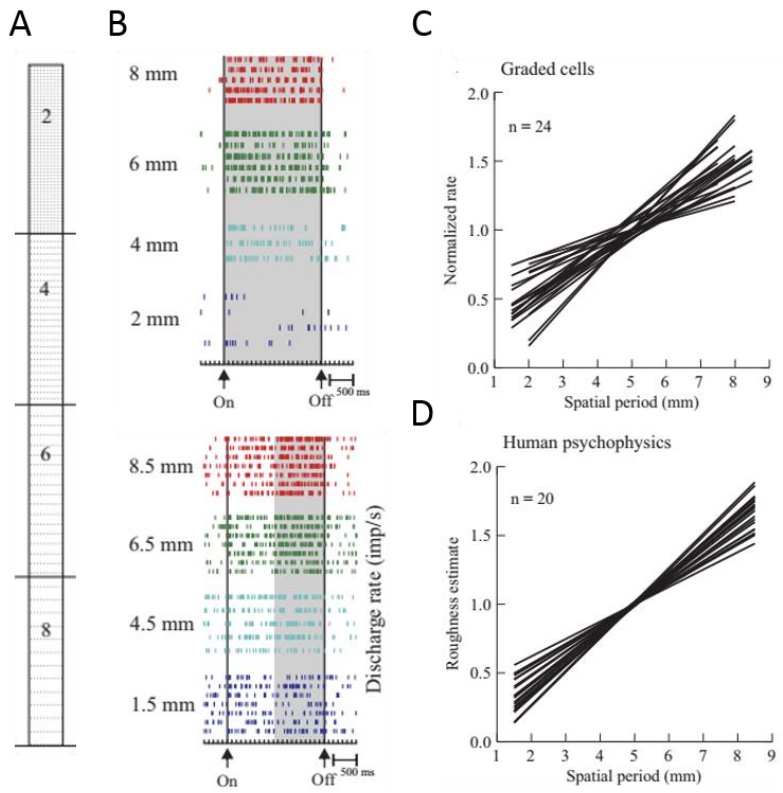

Figure I.7. **Firing rates in APC predict perceived roughness.** A| Four dot patterns whose interdot spacing varies from 2 to 8 mm. B| Spiking responses of two example APC neurons to the four stimuli. C| Responses of a subset of APC neurons ("graded cells") that show a steady increase in firing rate with spatial period. D| Human judgments of roughness increase with spatial period over the range tested. Responses of graded cells in APC mirror human judgments of roughness. Adapted from Bourgeon et. al. 2016.

While few studies have directly investigated texture representations in APC, a much broader body of work investigating neural coding in APC yields insights about texture processing in these cortical modules.

Spatial processing in APC

As tactile information propagates through APC from area 3b to 1, the selectivity of neurons for spatial features grows increasingly complex. In area 3b, neurons have elongated spatial receptive fields comprising both excitatory and inhibitory subfields (Figure I.8A) (DiCarlo et al., 1998; Sripati et al., 2006b), a receptive field structure that conveys to these neurons a selectivity for orientation (DiCarlo and Johnson, 2000; Bensmaia et al., 2008), drawing obvious analogies with neurons in primary visual cortex. The receptive fields of neurons in area 3b can be well approximated by a (linear) Gabor function (Bensmaia et al., 2008), which matches the computation that has been hypothesized to underlie the computation of roughness (see above). In contrast, neurons in areas 1 and 2 have larger, more complex

receptive fields that are more non-linear in their input (Hyvarinen and Poranent, 1978; Sripati et al., 2006b), which opens the possibility that these neurons will have more complex texture response properties.

Temporal Processing in APC

We are able to feel and distinguish skin vibrations whose frequencies span the range from less than 1 Hz to 1000 Hz. Vibrotactile frequency is encoded in in APC with two mechanisms: one rate-based, the other temporal. First, with amplitude constant, the firing rate increases with frequency up to about 100 Hz. Second, spikes tend to occur within a restricted phase of each vibratory cycle, so the response is entrained to the stimulus (Talbot et al., 1968; Salinas et al., 2000; Harvey et al., 2013). Thus, the temporal patterning in the response conveys information about frequency. As alluded to above, however, rate and temporal codes co-exist for frequencies less than 100 Hz and higher frequencies are encoded solely in the spike timing. It is interesting to note that, while somatosensory cortical neurons exhibit entrained responses up to 800 Hz (Figure I.8B) (Harvey et al., 2013), their counterparts rarely entrain beyond 50 Hz (Gao et al., 2016). Furthermore, studies with intracortical microstimulation suggest that somatosensory cortex is more sensitive than auditory cortex to finely timed patterns of stimulation (Yang and Zador, 2012). This result is counterintuitive given the much higher spectral resolution of the auditory system but is reconciled when considering that five synapses are interposed between the auditory periphery and primary auditory cortex, whereas the equivalent stretch along the somatosensory neuraxis comprises only three.

Combination of spatial and temporal codes in APC

In APC, even in area 3b, the earliest stage of cortical processing, signals from all three populations of tactile fibers are combined (Hyvärinen and Poranen, 1978; Pei et al., 2009). Indeed, most neurons in APC show sustained responses to a skin indentation, a signature of SA1 input (Pei et al., 2009), and nearly all

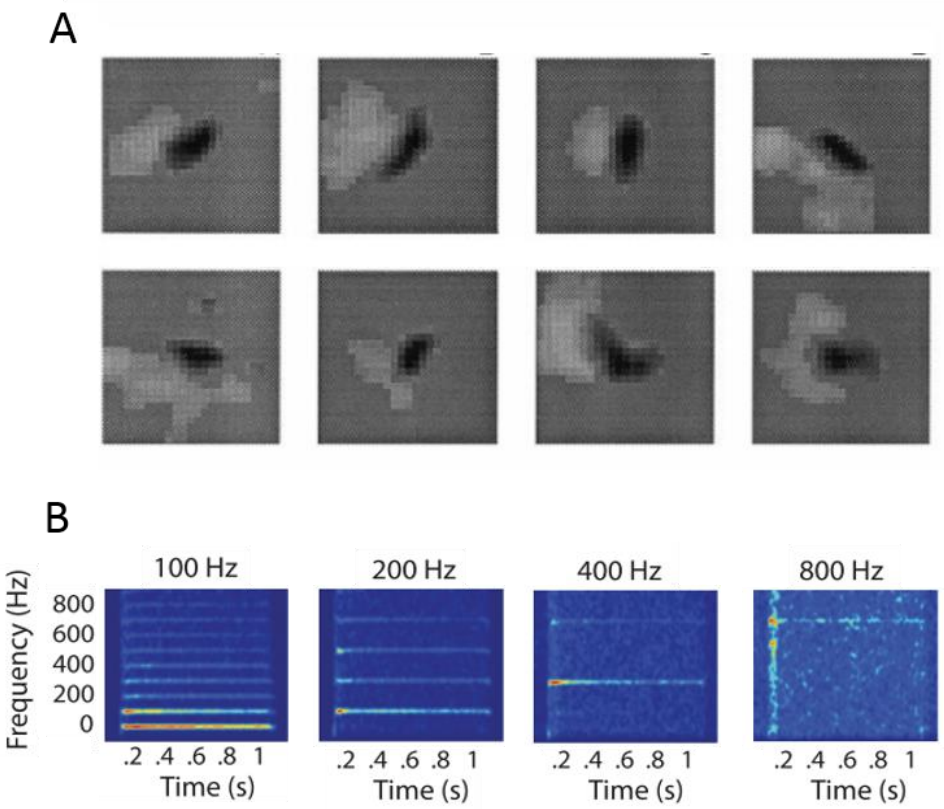

Figure I.8. **Spatial and temporal codes in APC.** A| Spatial receptive fields from eight example neurons in area 3b, as measured from spiking responses to a randomly distributed dot pattern scanned over the skin. In each 10x10 mm patch, darker colors represent excitatory regions and lighter colors represent inhibitory regions. Adapted from DiCarlo and Johnson 1998. B| Average spectrograms of APC responses to sinusoidal vibrations on the hand. Averages were taken over a subpopulation of APC neurons that phase-lock to high frequency vibrations (above 200 Hz, N=16). Some of these neurons exhibit phase locking up to 800 Hz. Adapted from Harvey et. al. 2013.

cells in APC also exhibit strong offset responses, a signature of RA and/or PC input (Sur et al., 1984; Pei et al., 2009). Furthermore, the responses to complex vibration responses in APC can only be explained by the integration of RA afferent-mediated and PC afferent-mediated streams of information (Saal et al., 2015). Thus, the spatial and temporal signals are integrated in cortex if not sooner. While SA1-like and RA-like properties seem to be distributed uniformly throughout cortex, the preponderance of neurons with strong PC input (Mountcastle et al., 1969) seems to be localized in area 1 (Paul et al., 1972; Hyvärinen and Poranen, 1978; Merzenich et al., 1978; Hyvärinen et al., 1980). These responses are

supported by anatomical evidence: the putative Pacinian-like region of somatosensory thalamus (VPi) projects densely to area 1 and sparsely to area 3b (Padberg et al., 2009).

Non-Sensory Modulation of APC Responses

The responses of APC neurons are relatively independent of the behavioral task or of the cognitive state of the animal. Indeed, while the trial-averaged stimulus responses of APC neurons are predictive of performance in a vibration discrimination task (Hernandez et al., 2000; Salinas et al., 2000), trial-to-trial variations of these responses do not seem to be related to the animal's choice (de Lafuente and Romo, 2005, 2006). Furthermore, attentional effects in APC are small; shifting attention from a visual task to a tactile task only modulates ~50% of neurons in APC, and those neurons only increase their responses by 30% or less (Hyvärinen et al., 1980; Hsiao et al., 1993; Meftah et al., 2002). This stable encoding of tactile events in APC stands in contrast to the strong task-dependence of neural responses in lateral parietal cortex, one of the primary recipients of signals from APC (Romo et al., 2002).

CONCLUSIONS

Previous studies investigating the spatial and temporal response properties of APC neurons have shown that (1) some APC neurons encode spatial information with receptive field comprising excitatory subfields flanked by inhibitory ones, in a way that is broadly analogous with primary visual cortex; (2) some APC neurons encode information about skin vibrations through both the strength and timing of their responses; (3) these two streams of information are integrated at the earliest stage of cortical processing (if not sooner). This previous work sets the stage for my dissertation project, which consists of characterizing how the response properties of neurons in somatosensory cortex give rise to neural representations that mediate our exquisite tactile sensitivity to texture.

REFERENCES

Abraira VE, Ginty DD (2013) The sensory neurons of touch. Neuron 79:618–639.

Bensmaia SJ, Denchev P V, Dammann JF, Craig JC, Hsiao SS (2008) The representation of stimulus orientation in the early stages of somatosensory processing. J Neurosci 28:776–786.

Bensmaia SJ, Hollins M (2003) The vibrations of texture. Somatosens Mot Res 20:33–43.

Bensmaïa SJ, Hollins M (2005) Pacinian representations of fine surface texture. Percept Psychophys 67:842–854.

Bensmaia SJ, Leung YY, Hsiao SS, Johnson KO (2005) Vibratory adaptation of cutaneous mechanoreceptive afferents. J Neurophysiol 94:3023–3036.

Birznieks I, Jenmalm P, Goodwin a W, Johansson RS (2001) Encoding of direction of fingertip forces by human tactile afferents. J Neurosci 21:8222–8237.

Birznieks I, Wheat HE, Redmond SJ, Salo LM, Lovell NH, Goodwin AW (2010) Encoding of tangential torque in responses of tactile afferent fibres innervating the fingerpad of the monkey. J Physiol 588:1057–1072.

Blake DT, Hsiao SS, Johnson KO (1997) Neural coding mechanisms in tactile pattern recognition: the relative contributions of slowly and rapidly adapting mechanoreceptors to perceived roughness. J Neurosci 17:7480–7489.

Boundy-Singer ZM, Saal HP, Bensmaia SJ (2017) Speed Invariance of Tactile Texture Perception. J Neurophysiol 118:jn.00161.2017.

Bourgeon S, Dépeault A, Meftah E-M, Chapman CE (2016) Tactile texture signals in primate primary somatosensory cortex and their relation to subjective roughness intensity. J Neurophysiol 115:1767–1785.

Brisben AJ, Hsiao SS, Johnson KO (1999) Detection of Vibration Transmitted Through an Object Grasped in the Hand. J Neurophysiol 81:1548–1558.

Burton H, Sinclair RJ (1994) Representations of tactile roughness in thalamus and somatosensory cortex. Can J Physiol Pharmacol 72:546–557.

Cadoret G, Smith a M (1996) Friction, not texture, dictates grip forces used during object manipulation. J Neurophysiol 75:1963–1969.

Callier T, Saal HP, Davis-Berg EC, Bensmaia SJ (2015) Kinematics of unconstrained tactile texture exploration. J Neurophysiol:jn.00703.2014.

Carlson M (1981) Characteristics of sensory deficits following lesions of brodmann's areas 1 and 2 in the postcentral gyrus of Macaca mulatta. Brain Res 204:424–430.

Chapman CE, Tremblay F, Jiang W, Belingard L, Meftah EM (2002) Central neural mechanisms contributing to the perception of tactile roughness. In: Behavioural Brain Research, pp 225–233.

Condon M, Birznieks I, Hudson K, Chelvanayagam DK, Mahns D, Olausson H, Macefield VG (2014) Differential sensitivity to surface compliance by tactile afferents in the human finger pad. J Neurophysiol 111:1308–1317.

Connor CE, Hsiao SS, Phillips JR, Johnson KO (1990) Tactile roughness: neural codes that account for psychophysical magnitude estimates. J Neurosci 10:3823–3836.

Connor CE, Johnson KO (1992) Neural coding of tactile texture: comparison of spatial and temporal mechanisms for roughness perception. J Neurosci 12:3414–3426.

Darian-Smith I, Johnson KO, LaMotte C, Kenins P, Shigenaga Y, Ming VC (1979a) Coding of incremental changes in skin temperature by single warm fibers in the monkey. J Neurophysiol 42:1316–1331.

Darian-Smith I, Johnson KO, LaMotte C, Shigenaga Y, Kenins P, Champness P (1979b) Warm fibers innervating palmar and digital skin of the monkey: responses to thermal stimuli. J Neurophysiol 42:1297–1315.

Darian-Smith I, Kenins P (1980) Innervation density of mechanoreceptive fibres supplying glabrous skin of the monkey's index finger. J Physiol 309:147–155.

Darian-Smith I, Sugitani M, Heywood J, Karita K, Goodwin AW (1982) Touching textured surfaces: cells in somatosensory cortex respond both to finger movement and to surface features. Science 218:906–909.

de Lafuente V, Romo R (2005) Neuronal correlates of subjective sensory experience. Nat Neurosci 8:1698–1703.

de Lafuente V, Romo R (2006) Neural correlate of subjective sensory experience gradually builds up across cortical areas. Proc Natl Acad Sci 103:14266–14271.

Delhaye B, Hayward V, Lefèvre P, Thonnard J-L (2012) Texture-induced vibrations in the forearm during tactile exploration. Front Behav Neurosci 6:37.

DiCarlo JJ, Johnson KO (2000) Spatial and temporal structure of receptive fields in primate somatosensory area 3b: effects of stimulus scanning direction and orientation. J Neurosci 20:495–510.

DiCarlo JJ, Johnson KO, Hsiao SS (1998) Structure of receptive fields in area 3b of primary somatosensory cortex in the alert monkey. J Neurosci 18:2626–2645.

Douglas PR, Ferrington DG, Rowe M (1978) Coding of information about tactile stimuli by neurones of the cuneate nucleus. J Physiol 285:493–513.

Fishkin SM, Pishkin V, Stahl ML (1975) Factors involved in visual capture. Percept Mot Ski 40:427–434.

Friedman D, Jones EG (1981) Thalamic input to areas 3a and 2 in monkeys. J Neurophysiol 45:59–85.

Friedman RM, Hester KD, Green BG, LaMotte RH (2008) Magnitude estimation of softness. Exp Brain Res 191:133–142.

Gao L, Kostlan K, Wang Y, Wang X (2016) Distinct Subthreshold Mechanisms Underlying Rate-Coding Principles in Primate Auditory Cortex. Neuron 91:905–919.

Geyer S, Schleicher A, Zilles K (1999) Areas 3a, 3b, and 1 of human primary somatosensory cortex: 1. Microstructural organization and interindividual variability. Neuroimage 10:63–83.

Ghosh S, Turman AB, Vickery RM, Rowe MJ (1992) Responses of cat ventroposterolateral thalamic neurons to vibrotactile stimulation of forelimb footpads. Exp Brain Res 92:286–298.

Guest S, Spence C (2003) Tactile dominance in speeded discrimination of textures. Exp Brain Res 150:201–207.

Harper R, Stevens SS (1964) Subjective hardness of compliant materials. Q J Exp Psychol 16:204–215.

Harvey MA, Saal HP, Dammann JF, Bensmaia SJ (2013) Multiplexing Stimulus Information through Rate and Temporal Codes in Primate Somatosensory Cortex. PLoS Biol 11.

Heller MA (1982) Visual and tactual texture perception: Intersensory cooperation. Percept Psychophys 31:339–344.

Heller MA (1989) Texture perception in sighted and blind observers. Percept Psychophys 45:49–54.

Hernandez A, Zainos A, Romo R (2000) Neuronal correlates of sensory discrimination in the somatosensory cortex. Proc Natl Acad Sci 97:6191–6196.

Ho H-N, Jones LA (2006) Contribution of thermal cues to material discrimination and localization. Percept Psychophys 68:118–128.

Hollins M, Bensmaia S, Karlof K, Young F (2000a) Individual differences in perceptual space for tactile textures: evidence from multidimensional scaling. Percept Psychophys 62:1534–1544.

Hollins M, Bensmaïa SJ, Washburn S (2001) Vibrotactile adaptation impairs discrimination of fine, but not coarse, textures. Somatosens Mot Res 18:253–262.

Hollins M, Fox A, Bishop C (2000b) Imposed vibration influences perceived tactile smoothness. Perception 29:1455–1465.

Hollins M, Risner SR (2000) Evidence for the duplex theory of tactile texture perception. Percept Psychophys 62:695–705.

Hsiao SS, O'Shaughnessy DM, Johnson KO (1993) Effects of selective attention on spatial form processing in monkey primary and secondary somatosensory cortex. J Neurophysiol 70:444–447.

Hudson KM, Condon M, Ackerley R, McGlone F, Olausson H, Macefield VG, Birznieks I (2015) Effects of Changing Skin Mechanics on the Differential Sensitivity To Surface Compliance By Tactile Afferents in the Human Finger Pad. J Neurophysiol:jn.00176.2014.

Hyvärinen J, Poranen A (1978) Receptive field integration and submodality convergence in the hand area of the post-central gyrus of the alert monkey. J Physiol 283:539–556.

Hyvärinen J, Poranen A, Jokinen Y (1980) Influence of attentive behavior on neuronal responses to vibration in primary somatosensory cortex of the monkey. J Neurophysiol 43:870–882.

Hyvarinen J, Poranent A (1978) Movement-sensitive and direction and orientation-selective cutaneous receptive fields in the hand area of the post-central gyrus in monkeys. J Physiol 283:523–537.

Johansson RS, Vallbo ÅB (1983) Tactile sensory coding in the glabrous skin of the human hand. Trends Neurosci 6:27–32.

Johansson RS, Westling G (1987) Signals in tactile afferents from the fingers eliciting adaptive motor responses during precision grip. Exp Brain Res 66:141–154.

Johnson K, Lamb G (1981) Neural mechanisms of spatial tactile discrimination: neural patterns evoked by braille-like dot patterns in the monkey. J Physiol:117–144.

Johnson KO (2001) The roles and functions of cutaneous mechanoreceptors. Curr Opin Neurobiol 11:455–461.

Johnson KO, Darian-Smith I, LaMotte C (1973) Peripheral neural determinants of temperature discrimination in man: a correlative study of responses to cooling skin. J Neurophysiol 36:347–370.

Johnson KO, Darian-Smith I, LaMotte C, Johnson B, Oldfield S (1979) Coding of incremental changes in skin temperature by a population of warm fibers in the monkey: correlation with intensity discrimination in man. J Neurophysiol 42:1332–1353.

Johnson KO, Phillips JR (1981) Tactile spatial resolution. I. Two-point discrimination, gap detection, grating resolution, and letter recognition. J Neurophysiol:1177–1192.

Johnson KO, Phillips JR (1988) A rotating drum stimulator for scanning embossed patterns and textures across the skin. J Neurosci Methods 22:221–231.

Jones EG (1975) Lamination and differential distribution of thalamic afferents within the sensory-motor cortex of the squirrel monkey. J Comp Neurol 160:167–203.

Jones EG (1983) Lack of collateral thalamocortical projections to fields of the first somatic sensory cortex in monkeys. Exp Brain Res 52:375–384.

Jones EG, Burton H (1976) Areal differences in the laminar distribution of thalamic afferents in cortical fields of the insular, parietal and temporal regions of primates. J Comp Neurol 168:197–247.

Jones EG, Friedman DP (1982) Projection pattern of functional components of thalamic ventrobasal complex on monkey somatosensory cortex. J Neurophysiol 48:521–544.

Julesz B (1962) Visual Pattern Discrimination. IRE Trans Inf Theory 8:84–92.

Julesz B (1981) Textons, the elements of texture perception, and their interactions. Nature.

Kaas JH (1983) What, if anything, is SI? Organization of first somatosensory area of cortex. Physiol Rev 63:206–231.

Katz D (1925) The World of Touch (Krueger LE, ed).

Klatzky RL, Lederman SJ (2010) Multisensory texture perception. In: Multisensory Object Perception in the Primate Brain, pp 211–230.

Klatzky RL, Lederman SJ, Matula DE (1993) Haptic Exploration in the Presence of Vision. J Exp Psychol Hum Percept Perform 19:726–743.

Klatzky RL, Lederman SJ, Metzger V a (1985) Identifying objects by touch: an “expert system”. Percept Psychophys 37:299–302.

Klatzky RL, Lederman SJ, Reed C (1989) Haptic Integration of Object Properties : Texture , Hardness , and Planar Contour. J Exp Psychol Hum Percept Perform 15:45–57.

Lamb GD (1983) Tactile discrimination of textured surfaces: psychophysical performance measurements in humans. J Physiol 338:551–565.

LaMotte RH (2000) Softness discrimination with a tool. J Neurophysiol 83:1777–1786.

LaMotte RH, Lu C, Srivasan MA (1996) Tactile neutral codes for the shapes and orientation of objects.

Somesthesis Neurobiol Somatosens Cortex:113–122.

Lederman SJ (1974) Tactile roughness of grooved surfaces: The touching process and effects of macro- and microsurface structure. Percept Psychophys 16:385–395.

Lederman SJ (1979) Auditory texture perception. Perception 8:93–103.

Lederman SJ (1981) The perception of surface roughness by active and passive touch. Bull Psychon Soc 18:253–255.

Lederman SJ (1983) Tactual roughness perception: Spatial and temporal determinants. Can J Psychol Can Psychol 37:498–511.

Lederman SJ, Abbott SG (1981) Texture perception: studies of intersensory organization using a discrepancy paradigm, and visual versus tactual psychophysics. J Exp Psychol Hum Percept Perform 7:902–915.

Lederman SJ, Klatzky RL (1987) Hand movements: A window into haptic object recognition. Cogn Psychol 19:342–368.

Lederman SJ, Loomis JM, Williams DA (1982) The role of vibration in the tactual perception of roughness. Percept Psychophys 32:109–116.

Lederman SJ, Thorne G, Jones B (1986) Perception of texture by vision and touch: multidimensionality and intersensory integration. J Exp Psychol Hum Percept Perform 12:169–180.

Macefield VG, Häger-Ross C, Johansson RS (1996) Control of grip force during restraint of an object held between finger and thumb: responses of muscle and joint afferents from the digits. Exp Brain Res 108.

Mackevicius EL, Best MD, Saal HP, Bensmaia SJ (2012) Millisecond Precision Spike Timing Shapes Tactile Perception. J Neurosci 32:15309–15317.

Manfredi LR, Baker AT, Elias DO, Dammann 3rd JF, Zielinski MC, Polashock VS, Bensmaia SJ (2012) The effect of surface wave propagation on neural responses to vibration in primate glabrous skin. PLoS One 7:e31203.

Manfredi LR, Saal HP, Brown KJ, Zielinski MC, Dammann JF, Polashock VS, Bensmaia SJ (2014) Natural scenes in tactile texture. J Neurophysiol 111:1792–1802.

McDermott JH, Simoncelli EP (2011) Sound texture perception via statistics of the auditory periphery: evidence from sound synthesis. Neuron 71:926–940.

Meftah E-M, Shenasa J, Chapman CE (2002) Effects of a cross-modal manipulation of attention on somatosensory cortical neuronal responses to tactile stimuli in the monkey. J Neurophysiol 88:3133–3149.

Merzenich MM, Kaas JH, Sur M, Lin C-S (1978) Double representation of the body surface within cytoarchitectonic area 3b and 1 in “S1” in the owl monkey (Aotus Trivirgatus). J Comp Neurol 181:41–73.

Mountcastle VB, Talbot WH, Sakata H, Hyvärinen J (1969) Cortical neuronal mechanisms in flutter-vibration studied in unanesthetized monkeys. Neuronal periodicity and frequency discrimination. J Neurophysiol 32:452–484.

Okamoto S, Nagano H, Yamada Y (2013) Psychophysical dimensions of tactile perception of textures. IEEE Trans Haptics 6:81–93.

Pack CC, Bensmaia SJ (2015) Seeing and Feeling Motion: Canonical Computations in Vision and Touch. PLoS Biol 13.

Padberg J, Cerkevich C, Engle J, Rajan AT, Recanzone G, Kaas J, Krubitzer L (2009) Thalamocortical connections of parietal somatosensory cortical fields in macaque monkeys are highly divergent and convergent. Cereb Cortex 19:2038–2064.

Paré M, Behets C, Cornu O (2003) Paucity of presumptive Ruffini corpuscles in the index finger pad of humans. J Comp Neurol 456:260–266.

Paré M, Smith AM, Rice FL (2002) Distribution and terminal arborizations of cutaneous mechanoreceptors in the glabrous finger pads of the monkey. J Comp Neurol 445:347–359.

Paul RL, Merzenich M, Goodman H (1972) Representation of slowly and rapidly adapting cutaneous mechanoreceptors of the hand in Brodmann's areas 3 and 1 of Macaca Mulatta. Brain Res 36:229–249.

Pei Y-C, Denchev P V, Hsiao SS, Craig JC, Bensmaia SJ (2009) Convergence of submodality-specific input onto neurons in primary somatosensory cortex. J Neurophysiol 102:1843–1853.

Phillips J, Johnson K (1981) Tactile spatial resolution. II. Neural representation of bars, edges, and gratings in monkey primary afferents. J Neurophysiol:1192–1203.

Phillips JR, Johnson KO, Hsiao SS (1988) Spatial pattern representation and transformation in monkey somatosensory cortex. Proc Natl Acad Sci 85:1317–1321.

Picard D, Dacremont C, Valentin D, Giboreau A (2003) Perceptual dimensions of tactile textures. Acta Psychol (Amst) 114:165–184.

Portilla J, Simoncelli EP (2000) A Parametric Texture Model Based on Joint Statistics of Complex Wavelet Coefficients. Int J Comput Vis 40:49–71.

Randolph M, Semmes J (1974) Behavioral consequences of selective subtotal ablations in the postcentral gyrus of Macaca mulatta. Brain Res 70:55–70.

Romo R, Hernández A, Zainos A, Lemus L, Brody CD (2002) Neuronal correlates of decision-making in secondary somatosensory cortex. Nat Neurosci 5:1217–1225.

Saal HP, Delhaye BP, Rayhaun BC, Bensmaia SJ (2017) Simulating tactile signals from the whole hand with millisecond precision. Proc Natl Acad Sci.

Saal HP, Wang X, Bensmaia SJ (2016) Importance of spike timing in touch: an analogy with hearing? Curr Opin Neurobiol 40:142–149.

Salinas E, Hernandez A, Zainos A, Romo R (2000) Periodicity and firing rate as candidate neural codes for the frequency of vibrotactile stimuli. J Neurosci 20:5503–5515.

Sathian K, Goodwin a W, John KT, Darian-Smith I (1989) Perceived roughness of a grating: correlation with responses of mechanoreceptive afferents innervating the monkey's fingerpad. J Neurosci 9:1273–1279.

Sherrick CEJ (1953) Variables affecting sensitivity of the human skin to mechanical vibration. J Exp

Psychol 45:273–282.

Sinclair RJ, Burton H (1991) Neuronal activity in the primary somatosensory cortex in monkeys (Macaca mulatta) during active touch of textured surface gratings: responses to groove width, applied force, and velocity of motion. J Neurophysiol 66:153–169.

Skedung L, Arvidsson M, Chung JY, Stafford CM, Berglund B, Rutland MW (2013) Feeling small: exploring the tactile perception limits. Sci Rep 3:2617.

Smith AM, Scott SH (1996) Subjective scaling of smooth surface friction. J Neurophysiol 75:1957–1962.

Srinivasan M a, LaMotte RH (1995) Tactual discrimination of softness. J Neurophysiol 73:88–101.

Sripati AP, Bensmaia SJ, Johnson KO (2006a) A continuum mechanical model of mechanoreceptive afferent responses to indented spatial patterns. J Neurophysiol 95:3852–3864.

Sripati AP, Yoshioka T, Denchev P, Hsiao SS, Johnson KO (2006b) Spatiotemporal receptive fields of peripheral afferents and cortical area 3b and 1 neurons in the primate somatosensory system. J Neurosci 26:2101–2114.

Stevens SS, Harris JR (1962) The scaling of subjective roughness and smoothness. J Exp Psychol 64:489–494.

Sur M, Wall JT, Kaas JH (1984) Modular distribution of neurons with slowly adapting and rapidly adapting responses in area 3b of somatosensory cortex in monkeys. J Neurophysiol 51:724–744.

Sutu A, Meftah E-M, Chapman CE (2013) Physical determinants of the shape of the psychophysical curve relating tactile roughness to raised-dot spacing: implications for neuronal coding of roughness. J Neurophysiol 109:1403–1415.

Talbot WH, Darian-Smith I, Kornhuber HH, Mountcastle VB (1968) The Sense of Flutter Vibration Comparison of the Human Capacity With Response Patterns of Mechanoreceptive Afferents From the Monkey Hand. J Neurophysiol 31:301.

Taylor MM, Lederman SJ (1975) Tactile roughness of grooved surfaces: A model and the effect of friction. Percept Psychophys 17:23–36.

Tremblay F, Ageranioti-Bélanger S a, Chapman CE (1996) Cortical mechanisms underlying tactile discrimination in the monkey. I. Role of primary somatosensory cortex in passive texture discrimination. J Neurophysiol 76.

Vega-Bermudez F, Johnson KO (1999) Surround Suppression in the Responses of Primate SA1 and RA Mechanoreceptive Afferents Mapped with a Probe Array. J Neurophysiol 81:2711–2719.

Weber AI, Saal HP, Lieber JD, Cheng J-W, Manfredi LR, Dammann JF, Bensmaia SJ (2013) Spatial and temporal codes mediate the tactile perception of natural textures. Proc Natl Acad Sci U S A 110:17107–17112.

Yang Y, Zador AM (2012) Differences in sensitivity to neural timing among cortical areas. J Neurosci 32:15142–15147.

Yau JM, Hollins M, Bensmaia SJ (2009) Textural timbre: The perception of surface microtexture depends in part on multimodal spectral cues. Commun Integr Biol 2:344–346.

Yoshioka T, Bensmaïa SJ, Craig JC, Hsiao SS (2007) Texture perception through direct and indirect touch:

An analysis of perceptual space for tactile textures in two modes of exploration. Somatosens Mot Res 24:53–70.

Yoshioka T, Craig JC, Beck GC, Hsiao SS (2011) Perceptual constancy of texture roughness in the tactile system. J Neurosci 31:17603–17611.

Yoshioka T, Gibb B, Dorsch a K, Hsiao SS, Johnson KO (2001) Neural coding mechanisms underlying perceived roughness of finely textured surfaces. J Neurosci 21:6905–6916.

Zhang HQ, Murray GM, Coleman GT, Turman a B, Zhang SP, Rowe MJ (2001) Functional characteristics of the parallel SI- and SII-projecting neurons of the thalamic ventral posterior nucleus in the marmoset. J Neurophysiol 85:1805–1822.

CHAPTER 1: THE NEURAL CODE FOR TACTILE ROUGHNESS IN THE SOMATOSENSORY NERVES

Justin D. Lieber[1], Xinyue Xia[2], Alison I. Weber[3], and Sliman Bensmaia[12]

[1]Committee on Computational Neuroscience, University of Chicago, Chicago, IL, 60637

[2]Department of Organismal Biology and Anatomy, University of Chicago, Chicago, IL, 60637

[3]Graduate Program in Neuroscience, University of Washington, Seattle, Washington, 98195

The authors declare no competing financial interests.

AUTHOR CONTRIBUTIONS

S.B. conceived of and designed the research; A.I.W. performed the experiments; J.D.L., X.X. analyzed the data; J.D.L. & S.J.B. prepared the manuscript.

ACKNOWLEDGMENTS

We would like to thank Zoe Boundy-Singer, Molly O'Donnell, and Kristine McLellan for assistance in collecting the psychophysical data, Vicky Polashock for providing us with profilometry on the textured surfaces, and Katie Long and Benoit Delhaye for comments on a previous version of this manuscript.

ABSTRACT

Roughness is the most salient perceptual dimension of surface texture but has no well-defined physical basis. Here, we seek to determine the neural determinants of tactile roughness in the somatosensory nerves. Specifically, we record the patterns of activation evoked in tactile nerve fibers of anesthetized Rhesus macaques to a large and diverse set of natural textures and assess what aspect of these patterns of activation can account for psychophysical judgments of roughness, obtained from human observers. We show that perceived roughness is determined by the variation in the population response, weighted by fiber type. That is, a surface will feel rough to the extent that the activity varies across nerve fibers and varies across time within nerve fibers. We show that this variation-based neural code can account not only for magnitude estimates of roughness but also for roughness discrimination performance.

INTRODUCTION

Everyday manual interactions activate multiple kinds of mechanoreceptors in the glabrous skin of the hand, each sensitive to different aspects of skin deformation. The nerve fibers that innervate these receptors inherit their response properties: slowly adapting type 1 (SA1) afferents respond preferentially to slowly-changing, local, large-amplitude skin deflections, Pacinian (PC) fibers prefer small-amplitude, high frequency oscillations that propagate large distances across the skin, and rapidly adapting (RA) afferents prefer local skin deformations over an intermediate range of frequencies. Signals from these three populations of afferents are routinely combined to extract sensory information from objects (Saal and Bensmaia 2014) to support interactions with them (Johansson and Flanagan, 2009). How information from these disparate sensory channels is integrated is not yet well understood.

The study of tactile texture processing is uniquely suited to address the integration of signals from the various modalities. Indeed, tangible textural features span a wide range of spatial scales, ranging from hundreds of nanometers (Skedung et al. 2013) to tens of millimeters (Connor et al. 1990a) and each tactile submodality (that is, SA1, RA, and PC fibers) is apt to encode textures over a subrange of spatial scales (Weber et al. 2013). SA1 fibers are sensitive only to surface features measured in millimeters. PC responses exhibit precise, texture-specific temporal spiking patterns to surface features on the order of micrometers but saturate with larger features. RA fibers are sensitive over a wide range of spatial scales but less sensitive than their SA1 and PC counterparts at the large and small extremes, respectively.

For many years, texture perception was thought to be primarily mediated by SA1 afferents, based on an elegant series of studies of the neural basis of perceived roughness, one of the major dimensions of texture (Hollins et al. 2000), in the somatosensory nerves (Connor et al. 1990a; Connor and Johnson 1992; Blake et al. 1997; Yoshioka et al. 2001). This conclusion, however, seems to have been an artifact of the Braille-like embossed dot patterns used in these studies, the processing of which happens to be dominated by the response of SA1 fibers (Goodman and Bensmaia 2017). Indeed, we have recently shown that all classes of nerve fibers convey texture information and contribute to our perceptual experience of texture (Weber et al. 2013).

Here, we investigate in more detail how signals from the different submodalities contribute to the tactile perception of roughness. To this end, we re-examine previously published recordings of neuronal responses evoked in the nerves of anesthetized non-human primates by natural textures and incorporate a new set of psychophysical judgments obtained from human observers to a previously collected one to establish how perception arises from nerve activity. First, we show that signals from all three afferent classes account for judgments of perceptual roughness across the full range of natural textures. Indeed, while SA1 responses are predictive of perceived roughness for coarsely textured

surfaces, RA responses provide much more finely graded information about roughness for both coarse and fine surfaces. Furthermore, PC responses are necessary to account for the familiar roughness of sandpapers, which evoke comparatively weak responses in SA1 and RA fibers. Second, we show that different afferents convey information about texture not in the strength of their responses but in their variation or inhomogeneity, as was first suggested in the aforementioned studies on roughness coding (Connor et al. 1990a). Moreover, we demonstrate that spatial variation in SA1 and RA afferents – the degree to which firing rates vary across fibers – and temporal variation in RA and PC fibers – the degree to which firing rates vary over time in *individual* fibers – determine how rough a surface will feel. Finally, we discuss how the hypothesized spatial and temporal variation computations are reflected in the responses properties of neurons in primary somatosensory cortex.

MATERIALS AND METHODS

The neurophysiological data and some of the psychophysical data (from the magnitude estimation experiment) were presented in a previous paper (Weber et al. 2013).

Stimuli

Textured surfaces were presented to the fingertips of both human participants (vibrometry, psychophysics) and non-human primates (neurophysiology) using a custom-built rotating drum stimulator (Weber et al. 2013)(Figure 1.1A). The fifty-five textures included gratings (height: 0.74 mm) and tetragonal arrays of embossed dots (truncated cones: height = 0.74 mm, base diameter = 1 mm, tip diameter = 0.5 mm, inter-dot spacing ranging from 2 to 6 mm, arranged as in Connor et al. 1990) created using a photosensitive polymer (Printight, Toyobo Co., Ltd.), which have been extensively used in previous roughness studies (Darian-Smith and Oke 1980; Phillips et al. 1988; Connor et al. 1990b; Cascio and Sathian 2001), as well as finer, more naturalistic textures such as fabrics and sandpapers

(Table 1, Figure 1.1B). Each textured strip (2.5 cm wide x 16 cm long) was wrapped around an acrylic drum (25.4 cm in diameter and 30.5 cm in length) to cover its surface completely. On each trial, the drum began to rotate and was lowered onto the fingertip when its desired speed had been achieved to exert a contact force of 50 g (± 10 g) on the finger. Textures were presented for 2.4, 1.2, or 0.8 s at 40, 80, and 120 mm/s, respectively, and the inter-stimulus interval was 3.5 s to prevent afferent adaptation (Bensmaia et al. 2005; Leung et al. 2005). In all analyses of neurophysiological data, we only consider neuronal responses during the steady-state period when both desired speed and force have been achieved.

Sequential scanning protocol. To reconstruct the spatial image conveyed by different afferent populations, we selected a subset of 12 textures to obtain spatial even plots (SEPs, cf. Johnson and Phillips 1988). Briefly, we repeatedly passed the texture stimulus over the receptive field of a nerve fiber, at 80 mm/s, with a 500 μm lateral shift (along the axis of rotation) between each presentation. Thus, a different patch of texture was scanned across the receptive field on each successive run (Johnson and Phillips 1988). Each texture was presented twice at 21 different locations along the axis of rotation, creating an SEP that was 1 cm wide. Because afferent responses are relatively similar across afferents of a given type, spike trains elicited in a single mechanoreceptive afferent by different portions of the stimulus can be used to estimate the spatial pattern of activation elicited by the stimulus across the afferent population (Figure 1.2B). Indeed, spatial variation computed from the responses of individual tactile fibers has been shown to provide a good approximation of the variation computed from different afferents (Yoshioka et al. 2001). Data from this protocol were used to compare spatial and temporal variation and revealed that these two quantities were highly correlated for the set of textures used.

Profilometry. The 3D surface profile of the 7x7 mm texture samples was recorded using a Laser Microscope (LEXT OLS4000; Olympus Corp., Tokyo, Japan), with a resolution of 2.5 µm in the x-y plane and 0.05 µm along the z axis. Our reported texture profiles are detrended for clarity and downsampled to a 10 µm resolution in the x-y plane.

Psychophysics

All procedures were approved by the Institutional Review Board of the University of Chicago and all subjects provided informed consent. Subjects sat with the left arm supinated and resting on a support under the drum. Stimuli were presented to the left index fingerpad of each subject. In the present study, we seek to relate psychophysical judgements obtained from human subjects to the responses of tactile fibers measured from anesthetized primates, as the response properties of afferents are quite similar in the two species (Johansson et al. 1982; Phillips et al. 1990, 1992).

Magnitude estimation experiments (8 subjects, 6m, 2f, ages 18-31): On each trial, the subject was passively presented with one of 55 textures (80 mm/s, 50 ± 10 g) and produced a rating proportional to its perceived roughness, where a rating of zero denoted a perfectly smooth surface. If texture B was perceived to be twice as rough as texture A, it was ascribed a number that was twice as large. Subjects were encouraged to use fractions and decimals. Each texture was presented once in each of 6 experimental blocks; ratings were normalized by the mean of each block and averaged, first within then across subjects. Ratings of roughness were highly consistent across subjects (inter-subject correlation: 0.91 ± 0.03, mean ± s.d.).

Roughness discrimination experiments (6 subjects, 3m, 3f, ages 19-31): For these experiments, a subset of 6 textures was selected from the fine group: fleece (fuzzy), velveteen, suede (cuddle), flannel, organza, wool gabardine. On each trial, the subject was passively presented with a pair of textures (for 1

s each, separated by a 1 s inter-stimulus interval, 15 unique comparisons, 80 mm/s, 50 ± 10 g) and judged which of the two felt rougher. Each pair of textures was presented 20 times in pseudorandom order. Roughness discrimination performance was consistent across the subjects (inter-subject correlation: 0.85 ± 0.16, mean ± s.d.).

Neurophysiology

Extracellular single-unit recordings were collected from the median and ulnar nerves innervating the distal fingertips of 6 Rhesus macaques (Macaca mulatta) using established procedures (Talbot et al. 1968; Muniak et al. 2007). Anesthesia was maintained using pentobarbital. Data were collected from 17 SA1 fibers, 15 RA fibers, and 7 PC fibers. Units were classified as SA1, RA, or PC using standard methods (Muniak et al. 2007). All procedures complied with the NIH Guide for the Care and Use of Laboratory Animals and were approved by the Animal Care and Use Committee of the University of Chicago.

Analysis

Our large, diverse stimulus set (Table 1.1) allowed us to test the hypothesis that different tactile submodalities are differentially informative about surface microgeometries at different spatial scales. Having noted that, excluding sandpapers, our textures naturally split into two clearly separated groups (Figure 1.1C), we split textures into three categories: (1) Fine textures; (2) coarse textures; and (3) sandpapers, which, while they tended to be rough, evoked qualitatively different responses in PC fibers than did other textures.

Temporal variation. As a starting point, we tested the hypothesis, put forth in our previous study (Weber et al. 2013), that perceived roughness could be predicted from the temporal variation in afferent responses with the caveat that the previously published analysis did not make a strong distinction between temporal and spatial variation (see below). To this end, we implemented a simple temporal

variation filter, with only two parameters, that allowed us to directly evaluate 1) the time scale over which roughness is computed and 2) the extent to which roughness relies on a rate code or a variation code. In our previously study (Weber et al. 2013), we had used a more complex filter to replicate results from one of the foundational papers on roughness coding (Connor and Johnson, 1992). However, in subsequent testing, we found that a simple filter achieved comparable fits as did the more complex one and consequently adopted it.

To compute variation, we first counted the number of whole and fractional inter-spike intervals (ISIs) within each 1 ms bin, an approach that yields variation values that increase smoothly with firing rate at low response rates in contrast to the standard binning technique (cf. Connor et al. 1990; Connor and Johnson 1992; Blake et al. 1997; Yoshioka et al. 2001). Next, we convolved these binned responses with a 1D variation filter:

$$f(t) = \left[p * \frac{t}{\sigma} + (1 - p)\right] \exp\left[\frac{-t^2}{2\sigma^2}\right]$$

where σ is the characteristic width (in ms) of the filter, and p, which ranges from 0 to 1, represents the strength of the bimodality in the filter: p=0 denotes Gaussian smoothing, p=1 denotes symmetric differentiation, analogous to the filters used in previous roughness studies (Connor et al. 1990a; Connor and Johnson 1992; Blake et al. 1997). This mathematical description of the filter was adopted as it captures the range of filters observed for the integration of afferent signals in somatosensory cortex (Saal et al. 2015). The resulting signal was then full-wave rectified – the equivalent of implementing two half-wave rectified, phase-inverted filters (cf. Connor and Johnson 1992) – then averaged to compute a single variation value per spike train (see Figure 1.3A). Note that the variation values obtained using half-wave and full-wave rectification were almost indistinguishable (R^2 = 1.0, 0.99, and 0.95 for SA1, RA, and PC fibers respectively).

Filters were fit individually to responses – from each afferent population separately – to textures that elicited an average of at least 10 spikes per second in that population (if too many low-spiking textures were included in the fitting, parameters became unstable). Variation was calculated for individual spike trains, then averaged over trials and afferents to get a mean variation value for each texture in each afferent population. Filter parameters were optimized to achieve the highest correlation between response variation and perceived roughness. The optimal *p* was 0.85, 0.90, and 1.0 for SA1, RA and PC afferents, respectively, suggesting strong differentiation (Figure 1.3B). The optimal σ was 20.7, 12.8, and 8.0 ms suggesting that SA1 responses are integrated over longer time windows than are their PC counterparts, with RA signals exhibiting intermediate integration times, consistent with previous findings (Saal et al. 2015). If these filters are interpreted in spatial terms (see below), then the corresponding distances between filter peaks are 3.36, 2.08, and 1.28 mm, respectively, given the scanning speed of 80 mm/s, consistent with previous findings (Connor et al. 1990a). These parameters are used for all analyses throughout the paper, with the exception of the speed analysis in Figure 1.9, in which σ is varied over a range (with *p* fixed at its optimal value).

Spatial variation. We sought to determine the degree to which temporal variation could be used as a proxy for spatial variation given our texture set. To this end, we measured the spatial variation in SA1 and RA responses of a subset of textures using previously established methods (developed by Connor and Johnson, 1992). Briefly, SEPs were binned in 0.5 mm x 0.5 mm bins (corresponding to 6.25 ms along the scanning direction), then convolved with a 2D Gabor filter:

$$f(x,y) = \sin\left\{\frac{2\pi[x * \sin(\theta) - y * \cos(\theta)]}{\lambda} + \varphi\right\} * \exp\left[\frac{-(x^2 + y^2)}{2{\sigma_s}^2}\right]$$

where (x, y) is the center of the filter, θ is the orientation of its sinusoidal component, λ is its spatial period, φ is the phase of the sinusoidal component relative to the center, and σ_s is the standard

deviation of the 2D Gaussian component. Spatial variation was calculated at a range of rotations and translations of the Gabor filter across the field of the SEP and then averaged to obtain the overall spatial variation. To compare temporal and spatial variation, we matched the shape of the spatial filter to that of the temporal filter, by setting $\sigma_s = 2 \cdot \sigma \cdot (80\text{mm/s})$, and $\lambda = 2.5 \cdot \sigma_s$, which yields filters with matched peak-to-peak distances. For SA1 and RA afferents, we measured the correlation between the mean temporal variation across the 21 rows of the SEP to the measured spatial variation of that same SEP, across all recorded cells, textures, and trials. We did not compute the spatial variation of PC responses as this population of tactile fibers innervates the skin too sparsely for a spatial code to be viable at the relevant spatial scales.

Model validation. To compare models with different numbers of parameters (e.g. single vs. multiple regressions), we performed a leave-one-out cross-validation procedure. For each texture, we refit our model on variation and roughness data from the 54 other textures, and used this new model to predict the roughness of the texture that was left out. Then, over the full set of 55 predicted values, we calculated the mean error normalized by total variance:

$$e = \frac{\sum_i (y_i - f_i)^2}{\sum_i (y_i - \bar{y})^2}$$

where f_i was the predicted roughness of ith texture, y_i the psychophysical roughness of ith texture, and $\bar{y}$ the mean measured roughness. For the non-cross-validated case, $1\text{-}e = R^2$. To test whether a given model provided significantly better predictions than another, we calculated a bootstrapped error (sampling textures with replacement 10000 times) and counted the proportion of times a given model performed more accurately than another.

These errors are summed over subsets of textures (fine, coarse, sandpaper) and reported in Figure 1.5A and Figure 1.8A. As our cross-validation procedure occasionally yielded large outliers (caused by an idiosyncratic sample), these errors are reported as medians and median absolute deviations.

Principal Components Analysis. We used principal components analysis (PCA) to characterize the extent to which the roughness signal was redundant across afferent populations. First, we treated the response variation response of each afferent as a separate dimension, yielding 55 points in a 39-dimensional space. Next, we normalized each afferent's response across textures such all three subpopulations of afferents (SA1, RA, PC) accounted for an equal proportion of the variance across the total space. Specifically, each response variation value was normalized by the standard deviation (across textures) of each afferent's variation values divided by the square root of the number of afferents of that type in the sample. Thus, each subspace (comprising 15, 17, and 7 dimensions corresponding to SA1, RA, and PC fibers) had unity variance, and the contribution to that variance of each fiber of each type was equal. Next, we used PCA to produce a sorted list of 39 orthonormal vectors (principal axes), the coordinates of the textures in this new orthonormal basis (principal components), and the variance explained by each basis. Finally, we performed regressions to quantify the relationship between individual principal components and roughness ratings. The main conclusions of the resulting analyses were consistent across strategies to normalize the variation values (including no normalization).

Afferent reliability. We characterized afferent reliability in two ways: 1) how reliably could two textures be discriminated based on the responses of an individual afferent? 2) how reliably could two textures be discriminated based on the responses of pairs of afferents? In other words, we wished to test the degree to which individual afferents conveyed consistent roughness signals and the degree to which different afferents conveyed roughness signals that were consistent with each other. To quantify within-fiber consistency, we computed how often comparisons based on single-trial responses of a given

afferent to each texture in a pair yielded results consistent with the comparison of the trial-averaged responses of that afferent to those two textures. That is, if texture t_2 had a larger mean variation than texture t_1, we assessed how often the variation in the single-trial response to t_2 was greater than that from t_1. We averaged this performance over all texture pairs to obtain a measure of how consistent each afferent's response was across repeated presentations of each texture. For each afferent class we averaged this performance over all cells, with a performance of 0.5 indicating no consistency, 1 indicating perfect consistency, and less than 0.5 indicating that the majority of afferents did not reflect the mean tendency.

To quantify across-fiber consistency, we computed how often comparisons of the mean variation from individual afferents gave results consistent with the comparison of the mean variation across afferents. That is, if texture t_2 had a larger mean variation (across trials and fibers) than texture t_1, we assessed how often the mean variation (across trials) in each afferent's responses to t_2 was greater than that the mean variation in another afferent's responses to t_1. To the extent that the ordinal relationship in the response variation was consistent across nerve fibers, this measure tended towards 1 (with 0.5 indicating no consistency).

Roughness discrimination. We implemented an ideal observer analysis to determine the extent to which a combined signal from all 3 afferent types could discriminate the roughness of pairs of textures. First, we combined single-trial variation values from equal numbers of SA1, RA, and PC afferents chosen at random, using weights from the full multiple regression. We measured the proportion of times that this new metric was higher for the rougher of the two textures (from magnitude estimation). The performance for a given texture pair was averaged over many combinations of trials and combinations of afferents to create a mean discrimination performance. We tested groups of afferents from sizes 3 to 21 (1 to 7 of each afferent type), and found that groups of size 15 (5 of each type) closely matched

psychophysical performance. We used an equal number of afferents of each type for this analysis – despite the fact that PC fibers innervate the skin much less densely than do RA or SA1 fibers – because the high-frequency vibrations evoked during texture scanning propagate long distances across the skin and activate PC afferents far from the contact area (Delhaye et al. 2012; Manfredi et al. 2012). This recruitment results in a substantial amplification of the PC signal and counters the effects of the lower innervation density of PC fibers.

As expected, ideal observer performance systematically improved as the roughness difference between two textures increased. To obtain best-fit curves of this relationship, we averaged the discrimination performance for each texture pair across nerve fibers of each type, and plotted this performance against the mean log ratio of roughness. Psychometric curves were fit with a sigmoid function:

$$f(r) = \frac{1}{1 + e^{-r/T}}$$

where *r* is the log ratio of variation or roughness, and T is a slope parameter that corresponds to the threshold log ratio given a criterion discrimination performance of 0.73 ($= \frac{1}{1+e^{-1}}$). The Weber fraction is then given by $e^{-T} - 1$. Note that the Weber fraction here is computed based on perceptual judgments rather than a physical continuum (as is typically done) and so cannot be directly compared to previously measured Weber fractions (based on grit size or spatial period, e.g.)(Miyaoka et al. 1999; Hollins et al. 2001; Sutu et al. 2013). However, we used the same perceptual judgments for the psychophysical and neurometric analyses, so the comparison of the two is appropriate.

RESULTS

We recorded the activity evoked in 17 SA1, 15 RA and 7 PC afferents as each of 55 textured surfaces was scanned across the finger using a rotating drum stimulator (Figure 1.1A). For the purposes of

comparison, stimuli were divided into three groups: 39 fine textures, which consisted mostly of fabrics, 10 coarse textures, which included Braille-like dot patterns, gratings, and coarse fabrics, and 6 sandpapers varying in grit size (from 150 to 800)(Table 1, Figure 1.1B). In paired psychophysical experiments, 8 human observers rated the perceived roughness of these same textures, also presented using the drum stimulator, in a free magnitude estimation paradigm (Figure 1.1C) and another 5 human observers performed a roughness discrimination task in which they judged which of two paired textures was rougher. We sought to understand which aspects of the activity in the three classes of afferents (Figure 1.2) accounted for reports of perceived roughness.

Predicting mean roughness judgments based on afferent responses

In a previous study using the same data, we showed that the variation in the responses evoked in the three classes of tactile nerve fibers, weighted by fiber type, was a reliable predictor of perceived roughness (Weber et al. 2013). Variation is defined as the inhomogeneity in the peripheral response, in space – how much does the response vary response across afferents? – or in time – how much does the response of individual afferents vary over time? We wished to further examine the relationship between neural response variation and roughness and assess how consistent this relationship was across the range of tangible textures. To quantify variation, we convolved afferent spike trains with a differentiating filter (Figure 1.3, see Methods). We first limited our analysis to coarse textures in an attempt to replicate results using dot patterns and gratings (Connor et al. 1990a; Connor and Johnson 1992; Blake et al. 1997). We found that variation in SA1 responses tended to outperform both RA and PC variation, consistent with previous studies (Figure 1.4, coarse textures in grey; R^2 = 0.90, 0.63, and 0. 80, for SA1, RA, and PC variation, respectively). In contrast, as previously reported (Weber et al. 2013), we found that SA1 variation was a poor predictor of perceived roughness of fine textures, and was easily outperformed by both RA and PC variation (Figure 1.4, blue. R^2 = 0.46, 0.91, and 0.67 for SA1, RA, and PC

variation). SA1 and PC signals were poor predictors of the roughness of sandpapers compared to RA afferents (Figure 1.4, red. R^2 = 0.62, 0.93, and 0.82 for SA1, RA, and PC variation). In fact, over the full range of textures, RA variation outperformed both SA1 and PC variation (leave-one-out cross-validation, p<0.05, R^2 = 0.72, 0.89, and 0.82 for SA1, RA, and PC variation). That SA1 responses performed poorly in the discrimination of sandpapers suggests that these nerve fibers are not simply coarse texture "specialists," as has been previously proposed (Hollins et al. 2001; Bensmaïa and Hollins 2005). Rather, aspects of the roughness signal seem to be distributed across fiber types.

While our data suggest that SA1 afferents cannot account for roughness, and that RA afferents provide the strongest linear relationship with roughness judgments, there is no reason to believe that any given perceptual function – texture perception, for example – will be mediated by a single population of afferents (Saal and Bensmaia 2014). In fact, we find that a linear combination of response variation in the three afferent types outperformed any individual afferent type (Figure 1.4D, R^2 = 0.94): all three predictors were significantly greater than zero (standardized regression, coefficients = 0.11, 0.25 & 0.25 for SA1, RA and PC, respectively; ΔR^2 F-test: $F(1,51)$= 6.5, 19.5 & 48.8 with, p<0.05) and the combined model performed significantly better than any model including only responses from a single afferent population (leave-one-out cross-validation, p<0.01) (cf. Weber et al. 2013). According to this model, then, RA and PC signals contribute to a greater extent to perceived roughness than do SA1 signals, a finding that stands in stark contrast to those of studies with embossed dot patterns and gratings.

PC signals are poor predictors of the roughness of dot patterns and gratings (Connor et al. 1990a; Yoshioka et al. 2001) and predict fine texture roughness less accurately than do RA afferents. Nevertheless, they were a significant predictor in the linear regression. One way to illustrate the role of PC afferents in texture perception is to examine their contribution to the coding of sandpapers. Specifically, if we compare a model built from just SA1 and RA signals to a model using all three

afferents, we find that adding PC afferents significantly reduced the error when predicting sandpaper roughness (Figure 1.5A, leave-one-out cross-validation, $p<0.001$). Indeed, SA1 and RA afferents consistently underestimate the relative roughness of sandpapers (see Figure 1.4A-B) but PC responses are nearly saturated for these textures (see Figure 1.4C). In other words, PC responses are the reason why sandpapers feel so rough (Figure 1.5B).

While texture responses differ across fiber types, they are all relatively good predictors of roughness. One possibility, then, is that roughness is determined by the shared variance across afferent types. To test this possibility, we ran a principal components analysis (see Methods) on the variation in texture-evoked responses (see Methods) and found that 60% of the variance in response variation was accounted by the first principal component. Importantly, this single dimension could predict roughness ratings nearly as well as our multiple regression of mean afferent variation (R^2 = 0.93). Furthermore, the 38 remaining principal axes, which in combination accounted for 40% of the response variance, explained essentially nothing about roughness (R^2 = 0.07). In other words, roughness may be best understood as the extent to which response variation covaries across afferent types.

Reliability of roughness signals

In the above analysis, we showed that mean psychophysical ratings of roughness could be accounted for from the sum of the mean variation in afferent responses, weighted by afferent type. Next, we wish to assess the reliability of this neural code for roughness. To this end, we investigated how reliable response variation was within and across fibers and assessed whether this neural population code could account for roughness discrimination performance.

First, we found that variation was highly consistent across repeated presentations of a stimulus for each afferent. Indeed, the ordinal relation in the response variations evoked by a pair of textures – i.e., which

of the two textures yielded the higher variation value – was highly consistent within fibers (mean within-afferent consistency, all texture pairs: 0.93, 0.95, and 0.91 for SA1, RA, and PC fibers, respectively). On the other hand, different afferents of a given type conveyed less consistent signals about roughness. That is, one fiber might yield a higher variation for texture A than for texture B while another fiber of the same type might reverse that relation (Figure 1.6A-C). SA1 fibers tended to be the most consistent for the coarse textures and RA fibers were the most consistent for fine textures and sandpapers, as well as over the full set of textures (Figure 1.6D)(mean across-fiber consistency, all texture pairs: 0.83, 0.88, and 0.79 for SA1, RA, and PC fibers). In other words, individual fibers are extremely consistent, but there is some disagreement across fibers of a given type as to the roughness of a texture and this disagreement, rather than stochasticity in the response, most likely drives the uncertainty in roughness judgments.

In the previous analysis, we assessed the consistency of response variation in each afferent population but did not directly address the relationship between these signals and perceived roughness. Next, then, we wished to gauge whether the combined signals *across* afferent populations could account for roughness discrimination measured in human observers. To this end, we measured the performance of 6 human subjects in a roughness discrimination task with a subset of 6 textures (yielding a total of 15 pairs)(Figure 1.7B). Performance on this discrimination task yielded a Weber fraction of 0.17; that is, a 17% increase in perceived roughness was perceived 73% of the time. Then, we performed an ideal observer analysis based on afferent responses, weighted by afferent type (using weights from the multiple regression performed on the roughness estimates), to examine how accurately the putative distributed neural code could predict the discrimination of surface roughness. We found that, to obtain a Weber fraction of 0.17 required only 15 nerve fibers (5 of each type) (Figure 1.7A). Orders of magnitude more fibers respond to a textured surface, but even individual tactile fibers have been shown to outperform human subjects (Arabzadeh et al. 2014). Furthermore, the patterns of confusions based on the psychophysical and neuronal data were highly correlated (R^2=0.85); that is, textures whose

roughness tended to be confused in the psychophysical experiments also tended to be confused in the neurometric analysis. Thus, a distributed code for roughness accounts not only for psychophysical ratings of roughness but also for roughness discrimination.

Does response rate or response variation determine roughness?

The above analyses were based on the premise, inspired by the work of Johnson and colleagues, that roughness was determined by the variation in afferent responses (Connor et al. 1990; Connor and Johnson 1992; Blake et al. 1997; Weber et al. 2013b). However, whether response rate or response variation determine roughness has been a point of contention (Sutu et al., 2012, but see Goodman and Bensmaia, 2017). With this in mind, we sought to reexamine the degree to which firing rates in populations of nerve fibers could account for perceptual judgments of roughness.

We found that a combined model using only firing rate was significantly outperformed by a model that used variation in afferent responses (p<0.001, leave-one-out cross-validation), an effect mostly driven by an improvement in predicting the roughness of coarse textures (Figure 1.8A). In light of this, we sought to examine why variation provides this advantage for some textures but not others. We found that variation increased with firing rate in a consistently monotonic manner for fine texture responses, but much more irregularly for coarse texture responses (Figure 1.8B-D). In other words, variation and firing rate are interchangeable for fine but not coarse textures, which explains why rate and variation are equally good at predicting the roughness of fine textures, but not that of coarse textures. Nonetheless, a single neural code – neural variation – accounts for perceived roughness across the range of tangible textures.

Does temporal or spatial variation determine roughness?

Another point of inquiry is whether spatial or temporal variation is the key determinant of perceived roughness (Connor and Johnson 1992). To compute the variability of the afferent response to texture, the nervous system could plausibly compute the variability over time within individual afferents (temporal variation) or compute the degree to which responses of spatially displaced afferents differ (spatial variation). As previously reported (Weber et al. 2013), for the subset of textures for which we were able to construct spatial event plots, we found that temporal and spatial variation were nearly identical (R^2=0.93, 0.98 for RA & SA1 afferents, respectively) and yielded indistinguishable predictions of perceived roughness (though in principle, they can be decoupled, see Connor and Johnson, 1992).

However, we also examined the dependence of the filters on scanning speed. Indeed, we might expect a simple temporal variation filter to be invariant to changes in texture speed. Conversely, if our temporal filter actually reflected a spatial computation, the temporal width would contract or dilate systematically with increases or decreases in scanning speed, to map to a spatial filter of constant width. In other words, if the filters do not scale with speed then they must be temporal. If filters do scale with speed, they may either be spatial, or a more complex version of a temporal filter the width of which is speed dependent. At each speed, we looked for the optimal timescale at which RA and SA1 response variation could best predict coarse texture roughness. We found that performance curves across speeds overlap closely when measured in spatial units, but not when measured in temporal units (Figure 1.9A-D, correlation between temporal/spatial curves – SA1: -0.08/0.95, RA: 0.11/0.99). In other words, our data are consistent with a model in which roughness is determined by spatial variation in SA1 and RA responses.

We found a similar, albeit weaker effect for PC afferents, whose responses showed more spatial than temporal constancy (Figure 1.9E-F, correlation between temporal/spatial curves – PC: 0.21/0.86). However, the innervation density of PC afferents is 1/7.5 mm^2, much sparser than 1/0.7 mm^2 and 1/0.6

mm^2 for SA1 and RA afferents (Darian-Smith and Kenins 1980), and much too low to carry out spatial differentiation corresponding to the width of the PC filter (1.28 mm peak-to-peak). To the extent that the PC variation filters exhibit constancy, it is likely mediated by a speed dependent temporal variation mechanism. Indeed, PC signals have been shown to be temporally differentiated by downstream neurons (Saal et al. 2015). Our results further suggest that the temporal differentiation filters that drive perceived roughness scale systematically with scanning speed.

DISCUSSION

Neural code for roughness

The main conclusions of the present study are that 1) all three afferent classes (SA1, RA and PC afferents) contribute to roughness perception and 2) the variation in afferent responses, rather than simply their strength, determines how rough a surface will feel. Consistent with previous reports (Connor et al. 1990a; Connor and Johnson 1992; Blake et al. 1997), SA1 fibers respond strongly to textured surfaces comprising coarse spatial features. The spatial variation in this population of nerve fibers accounts for the roughness of these surfaces better than their rate. While SA1 afferents set the limit of tactile acuity for patterns indented into the skin (Phillips and Johnson 1981), these nerve fibers are almost completely insensitive to small spatial features (measured in the hundreds of microns or less). Because most natural textures also comprise fine features, SA1 responses alone are insufficient to account for the tactile perception of texture.

While RA afferents contribute less to the perceived roughness of coarse textures than do their SA1 counterparts (cf. Blake et al., 1997a), these fibers are critical for the perceived roughness of textures whose features span a wide range of spatial scales. In a previous study, we proposed that RA fibers encode texture information in the temporal patterning of their responses, down to a precision of about

5 ms (Weber et al. 2013). Given the density of RA innervation, this population of fibers may also encode coarse spatial features in their spatial pattern of activation. RA signals may thus encode coarse surface features spatially and temporally and fine features temporally.

Finally, while PC fibers innervate the fingertip skin too sparsely to encode texture in their spatial pattern of activation, they produce strong responses to scanned surfaces that span the range of tangible textures (Weber et al. 2013). Whether the contribution of the PC signal is in the rates or in the variation is not clear: Our model's ability to predict texture roughness is unchanged if we replace PC variation with PC rate. The differentiation filter for PC responses may therefore not be necessary in the roughness computation. However, one might argue that the responses of all three afferent populations may be processed analogously to extract a given stimulus quantity (roughness), which would support the inclusion of PC variation. Furthermore, PC signals have been shown to be differentiated in cortex (see below).

In summary, all three populations of nerve fibers contribute to the perception of roughness. In fact, perceived roughness seems to be driven by a redundant signal carried by all three afferent populations. This finding adds to a body of evidence that signals from the three tactile submodalities are not functionally segregated, as was once believed, but rather are integrated to extract stimulus information and elicit in a tactile percept (Saal and Bensmaia 2014).

Spatial vs. temporal coding

A major limitation of the present study is the failure to conclusively distinguish spatial coding – where stimulus information is conveyed in the pattern of responses across populations of fibers – from temporal coding – where information is conveyed in temporal patterning in the spiking responses of individual fibers. Indeed, for the set of texture for which both could be explicitly measured and

compared, the spatial and temporal variation were highly correlated. We can exclude spatial coding in PC fibers, at least at the relevant spatial scales, given their sparse innervation and enormous RFs. We can also, in principle, exclude spatial coding for fine textures because their spatial periods are orders of magnitude smaller than what can be resolved spatially, even in SA1 and RA responses. However, we cannot exclude (and in fact believe it to be rather likely) that RA fibers encode coarse textural features both spatially and temporally. The main evidence for the spatial code for roughness is that the optimal variation filter scales with scanning speed as predicted by a spatial code. However, the ability to distinguish textures with spatial periods less than about 1 mm implies temporal coding in RA and PC fibers (Weber et al. 2013).

Downstream mechanisms

In the proposed model of roughness coding, the spatial representation of coarse features, carried by SA1 and perhaps RA fibers, is spatially differentiated at a specific spatial scale. The receptive fields of a large proportion of neurons in area 3b – characterized by an excitatory center flanked by one or more inhibitory subfields, separated by 2-4 mm (DiCarlo and Johnson 2000) – carry out precisely the implied computation. Indeed, the spatial variation filter used to predict roughness from afferent responses – the Gabor function – provides an accurate fit for this receptive field structure (Bensmaia et al. 2008). This spatial processing draws a strong analogy with vision: receptive fields in primary visual cortex are also well approximated by Gabor functions (Hubel and Wiesel 1959; Jones and Palmer 1987). The spatial differentiation structure in visual cortex is thought to be an adaptation to natural image statistics (Olshausen and Field 1996) and the same is likely true of its counterpart in somatosensory cortex (Pack and Bensmaia 2015).

In the model, the contribution of fine textural features to perceived roughness is driven primarily in the temporal variation of RA and PC afferents. In support of this hypothesis, a subpopulation of neurons in

area 3b perform a differentiation of their RA and PC input (Saal et al. 2015). That is, the contribution of RA and PC signals to the responses of many cortical neurons are well approximated using differentiating filters that are mathematically equivalent to those used to predict roughness.

Thus, both the spatial and temporal computations implied by the present model of roughness have been inferred from responses of neurons in somatosensory cortex in very different experimental contexts.

CONCLUSION

The perception of roughness is mediated by the three populations of tactile nerve fibers that innervate the glabrous skin of the hand. Perceived roughness is driven not by the strength of the response in these afferents but rather by the variation therein, either spatial (SA1, RA) or temporal (RA, PC). This model of roughness is bolstered by the fact that evidence for the implied variation computation has been observed in primary somatosensory cortex.

REFERENCES

Arabzadeh E, **Clifford CWG**, **Harris JA**, **Mahns DA**, **Macefield VG**, **Birznieks I**. Single tactile afferents outperform human subjects in a vibrotactile intensity discrimination task [Online]. *J Neurophysiol* 112, 2014. http://jn.physiology.org/content/112/10/2382.long [31 Jul. 2017].

Bensmaïa S, **Hollins M**. Pacinian representations of fine surface texture. *Percept Psychophys* 67: 842–854, 2005.

Bensmaia SJ, **Denchev P V**, **Dammann JF**, **Craig JC**, **Hsiao SS**. The representation of stimulus orientation in the early stages of somatosensory processing. *J Neurosci* 28: 776–786, 2008.

Bensmaia SJ, **Leung YY**, **Hsiao SS**, **Johnson KO**. Vibratory adaptation of cutaneous mechanoreceptive afferents. *J Neurophysiol* 94: 3023–3036, 2005.

Blake DT, **Hsiao SS**, **Johnson KO**. Neural coding mechanisms in tactile pattern recognition: the relative contributions of slowly and rapidly adapting mechanoreceptors to perceived roughness. *J Neurosci* 17: 7480–9, 1997.

Cascio CJ, **Sathian K**. Temporal cues contribute to tactile perception of roughness. [Online]. *J Neurosci* 21: 5289–96, 2001. http://www.ncbi.nlm.nih.gov/pubmed/11438604 [18 Nov. 2016].

Connor C, **Hsiao S**, **Phillips J**, **Johnson K**. Tactile roughness: neural codes that account for psychophysical magnitude estimates. *J …* , 1990a.

Connor CE, **Hsiao SS**, **Phillips JR**, **Johnson KO**. Tactile roughness: neural codes that account for psychophysical magnitude estimates. *J Neurosci* 10: 3823–36, 1990b.

Connor CE, **Johnson KO**. Neural coding of tactile texture: comparison of spatial and temporal mechanisms for roughness perception. *J Neurosci* 12: 3414–26, 1992.

Darian-Smith I, **Kenins P**. Innervation density of mechanoreceptive fibres supplying glabrous skin of the monkey's index finger. *J Physiol* 309: 147–155, 1980.

Darian-Smith I, **Oke LE**. Peripheral neural representation of the spatial frequency of a grating moving across the monkey's finger pad. *J Physiol* 309: 117–33, 1980.

Delhaye B, **Hayward V**, **Lefèvre P**, **Thonnard J-L**. Texture-induced vibrations in the forearm during tactile exploration. *Front Behav Neurosci* 6: 37, 2012.

DiCarlo JJ, **Johnson KO**. Spatial and temporal structure of receptive fields in primate somatosensory area 3b: effects of stimulus scanning direction and orientation. *J Neurosci* 20: 495–510, 2000.

Goodman JM, **Bensmaia SJ**. A variation code accounts for the perceived roughness of coarsely textured surfaces. *Sci. Rep.* .

Hollins M, **Bensmaïa S**, **Karlof K**, **Young F**. Individual differences in perceptual space for tactile textures:

evidence from multidimensional scaling. *Percept Psychophys* 62: 1534–1544, 2000.

Hollins M, **Bensmaia SJ**, **Washburn S**. Vibrotactile adaptation impairs discrimination of fine, but not coarse, textures. *Somatosens Mot Res* 18: 253–262, 2001.

Hubel DH, **Wiesel TN**. Receptive fields of single neurones in the cat's striate cortex. *J Physiol* 148: 574, 1959.

Johansson RS, **Flanagan JR**. Coding and use of tactile signals from the fingertips in object manipulation tasks. *Nat Rev Neurosci* 10: 345–359, 2009.

Johansson RS, **Landstrom U**, **Lundstrom R**. Responses of Mechanoreceptive Afferent Units in the Glabrous Skin of the Human Hand to Sinusoidal Skin Displacements. *Brain Res* 244: 17–25, 1982.

Johnson KO, **Phillips JR**. A rotating drum stimulator for scanning embossed patterns and textures across the skin. [Online]. *J Neurosci Methods* 22: 221–31, 1988. http://www.ncbi.nlm.nih.gov/pubmed/3361948 [28 Mar. 2017].

Jones JP, **Palmer LA**. The two-dimensional spatial structure of simple receptive fields in cat striate cortex. *J Neurophysiol* 58: 1187–1211, 1987.

Leung YY, **Bensmaia SJ**, **Hsiao SS**, **Johnson KO**. Time-course of vibratory adaptation and recovery in cutaneous mechanoreceptive afferents. *J Neurophysiol* 94: 3037–3045, 2005.

Manfredi LR, **Baker AT**, **Elias DO**, **Dammann 3rd JF**, **Zielinski MC**, **Polashock VS**, **Bensmaia SJ**. The effect of surface wave propagation on neural responses to vibration in primate glabrous skin. *PLoS One* 7: e31203, 2012.

Miyaoka T, **Mano T**, **Ohka M**. Mechanisms of fine-surface-texture discrimination in human tactile sensation. [Online]. *J Acoust Soc Am* 105: 2485–92, 1999. http://www.ncbi.nlm.nih.gov/pubmed/10212429 [28 Jul. 2017].

Muniak MA, **Ray S**, **Hsiao SS**, **Dammann JF**, **Bensmaia SJ**. The neural coding of stimulus intensity: linking the population response of mechanoreceptive afferents with psychophysical behavior. *J Neurosci* 27: 11687–11699, 2007.

Olshausen BA, **Field DJ**. Emergence of simple-cell receptive field properties by learning a sparse code for natural images. .

Pack CC, **Bensmaia SJ**. Seeing and Feeling Motion: Canonical Computations in Vision and Touch. *PLoS Biol* 13: e1002271, 2015.

Phillips J, **Johnson K**. Tactile spatial resolution. II. Neural representation of bars, edges, and gratings in monkey primary afferents. *J. Neurophysiol.* .

Phillips JR, **Johansson RS**, **Johnson KO**. Representation of braille characters in human nerve fibres. *Exp Brain Res* 81: 589–592, 1990.

Phillips JR, **Johansson RS**, **Johnson KO**. Responses of human mechanoreceptive afferents to embossed

dot arrays scanned across fingerpad skin. *J Neurosci* 12: 827–39, 1992.

Phillips JR, **Johnson KO**, **Hsiao SS**. Spatial pattern representation and transformation in monkey somatosensory cortex. *Proc Natl Acad Sci U S A* 85: 1317–21, 1988.

Saal HP, **Bensmaia SJ**. Touch is a team effort: interplay of submodalities in cutaneous sensibility. *Trends Neurosci* 37: 689–697, 2014.

Saal HP, **Harvey MA**, **Bensmaia SJ**. Rate and timing of cortical responses driven by separate sensory channels. *Elife* 4: 7250–7257, 2015.

Skedung L, **Arvidsson M**, **Chung JY**, **Stafford CM**, **Berglund B**, **Rutland MW**. Feeling small: exploring the tactile perception limits. *Sci Rep* 3: 2617, 2013.

Sutu A, **Meftah E-M**, **Chapman CE**. Physical determinants of the shape of the psychophysical curve relating tactile roughness to raised-dot spacing: implications for neuronal coding of roughness. *J Neurophysiol* 109: 1403–15, 2013.

Talbot WH, **Darian-Smith I**, **Kornhuber HH**, **Mountcastle VB**. The sense of flutter-vibration: comparison of the human capacity with response patterns of mechanoreceptive afferents from the monkey hand. *J Neurophysiol* 31: 301–34, 1968.

Weber AI, **Saal HP**, **Lieber JD**, **Cheng J-W**, **Manfredi LR**, **Dammann JF**, **Bensmaia SJ**. Spatial and temporal codes mediate the tactile perception of natural textures. *Proc Natl Acad Sci U S A* 110: 17107–12, 2013.

Yoshioka T, **Gibb B**, **Dorsch a K**, **Hsiao SS**, **Johnson KO**. Neural coding mechanisms underlying perceived roughness of finely textured surfaces. *J Neurosci* 21: 6905–16, 2001.

Figure 1.1. *Experimental apparatus, sample textures, and roughness judgments.* A| Rotating drum stimulator. B| The surface microstructure (profilometry) of 9 example textures, ordered from smoothest (top left) to roughest (bottom right, across rows, then columns). Fine textures are colored in cyan, coarse textures in grey, and sandpapers in red. C| Perceived roughness for each texture, split by texture group (C: coarse, F: fine, S: sandpaper). Each point represents a single texture. Bars denote mean roughness across the group, and error bars denote standard deviation. Units of roughness are such that the mean roughness of all 55 textures is normalized to 1.

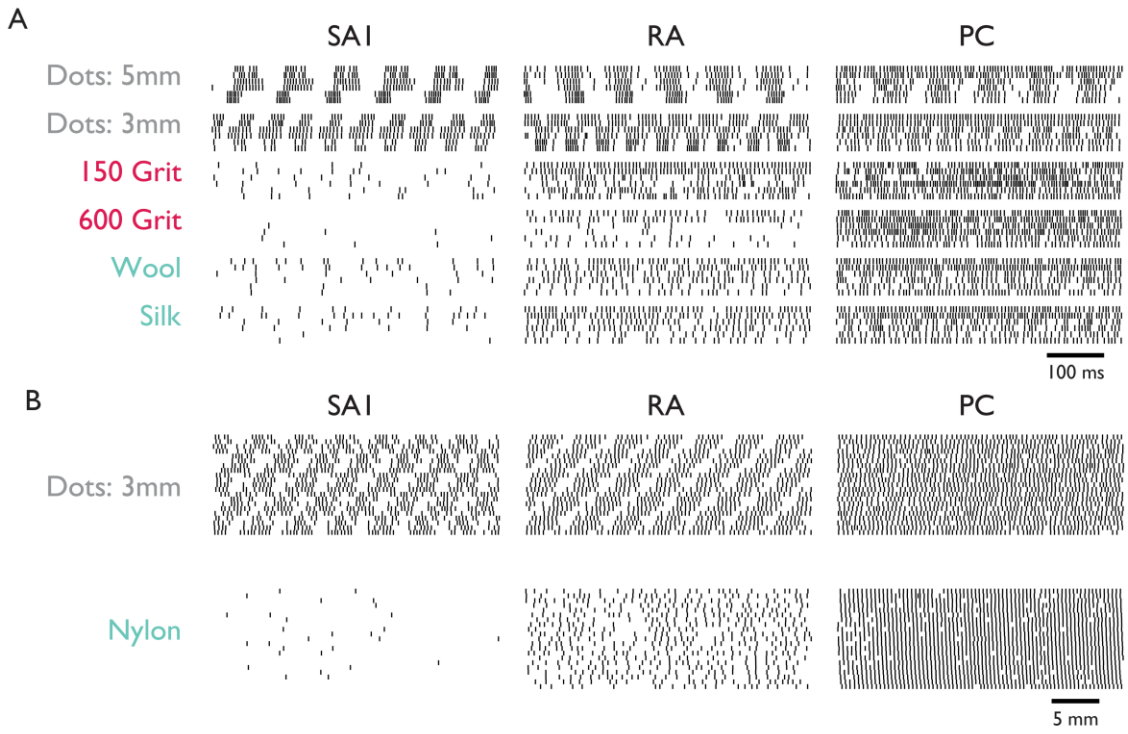

Figure 1.2. *Afferent responses to natural textures*. A| Spiking responses to 6 different textures from SA1, RA, and PC fibers (Responses to two repeated presentations of each texture from 3 example afferents of each type). Textures are ordered from roughest (top) to smoothest (bottom); colors correspond to the texture categories as in Figure 1. B| Spatial event plots for two textures reconstructed from the responses of one afferent of each type (5 mm corresponds to 62.5 ms at 80 mm/s) obtained in a dedicated protocol (see Methods). Each patch consists of repeated parallel scans of the texture across the receptive field of the afferent, each shifted perpendicular to the scanning direction by 0.5 mm, yielding a spatial image (Johnson and Phillips 1988).

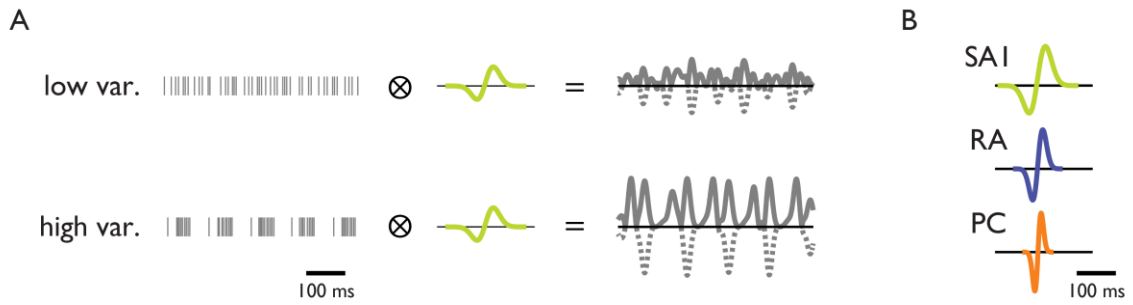

Figure 1.3. *Variation computation and filter shapes.* A| Spikes are binned and convolved with a temporal filter. The output of the filter is then rectified (all negative values [dashed line] are set to their absolute value [solid line]) and averaged to obtain a single variation value. B| Illustration of the variation filters used for SA1, RA and PC spiking data.

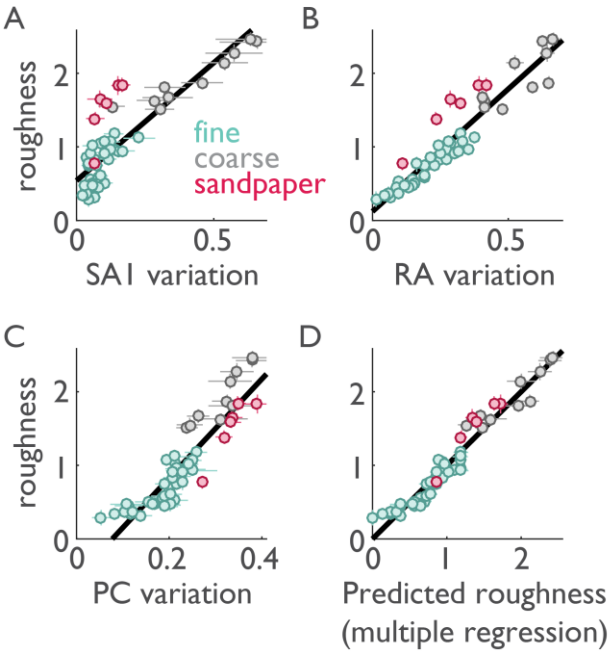

Figure 1.4. *Candidate neural codes for roughness*. A-C| Roughness ratings are plotted against SA1 variation (A, R^2=0.72), RA variation (B, R^2=0.89), and PC variation (C, R^2=0.82). Cyan markers denote fine textures, black markers coarse textures, and red markers sandpapers. Error bars denote standard error of the mean. Lines of best fit are plotted in black. D| Roughness ratings are plotted against the output of a multiple regression model that was fit on the mean variation values from all three afferent types (R^2=0.94, standardized regression weights = 0.11, 0.25 & 0.25 for SA1, RA and PC). Error bars denote standard error of the mean. (Reproduced from Weber et al. 2013).

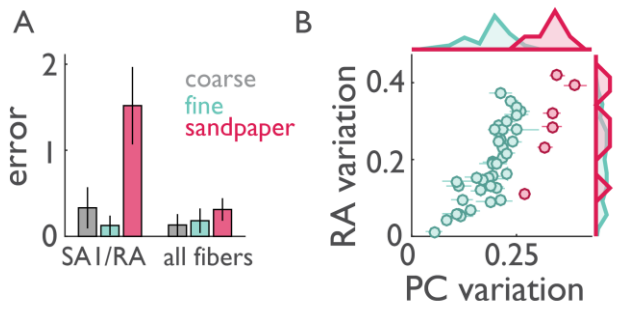

Figure 1.5. *PC contribution to roughness perception – the case of sandpapers*. A| Comparison between two regression models: one using only SA1/RA afferent responses, and one using all three afferent types. Cross-validated errors (leave-one-out procedure, see Methods) are plotted as medians +/- median absolute deviations. With PC variation, model performance significantly improves. B) RA variation vs. PC variation for fine textures and sandpapers. Each point represents the mean response across afferents to a single texture. Error bars denote standard errors. Marginal histograms are plotted on the sides. RA sandpaper responses are very similar to fine texture responses, despite the fact that sandpapers are significantly rougher. PC responses separate sandpapers from fine textures.

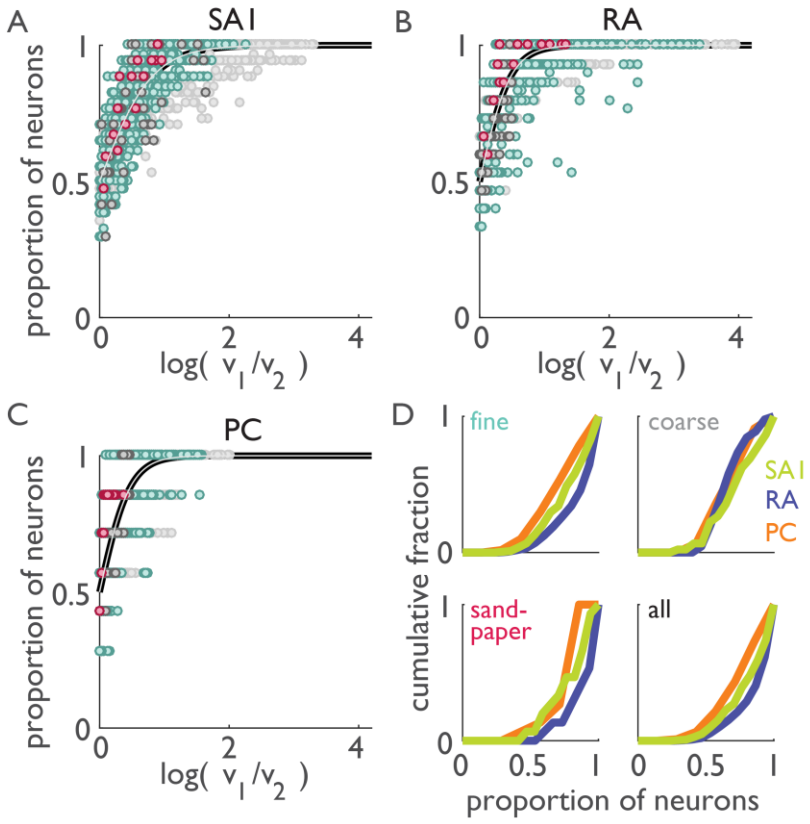

Figure 1.6. *Afferent reliability*. A-C| Across-fiber consistency: For every possible texture pair, the proportion of afferents with a higher mean variation for one texture than another is plotted against the log ratio of variation values (mean across afferents) for those textures. These values are plotted for SA1 (A), RA (B), and PC (C) fibers. Pairs of fine textures are plotted in cyan, coarse textures in black, and sandpapers in red. All other pairs (only mixed pairs, e.g. a sandpaper and a fine texture) are plotted in light grey. The black and grey line denotes the best fit sigmoid (see Methods). D| Cumulative distributions of across-fiber consistency (SA1 afferents in light green, RA afferents in dark blue, PC afferents in orange), for pairs of fine textures (top left), coarse textures (top right), and sandpapers (bottom left). All possible texture pairs are combined in the bottom right.

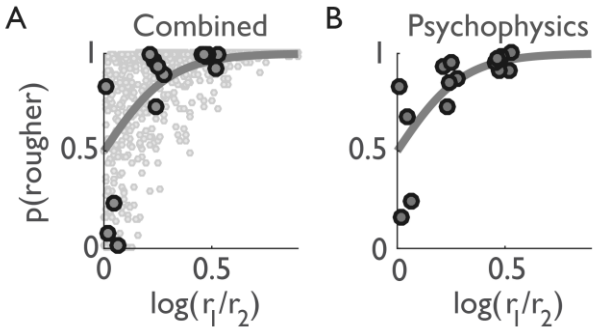

Figure 1.7. *Roughness discrimination*. A| Ideal observer analysis based on the summed (single-trial) variation of five afferents of each type, weighted by type, as a function of the roughness ratio (obtained in the magnitude estimation experiment) for every texture pair. Specifically, for a given pair of textures, r_1 (r_2) is the roughness rating for the rougher (smoother) of the two textures). A subset of these (larger black dots) were used in a roughness discrimination experiment. A best-fit curve is plotted in grey (threshold ratio = 0.15 yielding a Weber fraction = 0.17). Performance values below 50% fall within the margin of error of the mean ratings, highlighting the sensitivity of discrimination relative to magnitude estimation. B| Mean psychophysical performance of 7 human subjects on a roughness discrimination task, for all possible pairs of 6 different textures, plotted against the log ratio of roughness judgements. A best-fit curve is plotted in grey (Weber fraction = 0.17). Performance thresholds are similar for psychophysical and neurometric judgments of texture roughness.

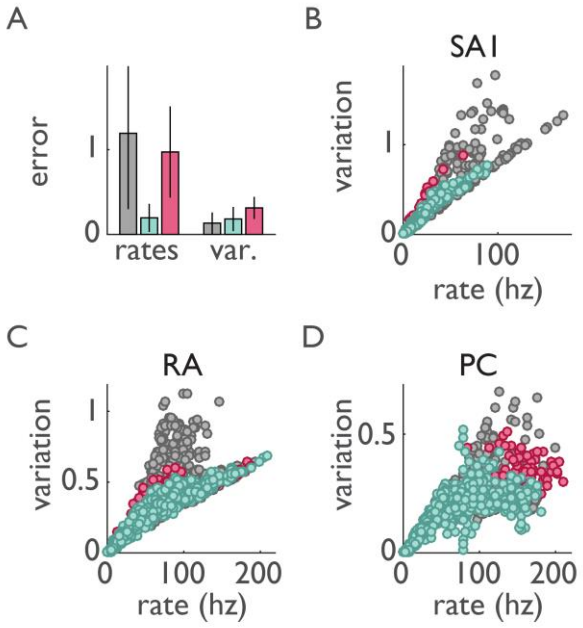

Figure 1.8. *Response rate vs. variation and roughness predictions*. A| Comparison between two models, one using only firing rates from all three afferent types, and one using response variation from all three afferent types. Cross-validated errors (leave-one-out procedure, see methods) are plotted as medians +/- median absolute deviations, and are broken down by texture subtype. The model using variation greatly reduces the error in predicting the roughness of coarse textures and sandpapers. B-D| Variation vs. firing rate for SA1 (A), RA (B), and PC fibers (C). Coarse texture responses exhibit a wider range of variation values for a given firing rate.

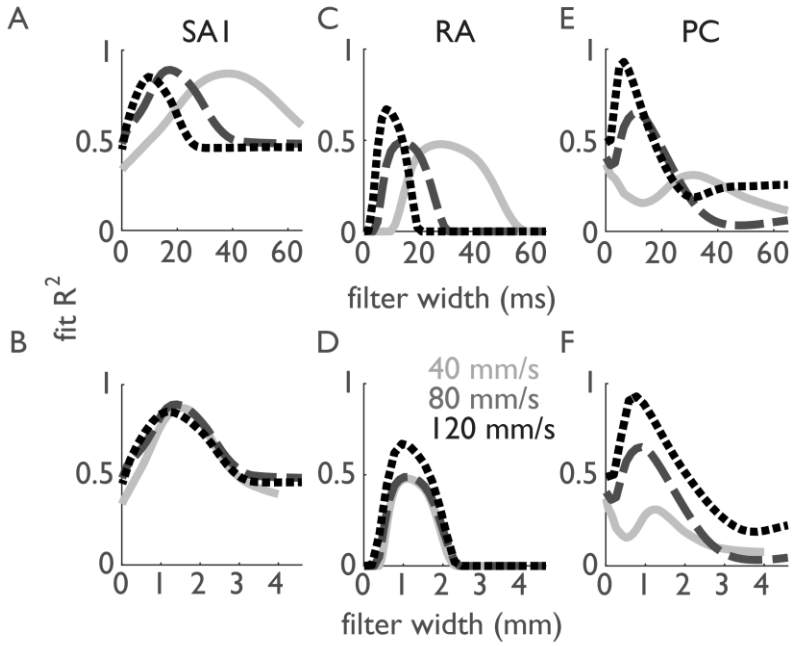

Figure 1.9. *Spatial vs. temporal variation and roughness predictions*. Coefficient of determination between variation and perceived roughness (coarse textures only) for SA1 (A), RA (B), and PC (C) afferents at three different speeds (40 mm/s solid, 80 mm/s long dash, 120 mm/s short dash) plotted against the filter width parameter σ (in ms, see Methods), as the other filter parameter (*p*) is held constant. R^2 values were rectified, such that when the correlation coefficient was negative ($r<0$), R^2 was set to 0. When these functions are plotted in spatial units (mm), the curves peak in the same location, particularly for SA1 and RA fibers, consistent with a spatial variation code for roughness, at least for SA1 and RA fibers.

Vinyl (20 gauge) [0.29, F]	Swimwear lining (polyester/spandex) [0.47, F]	Sparkle Vinyl Black [0.75, F]	Denim (cotton) [0.98, F]	Corrugated paper [1.63, C]
Faux leather (polyester) [0.32, F]	Sueded Cuddle (polyester) [0.47, F]	*Foam drapery tape [0.76, F]	Grating 3 mm (plastic) [1.01, F]	Sandpaper 320 grit [1.65, S]
Premier Velvet (polyester) [0.35, F]	Velvet [0.48, F]	Sandpaper 800 grit [0.77, S]	Stetch demin (cotton/Lycra) [1.04, F]	Embossed dots 2 mm (plastic) [1.67, C]
Grating 1 mm (plastic) [0.35, F]	*Leather, suede [0.50, F]	Designer wool [0.83, F]	*Silk, crinkled [1.07, F]	Grating 8 mm (plastic) [1.81, C]
Velour (polyester) [0.37, F]	Thin corduroy [0.51, F]	Chiffon [0.84, F]	Silk jacquard [1.08, F]	Sandpaper 240 grit [1.83, S]
*Microsuede (polyester) [0.37, F]	Satin [0.52, F]	Nylon (200 denier) [0.85, F]	Upholstery [1.12, F]	*Sandpaper 150 grit [1.84, S]
Stretch velvet [0.38, F]	Taffeta [0.56, F]	Silk, metallic (silk/metal) [0.90, F]	Wool, blend [1.18, F]	Grating 12 mm (plastic) [1.87, C]
Snowflake Fleece Fuzz (polyester) [0.44, F]	Careerwear Flannel (cotton) [0.58, F]	Wool crepe [0.92, F]	*Sandpaper 600 grit [1.39, S]	*Embossed dots 3 mm (plastic) [2.14, C]
Smooth leather [0.45, F]	Blizzard Fleece (polyester) [0.61, F]	Thick corduroy [0.93, F]	Hucktowel (cotton) [1.51, C]	Embossed dots 4 mm (plastic) [2.27, C]
Empire Velveteen (cotton) [0.46, F]	Organza [0.74, F]	Wool/rayon felt [0.94, F]	*Grating 5 mm (plastic) [1.55, C]	Embossed dots 6 mm (plastic) [2.42, C]
Snowflake Fleece Knit (polyester) [0.47, F]	Wool gabardine [0.75, F]	Medium corduroy [0.95, F]	Sandpaper 400 grit [1.58, S]	*Embossed dots 5 mm (plastic) [2.46, C]

Table 1.1. *Texture set.* All 55 textures are shown ordered by perceived roughness, by column then by row. In square brackets, we list the roughness of each texture and whether the textures were grouped as fine [F], coarse [C], or sandpapers [S]. Asterisks denote textures that are shown in Figure 1.1.

CHAPTER 2: HIGH-DIMENSIONAL REPRESENTATION OF TEXTURE IN THE SOMATOSENSORY CORTEX OF PRIMATES

Justin D. Lieber[1] and Sliman J. Bensmaia[2]

[1]Committed on Computational Neuroscience, University of Chicago

[2]Department of Organismal Biology and Anatomy, University of Chicago

The authors declare no competing financial interests.

ACKNOWLEDGEMENTS

We would like to thank Alison Weber and Ju-Wen Cheng for collecting the peripheral neural data, Frank Dammann, Michael Harvey, Erik Schluter and Oksana Lasowsky for assistance in setting up the cortical experiment, and Benoit Delhaye, Katie Long, Hannes Saal, and Jeffrey Yau for comments on a previous version of the manuscript. This work was supported by NINDS RO1 NS101325.

ABSTRACT

In the somatosensory nerves, the tactile perception of texture is driven by spatial and temporal patterns of activation distributed across three populations of afferents. These disparate streams of information must then be integrated centrally to achieve a unified percept of texture. To investigate the representation of texture in somatosensory cortex, we scanned a wide range of natural textures across the fingertips of Rhesus macaques and recorded the responses evoked in Brodmann's areas 3b, 1, and 2. We found that texture identity is reliably encoded in the idiosyncratic responses of populations of cortical neurons, which collectively yield a high dimensional representation of texture. Cortical neurons fall along a continuum in their sensitivity to fine vs. coarse texture, and neurons at the extrema of this continuum seem to receive their major input from different afferent populations. Finally, we show that cortical responses can account for several aspects of texture perception in humans.

INTRODUCTION

Our sense of touch endows us with an exquisite sensitivity to surface microstructure. We can perceive surface features that range in size from tens of nanometers[1] to tens of millimeters and integrate these to form a cohesive textural percept. In the somatosensory nerves, surface features at different spatial scales are encoded in different populations of afferents and rely on different neural representations. Coarse surface features are reflected in the spatial patterns of activation evoked in slowly adapting type-1 (SA1) and rapidly adapting (RA) afferents, whose small receptive fields give rise to a faithful neural image of surface elements measured in millimeters[2,3]. However, many tangible surface features are too fine and too close together to be encoded spatially because the spatial code is limited by the innervation density of the skin. To perceive these textures requires movement between skin and surface, thereby eliciting texture-specific skin vibrations, which are encoded in precisely timed spiking patterns in RA and

Pacinian corpuscle-associated (PC) afferents[4–9]. These spatial and temporal representations must be combined and synthesized to achieve a unified percept of texture, a process about which little is known.

While neurons in somatosensory cortex have been shown to encode information about texture, previous studies investigating cortical texture representations used surfaces with elements in the range of millimeters, such as Braille-like dot patterns[10] and gratings[11–13], which span only a small fraction of the wide range of tangible textures. We have previously shown that responses to such textures – which only engage the spatial mechanism – provide an incomplete view of the neural mechanisms that mediate the perception of texture[8,9].

To fill this gap, we examined how textures that span the tangible range are encoded in the responses of neurons in somatosensory cortex. To this end, we scanned a wide range of textures – including fabrics, furs, and papers, in addition to the traditional embossed dots and gratings – across the fingertips of (awake) Rhesus macaques and recorded the responses evoked in somatosensory cortex, including Brodmann's areas 3b, 1, and 2. First, we found that texture identity is faithfully encoded in somatosensory cortex and that this texture information is distributed across neurons exhibiting idiosyncratic texture responses. Second, we showed that the heterogeneity across somatosensory neurons is in part driven by differences in the submodality composition of their input (SA1, RA, PC). We then found the downstream recipients of the spatial and temporal codes observed at the periphery: a subpopulation of cortical neurons, receiving strong input from SA1 fibers, preferentially encodes coarse textural features whereas another population of neurons receives strong input from PC fibers and encodes fine surface features. Finally, we show that the responses of somatosensory neurons accounts for psychophysical reports of texture obtained from human observers.

RESULTS

We recorded the activity evoked in 141 neurons in somatosensory cortex from three animals (35 from area 3b, 81 from area 1, and 25 from area 2) with receptive fields on the distal fingertip, as each of 59 textured surfaces (Supplementary Table 1) was scanned across the finger using a rotating drum stimulator, which allows for precise control of scanning speed and indentation depth (Figure 2.1A-B). The objective was to determine the degree to which texture information is encoded in cortex, examine the nature of this representation, and assess the degree to which this representation can account for perception.

Texture information in somatosensory cortex

First, we examined the degree to which the responses of individual somatosensory neurons are modulated by texture (Figure 2.1C). We found that nearly every neuron responded to at least one texture (140/141 neurons with $p<0.05$, permutation test with Bonferroni correction), and that each texture significantly modulated the response of at least 20% of the neurons (0.23-0.72-92, min-median-max proportion of textures across cells, permutation test). To test whether these neurons carry texture-specific information, we built a simple linear classifier based on spike counts. Nearly all neurons yielded classification performance that was significantly above chance (mean ± s.d. of performance: 6.7% ±3.7% s.d., chance performance: 1.7%, 95% of neurons > chance), and the proportions of neurons that yielded better than chance performance were distributed similarly across areas 3b, 1 and 2 (97%, 96% and 88%, respectively, Supplementary Figure 2.S1A).

Next, we examined the degree to which texture identity is encoded in the responses of populations of somatosensory neurons (Figure 2.2A). To this end, we implemented our texture classifier using the responses of groups of neurons of varying size. We found that high classification performance could be achieved with a small population of somatosensory neurons (as few as 66 neurons yielded 97%

performance) and that the full population yields nearly perfect performance (Figure 2.2B). Classification performance was largely comparable across cortical modules (an average of 73%, 72%, 62%, for groups of 25 neurons in areas 3b, 1, 2, respectively, see Supplementary Figure 2.S1B). In summary, small populations of somatosensory neurons convey sufficient information to support texture identification for our large texture set.

Dimensionality of texture representation

Two factors drive the ability of neural populations to classify stimuli more accurately than do individual cells. First, as more neurons are included, the trial-to-trial variation in response is averaged out. Second, including more neurons can potentially increase the effective dimensionality of the representation if different neurons have different response properties. That is, insofar as different neurons respond to different aspects of a surface, these idiosyncratic responses will provide information beyond that available from simply averaging responses across cells. With this in mind, we sought to characterize whether the heterogeneity in texture responses across neurons provides texture-specific information beyond that found in the mean population response. We found that the population response collapsed onto a single dimension – the mean response – yielded 23% classification performance. In contrast, if the response of each neuron was taken as an independent dimension, the resulting representation yielded 99.4% classification performance. In fact, classification performance was robust even without the shared response signal. That is, if we removed this signal from individual cell responses by computing, for each neuron, the residuals of the regression of its responses with the population mean, as few as 66 cells achieved 92% accuracy and 112 cells achieved 97% (Supplementary Figure 2.S2). In other words, the heterogeneity of neural responses to texture is a major contributor to the texture signal in cortex.

We can further examine the dimensionality of texture responses – the degree to which somatosensory neurons respond heterogeneously to texture – by performing a principal components analysis (PCA). We find that much of the variance in neuronal responses is explained by the first principal component (Figure 2.3A) (65% proportion of variance explained from the 1st component, essentially the mean population firing rate), a signal that is strongly preserved across all three cortical areas (with inter-correlations across areas > 0.95, see Supplementary Figure 2.S3). Thus, while the heterogeneity of neuronal responses is critical to conveying information about individual textures, much of the variance in neuronal responses can be collapsed onto a single dimension. As discussed below, this prominent neuronal dimension has a clear perceptual correlate.

Next, we sought to examine the dimensionality of texture representations in terms of informativeness about texture identity rather than response variance. To this end, we measured dimensionality using a recently developed method that examines the degree to which dimensionality contributes to stimulus encoding (cf. Rigotti et al., 2013). Specifically, we trained a series of binary linear classifiers on the full cortical population response, and examined how classifier performance varied for different groups of textures (see Methods). The idea is that the dimensionality of a neuronal representation is reflected in the number of ways a stimulus space can be linearly split into two categories. We found that the cortical population could consistently classify arbitrary groupings of up to 22 textures, which suggests that the population response in somatosensory cortex is at least 21-dimensional, and likely larger. Indeed, our classifier-based estimate of dimensionality is not only capped by the dimensionality of the neuronal representation, but also by the size of the stimulus set and of the recorded neuronal population. We find that the dimensionality is still rapidly increasing as a function of neural group size for 141 cells (Figure 2.3C), so more neurons would likely yield a higher dimensional representation given our texture set[15]. In conclusion, populations of somatosensory neurons carry a high-dimensional representation of texture, which enables reliable encoding of texture identity.

Peripheral contribution to texture response heterogeneity

Next, we examined the degree to which the cortical response inherits its structure from the periphery, where texture signals are carried by three classes of low-threshold tactile nerve fibers. To this end, we leveraged previously obtained recordings of afferent responses (from 17 SA1, 15 RA, and 7 PC fibers) to a subset of 24 textures also used in the present study[8]. We then evaluated, using multiple regression, the extent to which the firing rates of SA1, RA and PC afferents evoked by these common textures could account for the firing rates of individual cortical cells. First, we found that the dominant afferent input differed between neurons (44.7%, 37.6% and 17.7% of neurons showed max input from SA1, RA, and PC afferents, respectively). Second, the responses of individual somatosensory neurons reflected submodality convergence as reflected by the fact that many cortical neurons were better explained by a combination of multiple afferents than they were by any single afferent (F-test: 28% with $p < 0.05$). Because this test has low statistical power given the small number of common stimuli, we also examined the adaptation properties of cortical neurons (that is, the dynamics of their responses to trapezoidal skin indentation[16]). We found that many neurons (69%) showed both significant responses during the sustained portion of the indentation, indicative of SA1 input, as well as significant responses upon the removal of the probe, indicative of RA or PC input (Supplementary Figure 2.S4). Overall, 80% of neurons displayed submodality convergence by one or both of these measures. Thus, even at the single-neuron level, the texture representation in somatosensory cortex is built from signals integrated across tactile submodalities.

We also examined what aspects of the high-dimensional cortical of texture in somatosensory cortex were inherited from structure in its peripheral inputs. To this end, we recalculated our PCA on both the peripheral and cortical population responses to their shared set of textures. We found the first principal axis in cortex to be highly correlated with its peripheral counterpart (r = 0.93). The second principal axis in cortex was correlated with its counterpart in the periphery, and separated neurons with strong SA1

input (and, to a lesser extent, RA input) from those with strong PC input. Indeed, the correlation between the second principal axis in cortex and SA1, RA, and PC regression coefficient was -0.43, -0.16, 0.76, respectively. Furthermore, neurons that receive strong PC input tended to produce texture responses that were correlated with each other but uncorrelated with the responses of neurons driven primarily by SA1 or RA responses (Figure 2.4), reflecting the stark difference in response properties of these two sources of input. Interestingly, the most strongly PC-like cells were predominantly located in area 1 (10/12 of cells with normalized PC weight > 0.8, the other two in area 2, see Supplementary Figure 2.5). Thus, the second dimension of variance in the cortical response has, at one extreme, SA1-like neurons and, at the other extreme, PC-like ones. Two other pairs of principal components in periphery and cortex were also correlated (3 & 3, 4 & 5), but their meaning is unclear, and no relationship was observed in any combination of the remaining PCs. Thus, the first few principal axes of the texture representation in cortex are inherited from the periphery but much of the structure in the cortical representation cannot be explained straightforwardly from the relative strengths of SA1, RA, and PC input.

Coding of texture at different spatial scales

At the periphery, texture-specific surface features are encoded through multiple mechanisms. Coarse surface features – measured in millimeters – are encoded in the spatial pattern of activation across of SA1 fibers[17] (and perhaps RA fibers as well[9]). In contrast, fine surface features – typically measured in the tens or hundreds of microns – elicit characteristic vibrations in the skin during texture scanning[18]. These vibrations (and by extension, textural features) are encoded in precisely timed, texture-specific temporal patterns in RA and PC fibers[8]. Next, then, we sought to examine how these peripheral codes for texture were reflected in cortical responses to texture.

First, we tested the hypothesis that a subpopulation of somatosensory neurons act as *spatial* filters, well suited to extract information about *coarse* textural features, as has been previously proposed [19,20]. We also wished to assess the spatial scale over which such a mechanism might operate. To this end, we first characterized the spatial receptive fields of somatosensory neurons using well-established techniques (Supplementary Figure 2.S6A-B). Using this approach, neurons have been shown to encode spatial features with excitatory subfields flanked by inhibitory ones[10], analogous to simple cells in primary visual cortex[21]. Consistent with previous reports, the measured receptive fields exhibited well defined excitatory subfields (average 12.7 mm^2, range 3.1-37.4 mm^2) and inhibitory subfields (average 12.8 mm^2, range 0-42.6 mm^2) (Supplementary Figure 2.S6C). Inhibitory subfields tend to lag behind excitatory subfields in the scanning direction (93% (62/67), average 2.5 mm lag) (Supplementary Figure 2.S6D). Importantly, the spatial period of the subfield – that is, the distance between excitatory and inhibitory subfields – spanned a range between 2 and 4 mm (Supplementary Figure 2.S7E). Thus, the spatial structure of cortical receptive fields is well suited to extract information about coarse features, but not fine ones. Note that this receptive field structure is ideally suited to compute the spatial derivative of the neural image, which has been shown to drive perceived roughness[9,17]. Interestingly, while PC fibers have substantially larger receptive fields than do SA1 or RA fibers, this tendency was not reflected in cortex. Indeed, PC-like somatosensory neurons did not have larger receptive fields than did SA1- or RA-like ones (excitatory subfield size: average 12.1 mm^2, inhibitory subfield size: average 13.1 mm^2, average 2.3 mm lag at 80 mm/s, see Supplementary Figure 2.S6).

Next, we examined the cortical manifestation of the *temporal* code for *fine* textural features carried at the periphery by RA and PC fibers. A characteristic feature of PC (and to some extent RA) responses to texture is the elicitation of high-frequency spiking patterns (> 50 Hz) that are highly informative about texture identity as they reflect the succession of fine textural features moving across their receptive fields[8]. To explore the presence of such timing signals in the responses of somatosensory neurons, we

designed two finely textured 3D patterns – gratings with spatial periods of 0.5 and 1 mm – to elicit skin vibrations at 160 and 80 Hz, respectively (given a scanning speed of 80 mm/s). We anticipated that these highly periodic components would be readily identifiable in the cortical responses, and might potential encode fine textural features. We found that a subpopulation of somatosensory neurons produced phase-locked responses to these and other fine textures (Supplementary Figure 2.S8) with periodic components, providing a strong analog to the temporal code observed at the periphery. As expected, phase-locked responses were stronger among somatosensory neurons with PC-like responses than among their SA1-like counterparts (Figure 2.5A-B). Indeed, while the spiking patterns of both sets of neurons consistently reflected the periodic structure of coarse features, PC-like responses much more reliably reflected the periodic structure of fine features, even if these were embedded among coarse features. Neurons with PC input are thus well suited to convey information about fine textural features.

In light of these observations, we wished to assess the respective abilities of these two subpopulations of neurons – SA1-like and PC-like – to convey information about fine and coarse features. To this end, we examined the responses of these two neuronal populations to 3D-printed surfaces (Supplementary Figure 2.S9) in which coarse and fine features were parametrically combined (Figure 2.5A). We found that SA1-like neurons responded significantly more strongly to textures with coarse features than without, exhibiting only weak firing rate modulation to the presence of fine features (20.7 vs. 2.40 spikes/s for coarse vs. fine, respectively, $p < 0.001$, paired t-test). Conversely, PC-like neurons responded more strongly to textures with fine features than to those without, and their rates were nearly independent of the presence or absence of coarse features (2.0 vs. 15.9 spikes/s, $p<0.01$). Accordingly, SA1-like neurons were significantly better at discriminating coarse features – independent of the fine features – than were their PC-like counterparts ($p<0.05$, permutation test), and PC-like neurons were significantly better at discriminating fine features – independently of the coarse features – than were

SA1-like neurons ($p<10^{-4}$, permutation test) (Figure 2.5C). In conclusion, then, different subpopulations of somatosensory neurons preferentially encode textural features at different spatial scales.

The cortical basis of tactile texture perception

Next, we examined how these different populations of neurons might account for the perception of texture, an important step in establishing a neural code[17,22,23]. To this end, we first investigated whether the responses of neurons in somatosensory cortex could account for judgments of roughness obtained from human subjects. We found that the firing rates of most somatosensory neurons (92%) were significantly positively correlated with roughness judgments (r = 0.59 ± 0.27, mean + std dev for individual cells, 130/141 cells with significantly positive correlation at $p<0.05$, permutation test) and that the first principal component of the population response was a good predictor of roughness (Figure 2.6A, r = 0.88), a consistent effect across all three cortical areas (all $r>0.85$, Supplementary Figure 2.S10).

As the sensory space of texture comprises many dimensions[24], we next examined the degree to which neuronal responses could account for dissimilarity judgments of texture, which reflect sensory aspects beyond roughness. For this analysis, we determined the degree to which judgments of dissimilarity mirrored differences in the evoked neuronal responses. We carried out this analysis on data obtained from two sets of texture pairs: one in which textures differed in their coarse spatial features (Coarse Group: 3 fabrics and 2 dot patterns, yielding 10 pairs) and one that comprised textures mostly lacking coarse spatial features (Fine Group: 13 fabrics, 78 pairs). First, we examined the ability of afferent responses to predict perceived dissimilarity. We found that SA1 responses best accounted for the dissimilarity of textures with different coarse spatial features (Coarse Group: correlation between firing rates and perceived dissimilarity = 0.78, 0.41, 0.17 for groups of 7 SA1, RA, and PC fibers, respectively), and PC responses best accounted for the perceived dissimilarity of finely textured fabrics (Fine Group: r = 0.37, 0.39, 0.56 for groups of 7 SA1, RA, and PC fibers). When we carried out the same analysis based

on cortical responses, we found that SA1-like neurons best accounted for the perceived dissimilarity of Coarse Group pairs (r = 0.70, 0.24, 0.26 for groups of 7 SA1-like, RA-like, and PC-like neurons, respectively) and PC-like neurons best accounted for that of Fine Group pairs (r = 0.31, 0.26, 0.67 for groups of 7 SA1-like, RA-like, and PC-like neurons, respectively). Results from this analysis further supports the hypothesis that different subpopulations of neurons encode textures at different spatial scales: SA1-like neurons are specialists for coarse textural features and PC-like neurons are specialists for fine ones.

DISCUSSION

While texture responses in cortex are dominated by a common signal that encodes roughness, the heterogeneity of responses across individual somatosensory neurons carries considerable information about texture identity. One identifiable way in which neurons differ is in the degree to which their responses reflect SA1 afferent input vs. PC afferent input, a continuum rather than a dichotomy as evidenced by the continuous distribution of regression coefficients (Figure 2.4A). However, cortical responses to texture are more complex than just a linear combination of afferent responses. While we find four shared dimensions between the peripheral and cortical representations of texture, our binary classification analysis shows that the effective number of dimensions is much larger than just four (Figure 2.3B).

The increase in dimensionality can be accounted for, at least in part, by well-documented cortical transformations of peripheral input. Indeed, individual cortical neurons receive convergent input from different combinations of afferent types and each neuron acts as a spatial[10,25] and/or temporal[26] filter, the shape of which is specific to that neuron. The relative contribution of RA and PC input and the way these signals are integrated also differs from neuron to neuron. While these spatial and temporal filters are often estimated using linear models, this integration of peripheral input is subject to the nonlinear

motifs of neural processing, including thresholds[10,26,27], synaptic depression[27–29], and divisive normalization[30–33]. Each cortical neuron, then, preferentially encodes a particular set of spatial and/or temporal features in the texture-induced skin deformation, and the associated non-linear transformations result in a high dimensional representation of texture.

The multidimensional nature of the texture representation in somatosensory cortex, broadly analogous to that found in visual representations of shape for example[34–36], reflects the complexity of the sensory space of textures. While some of this space can be described by a small number of commonly identified sensory dimensions – roughness, hardness, stickiness, and warmth[24] –, much of it cannot. That is, the roughness, hardness, stickiness, and warmth of a texture defines it only partially. Many adjectives to describe texture – fuzzy, bumpy, silky, to name just a few – evoke additional textural features not captured in low-dimensional descriptions. This rich sensory space arises from a complex neural space.

As described above, somatosensory neurons fall along a continuum – captured in the second principal component of their responses – that seems to be determined by their peripheral inputs. The position of a neuron along this axis relates to the spatial scale of the textures it is best suited to encode. At one end of the continuum, SA1-like neurons encode coarse textural elements; at the other end, PC-like neurons encode fine features. This differential spatial sensitivity is reflected in the ability of neurons to convey information about texture: SA1-like responses best distinguish textures with different coarse features while PC-like responses best distinguish textures with different fine features. These differences are also reflected in the ability of neuronal populations to predict perceptual judgments of texture: SA1-like neurons account for the perception of coarse features; PC-like neurons account for the perception of fine features.

In the peripheral nerve, coarse and fine textures are encoded through two mechanisms, a spatial code and a temporal one, respectively. Somatosensory neurons are well suited to extract coarse textural

features measured in millimeters as evidenced by the spatial dimensions of their receptive fields (Supplementary Figure 2.S5)[10,21]. As discussed above, the idiosyncratic receptive field structure of individual neurons (Supplementary Figure 2.S5B, Supplementary Figure 2.S6) confers to them idiosyncratic preferences for coarse textural features and likely drives, in part, the heterogeneity of texture responses. Furthermore, the computation that such receptive fields imply – of spatial variation – has been shown to drive perceived roughness. Thus, while spatial variation in afferent responses predicts roughness judgments[8,9,22,37], cortical firing rates predict roughness judgments because they reflect the output of this differentiation computation.

At the periphery, however, the spatial mechanism cannot account for the perception of fine features due to limitations of the skin to transmit those features to the receptors[2,38,39] and limitations set by the cutaneous innervation density [40]. At submillimeter scales, RA and particularly PC afferents have been shown to encode texture in precise temporal spiking patterns evoked when a finely textured surface slides across the skin[8]. While these temporal patterns are inherited by the PC-like neurons in somatosensory cortex (Figure 2.5A), their role in texture coding remains to be elucidated. Indeed, textures in our set can be classified accurately based on cortical firing rates, without taking into account the precise spike timing. One possibility is that the texture information conveyed by spike timing in cortex is redundant with the texture information conveyed by the rates. Consistent with this view, somatosensory neurons have been shown to implement temporal variation computations[26], which confer to them a sensitivity to the temporal properties of the response. The form of these computations can widely vary from neuron to neuron, and this documented heterogeneity likely also contributes to the observed heterogeneity in texture responses. This transformation allows for the possibility, in principle, that all the relevant texture information in spike timing has been converted to a rate code in cortex.

We have previously shown that frequency perception relies on the spike patterning of somatosensory responses[41]. These divergent findings for vibration and texture can be reconciled by a model where temporal patterning in somatosensory cortex encodes information about the skin's behavior, e.g. the frequency of skin vibrations[18], divorced of any ethological meaning. Texture perception involves the identification of spatio-temporal patterns of skin deformations produced by a meaningful stimulus, a textured surface. In this case, the relevant patterns are encoded in the rates even though the skin-related signal is still present in the temporal patterning and is perceptually available independently of the texture. Alternatively, this timing signal may be informative for some textures, but redundant with the rate signal in our specific texture set. To establish the role of temporal signals in cortical representations of texture will require the construction of finely textured surfaces designed to draw out this temporal component.

METHODS

Experimental methods

Behavioral training

Before the beginning of recording sessions, all animals were trained to sit in a primate chair with their heads fixed and arms restrained as they were habituated to the experimental apparatus. During the task, the arm was stabilized in a supinated position with a custom-built cast (Polycaprolactone, lined on the interior with foam padding for comfort). The animal was trained to keep its hand still for the duration of the recording protocols, and a protocol was restarted from the beginning if the finger moved. Stability was further maintained by loosely taping the non-stimulated fingers down, and applying a small amount of glue to the fingernail of the stimulated finger to keep it in stable contact with the hand holder.

To maintain alertness during recording, the animals performed a simple visual brightness discrimination task [41]. Briefly, the animals fixated on a small square presented in the center of a monitor located in front of the tactile stimulator. After approximately 1-2s of fixation, two circles of different luminance appeared to the left and right of the fixation point. The animal was given a liquid reward (juice or water, depending on the animal's preference) for making a saccade to the brighter target. The task was kept sufficiently challenging by adjusting the relative luminance of the targets and the fixation time. Eye movements were tracked using Arrington Research Eye Tracker (ViewPoint PC-60, Arrington Research) and visual stimuli were presented using in-house software based on the OpenGL library.

Surgery

Procedures were approved by the University of Chicago Institutional Animal Care and Use Committee. First, a custom-built head-post was secured to the skull and allowed to osseointegrate for 1.5 months before fixing the head. Once the animals were sufficiently habituated to the test apparatus and visual task, a recording chamber (22 mm internal diameter) was attached to the skull using bone cement such that it circumscribed the hand representation in somatosensory cortex, and a craniotomy was made over the internal diameter of the chamber. All surgical procedures were performed under sterile conditions; anesthesia was induced with ketamine and dexmedatomadine, and maintained with a surgical plane of isofluorane and occasional redosing of dexmedatomadine[42]. Post-surgery, anesthesia was reversed with atipamezole.

Neurophysiological procedures

Extracellular recordings were made in the postcentral gyri of three hemispheres of three macaque monkeys (all male, 6-8 yrs old, 8-11 kg) using previously described techniques[41]. On each recording day, a multielectrode microdrive (NAN Instruments) was loaded with three electrodes (tungsten, Epoxylite insulated, FHC Inc.) and electrodes were lowered normal to the cortical surface, through a custom-

designed 3D-printed guide tube system that arranged the electrodes in a line 650 microns apart tip-to-tip. The electrodes were then driven into the cortex until they encountered neurons from areas 3b, 1, and 2 of somatosensory cortex with RFs on the distal fingerpad.

The transition from area 1 to area 3b exhibits a characteristic progression of RF locations. As one descends from the cortical surface through area 1 into area 3b near the central sulcus, the RFs progress from the medial and proximal finger pads to the palmar whorls. As one enters area 3b, RFs proceed back up the finger, transitioning from proximal, to medial, and ultimately to distal pads. Because responses from the distal pad were never encountered in the more superficial regions of 3b (where the palmar whorls or proximal pad typically were most responsive), there was never any uncertainty about the anatomical area from which area 3b recordings originated. The representation of the digits in area 2 lies just caudal to, and mirrors that of area 1. Thus, as one proceeds caudally, one first encounters the proximal, then medial, then distal pads. As one enters area 2, RFs remain on the distal pads and then proceed down the finger as one further proceeds caudally. The most salient feature identifying area 2 is the presence of neurons with proprioceptive response properties; that is, neurons that respond preferentially to movements of the joints. Because the distal finger pad representations in areas 1 and 2 are adjacent, we used the presence of proprioceptive responses to inform the areal classification.

We recorded from neurons whose RFs were located on the distal pads of digits 2–5. On roughly every second day of recording, the electrode array was shifted 200 mm along the postcentral gyrus until the entire representation of digits 2–5 had been covered. At the end of the recording day, the electrodes were withdrawn and the chamber was filled with sterile saline and sealed. Recordings were obtained from neurons in areas 3b, 1, and 2 that met the following criteria: (1) action potentials were well isolated from the background noise, (2) the RF included at least one of the distal finger pads on digits 2-5, (3) the finger could be positioned such that the textured surface impinged on the center of the RF, and (4) the neuron was clearly driven by light cutaneous touch. Isolations had to be maintained for at

least 30 minutes to complete 5 repetitions of the basic texture protocol. When held for longer, additional protocols were run (see below).

Stimulus presentation

Textured surfaces were presented to the fingertips of awake macaque monkeys using a custom-built rotating drum stimulator like those used in previous studies [8,43], but larger and more precise. The drum was attached to a rotation motor (Animatics SmartMotor SM23165D) via a 1:100 gearbox (Animatics), which provided precise control of rotational position (± 200 µm) and velocity (± 1.1 mm/s). The motor was attached to a vertical stage (Newport IMS100V), which could achieve depths over a range of 4 cm at a precision of 2 microns. The vertical stage was attached to another horizontal stage (Newport IMS400CCHA) allowing smooth displacement over 40 cm at a precision of 4 microns. Thus, we achieved precise horizontal, vertical, and rotational positioning of textures, allowing 60 different slots (12 rows, 5 textures per row) in which texture strips (2.5 cm wide by 16 cm long) could be mounted to the drum (25.5 cm in diameter and 30 cm in length). The inter-stimulus interval was at least 3 s between stimulus presentations, to allow the drum to reposition and to prevent neural adaptation.

One of the available slots was dedicated to a small load cell placed on the surface of the drum (Futek LSB200 2 lb, 1-axis, parallel to indentation), whose function was to ensure a consistent level of pressure was exerted on the finger across recording sessions. Each day, after the animal's hand and finger were stabilized in place, the drum was rotated and translated such that the load cell was pressed lightly (to a force of 15 ± 3 g) into the animal's fingertip. This position was used as a reference point for all protocols, to ensure that stimulation was consistent across days and across fingers.

Stimuli

Texture samples were mounted on individual strips of magnetic tape (5 x 16 cm), which were then attached to a complementary sheet of magnetic tape fixed to the surface of the drum. This allowed for

simple removal and replacement when textures became mechanically damaged or worn through use. In total, 59 different textures were mounted on the drum, including a wide array of natural textures such as papers, fabrics, furs, and upholsteries with coarse periodic structure, as well as tetragonal arrays of embossed dots [22], and 3D-printed gratings and dots. 24 of these textures were also used in a previous experiment on peripheral afferents [8] (see Supplementary Table 1).

Textures were presented at a speed of 80 mm/s and at a force of 15 g. To find the displacement equivalent to this desired force, a set of calibration readings were taken offline using a 2nd load cell mounted at the location of the hand. First, a standard reference point was found by indenting the drum-mounted load cell into the 2nd load cell, to a force of 15 g. Then, individual textures were repeatedly indented into the 2nd load cell to find the displacement (relative to the calibration point) necessary to achieve the calibration force (15 g). Finally, during recording, we scanned our textures over the finger according to these standard displacements relative to the reference point, measured daily.

Adaptation protocol

One way to assess the submodality composition of a neuron is to measure its response to a skin indentation. Indeed, SA1 fibers are the only ones to respond during the sustained portion of the indentation whereas RA and PC fibers are the only ones to respond during the offset of the indentation. To the extent that a cortical neuron exhibits both of these properties, we can infer that it receives convergent input from multiple classes of tactile fibers. With this in mind, we measured the response of cortical neurons to a probe indented into the skin. Specifically, we indented the drum-mounted load cell (a cylinder of diameter 7 mm, see above) vertically into the skin to the 15 g reference point, and held the indentation for 500 ms, before removing it from the skin (5 mm/s indentation/removal speed). This indentation was repeated 60 times, with an inter-trial interval of 500 ms. We completed this protocol for 94 neurons (28, 57, and 9 from areas 3b, 1, and 2, respectively).

Spatial receptive fields

In order to systematically measure the spatial receptive field of individual cortical neurons, we designed a 3D-printed random dot array following a previously described approach [10] (truncated cones: 0.5 mm dot height, 1 mm base diameter, 0.5 mm top diameter, 10 dots/cm^2, dots uniformly distributed, 5 cm x 16 cm). The random dot pattern was scanned over the skin 100 times but, after each scan, the drum was stepped 400 microns along its axis of rotation. A full uninterrupted protocol was completed (~10 minutes), for 72 neurons (27, 37, and 8 from areas 3b, 1, and 2, respectively).

Peripheral recordings

We have previously reported the responses of 15 SA1 fibers, 13 RA fibers, and 7 PC fibers to 55 different texture stimuli (see ref. [8] for details). Briefly, we collected extracellular single-unit recordings from the median and ulnar nerves of six anesthetized (isoflurane) Rhesus macaques as texture stimuli were presented to the distal digits of the hand at a speed of 80 mm/s. Each texture was presented to each fiber at least twice.

Magnitude estimation

All procedures were approved by the Institutional Review Board of the University of Chicago and all subjects provided informed consent. Subjects sat with the right arm supinated and resting on a support under the drum. Stimuli were presented to the right index fingerpad of each subject.

Roughness scaling (6 subjects, 5m, 1f, ages 18-24): On each trial, the subject was presented with one of 59 textures (80 mm/s, 25 ± 10 g) and produced a rating proportional to its perceived roughness, where a rating of zero denoted a perfectly smooth surface. If texture B was perceived to be twice as rough as texture A, texture B was ascribed a number that was twice as large as texture A. Subjects were encouraged to use fractions and decimals if necessary. Each texture was presented once in each of 6

experimental blocks; ratings were normalized by the mean of each block and averaged, first within then across subjects. Ratings of roughness were consistent across subjects (subject correlation to the mean: r=0.87 ± 0.079, mean ± std. dev.).

Dissimilarity scaling (10 subjects, 10f, ages 19-24): In these experiments, two subsets of textures were used. The first comprised 5 textures (Group A: silk, microsuede, upholstery, 4 mm embossed dots, 5 mm embossed dots), and the second 13 textures (Group B: suede, chiffon, nylon (200 denier), denim, hucktowel, silk, microsuede, wool, satin, metallic silk, upholstery, thin corduroy, thick corduroy). On each trial, the subject was presented with a pair of textures (for 1 s each, separated by a 1 s inter-stimulus interval, 78 unique comparisons, 80 mm/s, 25 ± 10 g) and produced a rating proportional to the perceived dissimilarity of the pair, where 0 denotes (perceived) identicalness. Each pair of textures was presented 3 times in pseudorandom order. Texture dissimilarity ratings were correlated across subjects (subject correlation to the mean, Group A: r=0.88 +/- 0.10, Group B: 0.65 ± 0.12, mean ± std. dev.).

Analysis

Basic analyses of firing rate

Because the stimulus epoch over which a texture was moved into the skin evoked a large phasic response that lasted about 200 ms, we excluded this response from our analysis. For each trial, the baseline firing rate was measured in the 500-ms period before drum's initial contact with the skin.

To test whether textures responses were significantly above baseline firing rates, we first created a distribution of baseline responses for each cell. We then measured how often each cell's texture firing rate response (averaged across 5 repetitions) was greater than the average of 5 random draws from the baseline distribution. We set significance at $p<0.05$ for all textures, Bonferroni corrected for 8319 comparisons (141x59).

For data from the indented probe protocol, we measured the trial-by-trial firing rate over stimulus epochs: 1) background activity, measured between 1 s and 500 ms before the probe was indented into the skin, 2) sustained response activity, measured during the 500 ms hold period, and 3) offset response activity, measured between 100 and 300 ms after the probe started lifting off the skin. We report that a neuron has a significant sustained/offset response if its texture elicited firing rate was significantly different from baseline (two-sided t-test for sustained/offset-baseline, significant if $p<0.05$). To quantify the relative magnitude of the sustained and offset responses, we calculated the fraction of the combined sustained and offset responses that was carried by the offset response:

$$f_o = \frac{|r_o - r_b|}{|r_o - r_b| + |r_s - r_b|}$$

where r_o is the firing rate at the offset, r_s is the firing rate during the sustained phase, and r_b is the baseline firing rate.

Texture classification

To assess the degree to which neuronal responses carry information about texture identity, we assessed the degree to which we could classify textures based on the neuronal responses they evoke. To this end, we implemented a nearest neighbor classifier. First, for each neuron, we averaged 4 of the 5 available repetitions of each texture presentation, leaving 1 repetition out, yielding 59 vectors of mean responses and 59 vectors of single-trial responses. Next, we computed the distance between each single-trial response and each mean response. For each single trial response, the mean response yielding the lowest distance was selected. If the selected mean responses and the single trial responses corresponded to the same texture, classification was correct. Performance was averaged across all textures, and then again across 25 shuffles of which repetitions were left out. This procedure was repeated for neuron groups of different sizes.

We wished to examine how well the cortical population could classify texture with the mean intensity signal removed. First, we calculated each texture's mean firing rate response across the full neural population. Then, we used regression to predict each individual cell's texture responses from the population texture responses. Thus, for every cell, we had a "best fit" firing rate for each texture based on the population firing rate response. Finally, we subtracted these best fit firing rates from the true firing rates, so that for each cell we had a set of "residual responses." These residual responses were used in the classification described above.

Principal components analysis

We applied a principal components analysis (PCA) to population responses to determine their major axes of variation. Specifically, we treated each cortical neuron as a signal, and each texture response as an observation in 141-dimensional space. To compare the main axes of variation in the responses of tactile fibers and cortical neurons, we also performed PCA on the responses of afferents (N = 39) and cortical neurons using only the responses to the 24 textures that were used in both the peripheral and cortical experiments.

We measured the correlation between peripheral and cortical values for every possible pairing of the principal components (23x23=529 possible comparisons). To determine whether the correlations were significant we repeated these regressions on bootstrapped data, using separate, random permutations of the peripheral and cortical texture identities (5000 permutations). We calculated significance as the proportion of times our measured correlation was greater than our bootstrapped correlations, Bonferroni-corrected for 529 multiple comparisons.

Binary classification and dimensionality

The dimensionality of the cortical population response estimated from PCA comprises both a component that carries texture information and a component that does not. To estimate the texture-

related component of the dimensionality, we adapted a method from Rigotti et. al.[14] that assesses the number of informative dimensions by quantifying the ability of the population representation to perform arbitrary linear binary classifications of the state space (in this case textures). The idea is, to the extent that the texture set can be arbitrarily split into *D* categories, the neural space comprises *D* dimensions relevant to texture coding. First, we randomly select N neurons and T textures. We choose one (of the 2^T possible ways) of splitting the T textures into two groups, and test whether a binary classifier could successfully discriminate between the two groups using the N-dimensional population response. Specifically, we train a support vector machine with a linear kernel (with the *fitcsvm()* function in Matlab) on four randomly selected (of five, with replacement) responses to each texture, each yielding an N-dimensional vector of firing rates. We then use the remaining left-out response from each cell to build a single N-dimensional test vector for each texture, which is used to test the performance of the binary classifier. Performance is averaged over 50 repetitions of the trial-shuffling procedure, to get a mean performance for this set of cells and texture groups. If this mean performance is greater than 75%, we count this binary classification as "implementable" by the population response. The functions in Figure 2.3B represent the proportion of "implementable" conditions, measured over 500 random selections of cells and texture groupings. Data are fit with sigmoids:

$$p(T) = \exp(-(T/\beta)^{\alpha})$$

the intersection of this curve *p(T)* = 0.95 is taken as the critical value T* for each population size. A population that can successfully classify T* textures has an effective dimensionality of T*-1. Thus, in Figure 2.3C, we report the dimensionality for a population size N as *D = max(T* -1,0)*.

Estimating submodality input

We wished to assess the relative contributions of the three populations of tactile fibers to the response of each neuron in somatosensory cortex, having previously shown that a majority of cortical neurons

receive convergent input from multiple modalities, even in area 3b [44,45]. While afferent input is not integrated linearly, we estimated the relative strength of that input using a linear model. Specifically, we used a multiple regression to predict the standardized (z-scored) mean texture responses of each cortical neuron to a set of 24 textures (see above) from the standardized (z-scored) mean responses of SA1, RA, and PC afferents to those same textures. We used these normalized regression weights as measures of the relative strength of SA1, RA, and PC afferent input into each neuron.

Spatial receptive fields

To characterize the spatial receptive field of each cortical neuron, we adopted an approach described in detail in ref. [10]. In brief, we first binned spiking responses to the receptive field protocol (see above) in 100 micron (1.25 ms) bins. The 100 runs – each corresponding to the response during one scan of the random dot pattern, each scan radially displaced from the previous one by 400 microns – were combined into a neural image (spatial even plot, cf. ref. [43]), which was then cross-correlated with a reconstruction of the stimulus (binned into 100x100 micron bins) to find an optimal alignment. Then, we used a spike-triggered average (STA) of the stimulus to find the mean stimulus values that were spatially aligned to any given spike.

To calculate receptive field properties, we first smoothed the STA with a 0.3 mm std. dev. Gaussian filter. Next, all bins with an absolute amplitude less than 20% of the RF's peak amplitude were set to zero. Finally, we required 1) that every non-zero bin have at least two of the four adjacent bins be nonzero and 2) that isolated regions of the RF have areas of at least 0.7 mm^2. Cells that did not meet these criteria were set to zero. To calculate excitatory & inhibitory area, we summed the area occupied by bins in the RF with positive/negative values, respectively. To calculate the scanning distance between excitatory and inhibitory subfields, we first found the center-of-mass for the excitatory and inhibitory bins in each RF, and then calculated the distance between them along the scanning direction.

Frequency analysis

Spiking responses in the nerve have been shown to phase-lock at high frequencies to texture-elicited skin vibrations [46], and spiking responses in somatosensory cortex have been shown to phase-lock to high-frequency skin vibrations imposed by a shaker [41]. To reveal any phase-locking in the cortical responses to texture, we first binned spike trains into 0.3 ms bins. Next, we computed the fast Fourier transform of that binned spike train and, from it, the amplitude spectrum. Finally, we computed the mean amplitude spectrum across repeated presentations for each texture and neuron. To assess whether we could match the surface profile of textures to their neural responses based on their respective frequency compositions, we measured the mean correlation between the surface profile spectrum and its neural counterpart.

Discriminability of 3-D printed textures

We wished to assess whether neurons in somatosensory cortex are more sensitive to differences in the coarse structure or fine structure of a textured surface. To this end, we measured neuronal responses to nine 3D-printed textures that parametrically combined three coarse patterns (blank, 7.7 mm spaced dots, 5 mm-period grating) and three fine patterns (blank, 1 mm-period grating, and 500 μm-period grating). We then measured the discriminability of pairs of textures from their respective distributions of responses. Specifically, we sought to determine whether two textures with identical fine structure, but different coarse structure could be discriminated from the responses of an individual neuron. For each fine pattern, we had three different coarse patterns (and vice versa for each coarse pattern), and thus 3 different pairwise comparisons. To quantify the discriminability of each pair from each neuron's responses, we measured a sensitivity index (*d'*):

$$d' = \frac{|\mu_1 - \mu_2|}{\sqrt{\frac{1}{2}(\sigma_1^2 + \sigma_2^2)}}$$

where μ is the mean firing rate response to a texture and σ^2 is the variance in firing rate across repeated presentations of that texture. These values were averaged across conditions and subpopulations of cells (Figure 2.5C). To calculate the statistical significance of these differences across neural subpopulations, we repeated this averaging on permutations the same data set with responses shuffled (50000 permutations). We calculated significance as the proportion of times our measured difference was greater than that computed from shuffled data.

Dissimilarity correlation

We sought to determine whether we could account for psychophysical judgments of texture dissimilarity obtained from human observers to neuronal responses in somatosensory cortex. To this end, we computed the Euclidean distance between the two population vectors for each of the two textures, each element of which is the mean firing rate of each neuron in the set. This distance was then compared with the psychophysical judgment of texture dissimilarity.

REFERENCES

1. Skedung, L. *et al.* Feeling small: exploring the tactile perception limits. *Sci. Rep.* **3,** 2617 (2013).

2. Phillips, J. & Johnson, K. Tactile spatial resolution. II. Neural representation of bars, edges, and gratings in monkey primary afferents. *J. Neurophysiol.* 1192–1203 (1981).

3. Johnson, K. & Lamb, G. Neural mechanisms of spatial tactile discrimination: neural patterns evoked by braille-like dot patterns in the monkey. *J. Physiol.* 117–144 (1981).

4. Hollins, M., Bensmaïa, S. J. & Washburn, S. Vibrotactile adaptation impairs discrimination of fine, but not coarse, textures. *Somatosens. Mot. Res.* **18,** 253–262 (2001).

5. Hollins, M. & Risner, S. R. Evidence for the duplex theory of tactile texture perception. *Percept. Psychophys.* **62,** 695–705 (2000).

6. Hollins, M., Bensmaia, S. J. & Roy, E. A. Vibrotaction and texture perception. *Behav. Brain Res.* **135,** 51–56 (2002).

7. Bensmaïa, S. & Hollins, M. Pacinian representations of fine surface texture. *Percept. Psychophys.* **67,** 842–854 (2005).

8. Weber, A. I. *et al.* Spatial and temporal codes mediate the tactile perception of natural textures. *P Natl Acad Sci Usa* (2013). doi:10.1073/pnas.1305509110

9. Lieber, J. D., Xia, X., Weber, A. I. & Bensmaia, S. J. The Neural Code for Tactile Roughness in the Somatosensory Nerves. *J. Neurophysiol.* (2017).

10. DiCarlo, J. J., Johnson, K. O. & Hsiao, S. S. Structure of receptive fields in area 3b of primary somatosensory cortex in the alert monkey. *J. Neurosci.* **18,** 2626–45 (1998).

11. Darian-Smith, I., Sugitani, M., Heywood, J., Karita, K. & Goodwin, A. Touching textured surfaces: cells in somatosensory cortex respond both to finger movement and to surface features. *Science* **218,** 906–9 (1982).

12. Sinclair, R. J. & Burton, H. Neuronal activity in the primary somatosensory cortex in monkeys (Macaca mulatta) during active touch of textured surface gratings: responses to groove width, applied force, and velocity of motion. *J. Neurophysiol.* **66,** 153–69 (1991).

13. Tremblay, F., Ageranioti-Bélanger, S. a & Chapman, C. E. Cortical mechanisms underlying tactile discrimination in the monkey. I. Role of primary somatosensory cortex in passive texture discrimination. *J. Neurophysiol.* **76,** 3382–3403 (1996).

14. Rigotti, M. *et al.* The importance of mixed selectivity in complex cognitive tasks. *Nature* **497,** 585–590 (2013).

15. Pachitariu, M. *et al.* Suite2p: beyond 10,000 neurons with standard two-photon microscopy. *bioRxiv* 61507 (2016). doi:10.1101/061507

16. Pei, Y.-C. C., Denchev, P. V., Hsiao, S. S., Craig, J. C. & Bensmaia, S. J. Convergence of submodality-specific input onto neurons in primary somatosensory cortex. *J. Neurophysiol.* **102,** 1843–1853 (2009).

17. Connor, C. E. & Johnson, K. O. Neural coding of tactile texture: comparison of spatial and temporal mechanisms for roughness perception. *J. Neurosci.* **12,** 3414–26 (1992).

18. Manfredi, L. R. *et al.* Natural scenes in tactile texture. *J. Neurophysiol.* **111,** 1792–802 (2014).

19. DiCarlo, J. J., Johnson, K. O. & Hsiao, S. S. Structure of receptive fields in area 3b of primary somatosensory cortex in the alert monkey. *J. Neurosci.* **18,** 2626–45 (1998).

20. Yoshioka, T., Gibb, B., Dorsch, a K., Hsiao, S. S. & Johnson, K. O. Neural coding mechanisms underlying perceived roughness of finely textured surfaces. *J. Neurosci.* **21,** 6905–16 (2001).

21. Bensmaia, S. J., Denchev, P. V, Dammann, J. F., Craig, J. C. & Hsiao, S. S. The representation of stimulus orientation in the early stages of somatosensory processing. *J Neurosci* **28,** 776–786 (2008).

22. Connor, C. E., Hsiao, S. S., Phillips, J. R. & Johnson, K. O. Tactile roughness: neural codes that account for psychophysical magnitude estimates. *J. Neurosci.* **10,** 3823–36 (1990).

23. Blake, D. T., Johnson, K. O. & Hsiao, S. S. Monkey cutaneous SAI and RA responses to raised and depressed scanned patterns: effects of width, height, orientation, and a raised surround. *J Neurophysiol* **78,** 2503–2517 (1997).

24. Hollins, M., Bensmaia, S., Karlof, K. & Young, F. Individual differences in perceptual space for tactile textures: evidence from multidimensional scaling. *Percept. Psychophys.* **62,** 1534–1544 (2000).

25. DiCarlo, J. J. & Johnson, K. O. Spatial and temporal structure of receptive fields in primate somatosensory area 3b: effects of stimulus scanning direction and orientation. *J. Neurosci.* **20,** 495–510 (2000).

26. Saal, H. P., Harvey, M. A. & Bensmaia, S. J. Rate and timing of cortical responses driven by separate sensory channels. *Elife* **4,** 7250–7257 (2015).

27. Priebe, N. J. & Ferster, D. Mechanisms of Neuronal Computation in Mammalian Visual Cortex. *Neuron* **75,** 194–208 (2012).

28. Chung, S., Li, X. & Nelson, S. B. Short-term depression at thalamocortical synapses contributes to rapid adaptation of cortical sensory responses in vivo. *Neuron* **34,** 437–446 (2002).

29. Katz, Y., Heiss, J. E. & Lampl, I. Cross-whisker adaptation of neurons in the rat barrel cortex. *J. Neurosci.* **26,** 13363–72 (2006).

30. Carandini, M. & Heeger, D. J. Normalization as a canonical neural computation. *Nature Reviews Neuroscience* **13,** 51–62 (2012).

31. Brouwer, G. J., Arnedo, V., Offen, S., Heeger, D. J. & Grant, A. C. Normalization in human somatosensory cortex. *J. Neurophysiol.* **114,** 2588–2599 (2015).

32. Reed, J. L., Qi, H.-X. & Kaas, J. H. Spatiotemporal Properties of Neuron Response Suppression in Owl Monkey Primary Somatosensory Cortex When Stimuli Are Presented to Both Hands. *J. Neurosci.* **31,** 3589–3601 (2011).

33. Reed, J. L. *et al.* Response Properties of Neurons in Primary Somatosensory Cortex of Owl Monkeys Reflect Widespread Spatiotemporal Integration. 2139–2157 (2010).

doi:10.1152/jn.00709.2009.

34. Brincat, S., Siegel, M., von Nicolai, C. & Miller, E. K. Gradual progression from sensory to task-related processing in cerebral cortex. *bioRxiv* 195602 (2017).

35. Lehky, S. R., Kiani, R., Esteky, H. & Tanaka, K. Dimensionality of Object Representations in Monkey Inferotemporal Cortex. *Neural Comput.* **26,** 2135–2162 (2014).

36. Cowley, B. R., Smith, M. A., Kohn, A. & Yu, B. M. Stimulus-Driven Population Activity Patterns in Macaque Primary Visual Cortex. *PLoS Comput. Biol.* **12,** (2016).

37. Goodman, J. M. & Bensmaia, S. J. A variation code accounts for perceived roughness. (2017).

38. Sripati, A. P., Yoshioka, T., Denchev, P. V, Hsiao, S. S. & Johnson, K. O. Spatiotemporal receptive fields of peripheral afferents and cortical area 3b and 1 neurons in the primate somatosensory system. *J Neurosci* **26,** 2101–2114 (2006).

39. Sripati, A. P., Bensmaia, S. J. & Johnson, K. O. A continuum mechanical model of mechanoreceptive afferent responses to indented spatial patterns. *J. Neurophysiol.* **95,** 3852–3864 (2006).

40. Johansson, R. & Vallbo, Å. Tactile sensibility in the human hand: relative and absolute densities of four types of mechanoreceptive units in glabrous skin. *J. Physiol.* 283–300 (1979).

41. Harvey, M. A., Saal, H. P., Dammann, J. F. & Bensmaia, S. J. Multiplexing stimulus information through rate and temporal codes in primate somatosensory cortex. *PLoS Biol.* **11,** e1001558 (2013).

42. Theriault, B. R., Reed, D. A. & Niekrasz, M. A. Reversible medetomidine/ketamine anesthesia in captive capuchin monkeys (Cebus apella). in *Journal of Medical Primatology* **37,** 74–81 (2008).

43. Johnson, K. O. & Phillips, J. R. A rotating drum stimulator for scanning embossed patterns and textures across the skin. *J. Neurosci. Methods* **22,** 221–31 (1988).

44. Saal, H. P., Harvey, M. A. & Bensmaia, S. J. Rate and timing of cortical responses driven by separate sensory channels. *Elife* **4,** (2015).

45. Pei, Y.-C. C., Denchev, P. V., Hsiao, S. S., Craig, J. C. & Bensmaia, S. J. Convergence of submodality-specific input onto neurons in primary somatosensory cortex. *J. Neurophysiol.* **102,** 1843–1853 (2009).

46. Weber, A. I. *et al.* Spatial and temporal codes mediate the tactile perception of natural textures. *Proc. Natl. Acad. Sci. U. S. A.* **110,** 17107–17112 (2013).

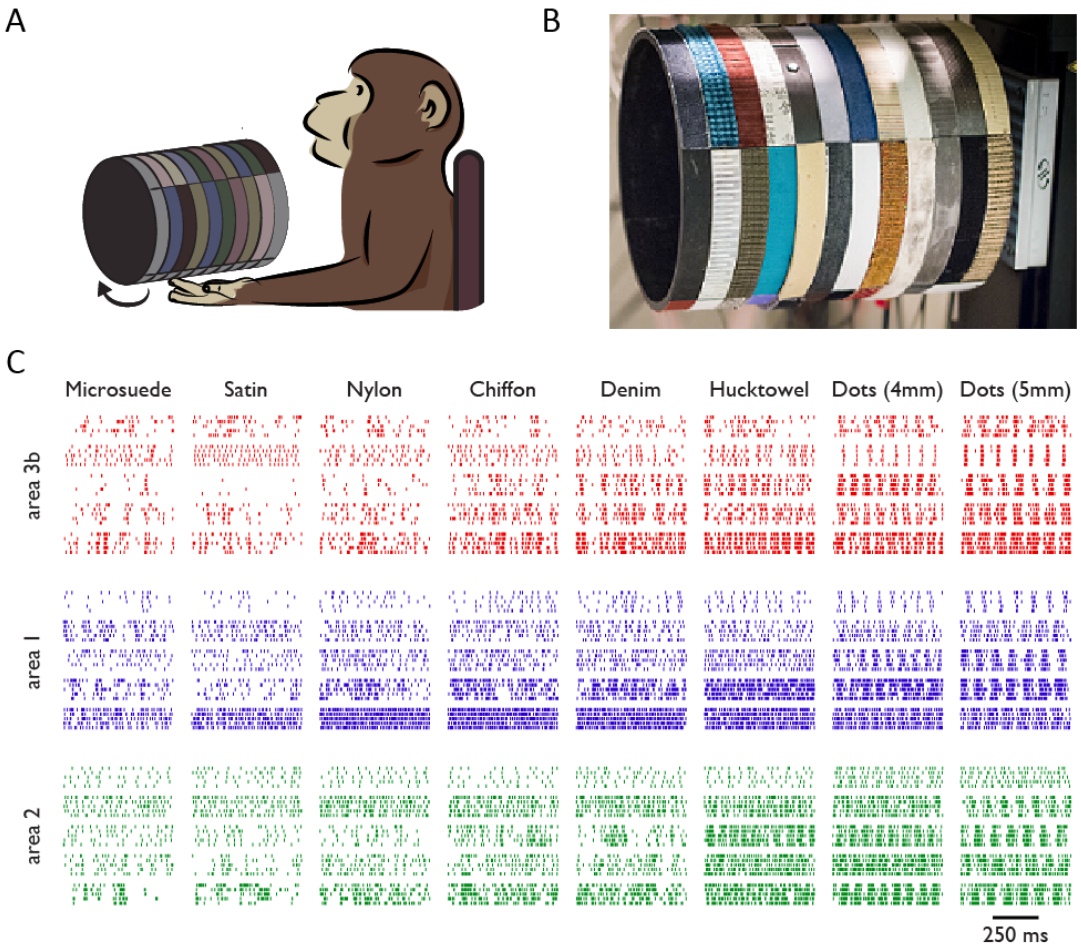

Figure 2.1. **Experimental apparatus and sample responses.** A| Textures were passively presented to the fingerpad of an awake macaque. B| The rotating drum stimulator – on which the 59 textures were mounted – allows a surface to be scanned across the fingertip at a precise and repeatable speed and depth of indentation into the skin. C| Sample spiking responses of 5 neurons each in areas 3b, 1, and 2 to 5 repetitions of 8 textured surfaces.

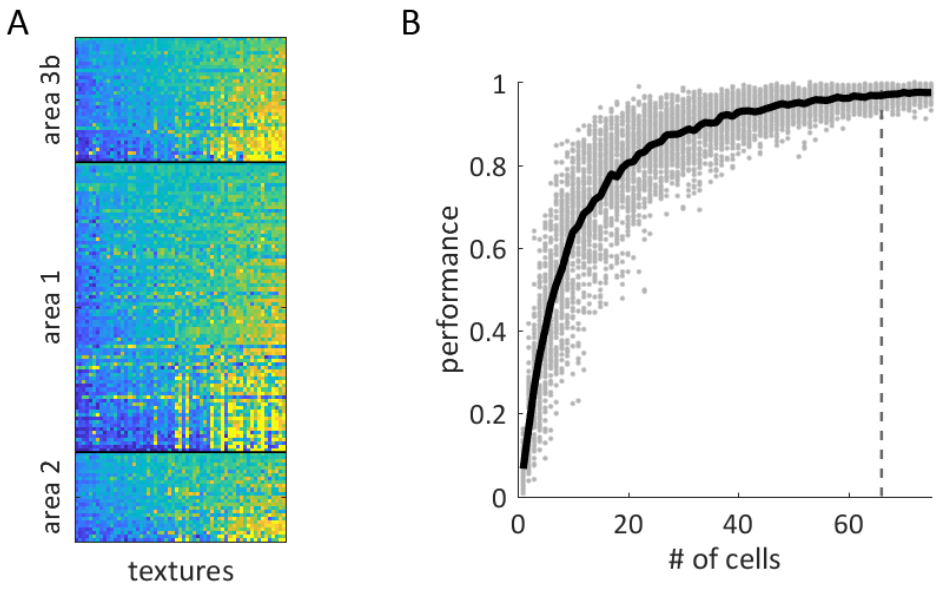

Figure 2.2. **Texture classification performance based on cortical responses**. A| The mean firing rate (across repetitions) evoked by each of 59 textures (columns) in somatosensory neurons, broken up by cortical module. Firing rates are normalized within neuron for display purposes, and range from low (blue) to high (yellow) firing rates. Textures are sorted according to the first principal component of the population response from lowest to highest. Cells are ordered first by area, then by variance of their firing rates across textures. Somatosensory neurons exhibit heterogeneous responses to textures. B| Textures were classified according to the responses they evoked in somatosensory neurons. As expected, classification performance improved as more responses were included. Gray dots denote the performance of individual neuronal groups, the black trace denotes the mean as a function of group size. Groups of 66 cells, marked by the grey dashed line, yield a near-asymptotic performance of 97%.

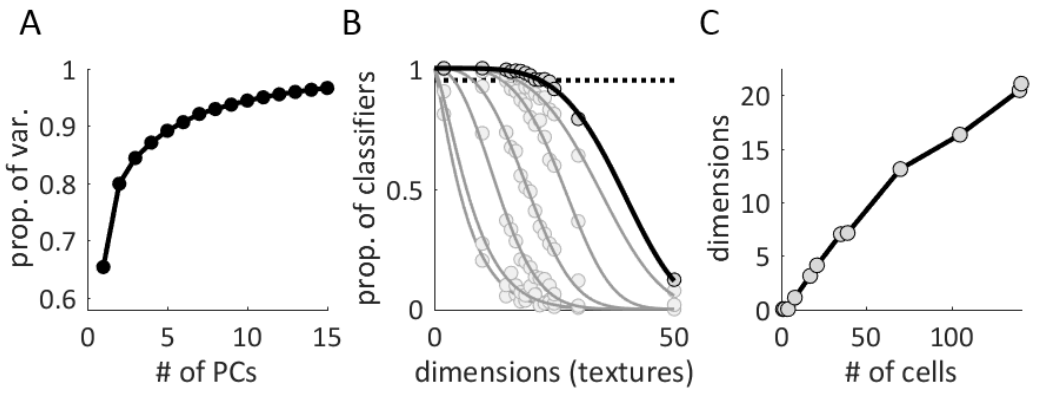

Figure 2.3. **Dimensionality of the cortical representation of texture**. A| We performed a principal components analysis on the population response to texture and show the cumulative scree plot for the first 15 principal components. The bulk of the response variance is carried in the first few components. B| Fraction of the number of implementable binary classifications as a function of the number of textures included in the classification. That is, we can split almost any collection of 22 textures (~95% of groups, dotted line) into two arbitrary groups and distinguish those groups (performance > 0.75) with a binary classifier. From this analysis, we estimate the population representation of texture (for these 141 cells) to be at least 21-dimensional. The same analysis, performed on smaller subsets of cells, is plotted in grey (from left to right, N=1, 2, 17, 35, 70, 105). C| The number of dimensions estimated from the binary classification analysis is still rapidly rising with group size up to 141, suggesting that the population representation of texture is larger than 21-dimensional across the full cortical population.

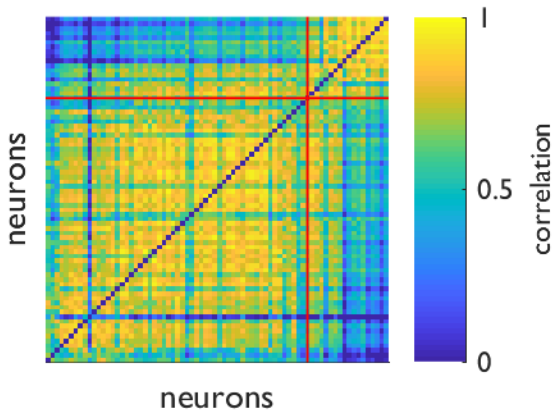

Figure 2.4. **The heterogeneity of cortical responses can be in part attributed to differences in submodality input.** Correlation matrix of texture-elicited firing rates with each row and column corresponding to a different neuron. Cells are ordered by their PC regression weight, from least PC-like (bottom left) to most PC-like (top right). The red line divides neurons with PC regression weights greater than or less than 0.5. The most PC-like cells in somatosensory cortex tend to cluster, showing firing rate responses that are distinct from the rest of the cortical population.

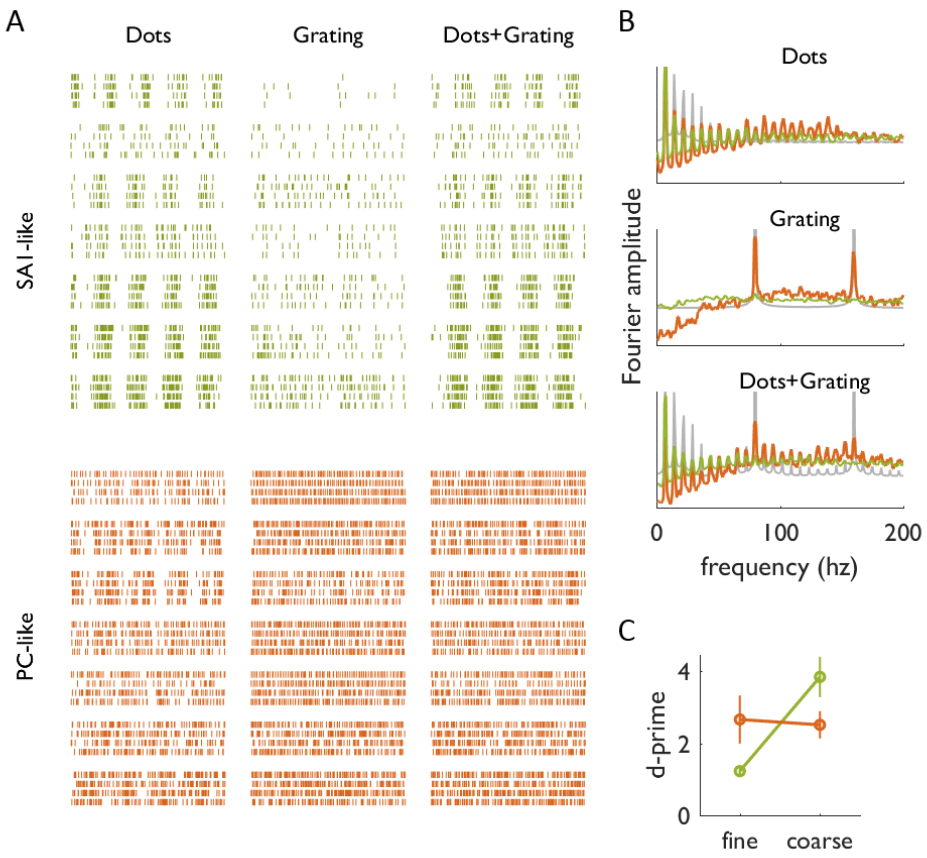

Figure 2.5. **Encoding of coarse and fine features in somatosensory cortex**. A| Example spiking responses are plotted from 7 SA1-like neurons (green, cells with SA1 regression coefficient > 0.5, N=53) and PC-like neurons (orange, cells with PC regression coefficient > 0.5, N=23) in response to 5 repeated presentations of 3 different textures: dots spaced 7.7 mm apart, a 1 mm-period grating, and a superposition of the dots with the grating. B| Mean amplitude spectrum of the responses of SA1-like neurons (green) and PC-like cells (orange) to the same 3 textures as in A. PC-like cells exhibit high-frequency phase-locking to the temporal period of the grating (80 Hz), even when the dots are present, while SA1-like cells do not. C| Discriminability (*d'*) of textures based on the firing rates they evoke in SA1-like and PC-like neurons (green and orange, respectively). Error bars denote the bootstrapped

standard errors of the mean across cells and texture pairs. While PC-like cells are sensitive to both coarse and fine features, SA1-like cells are sensitive only to coarse ones.

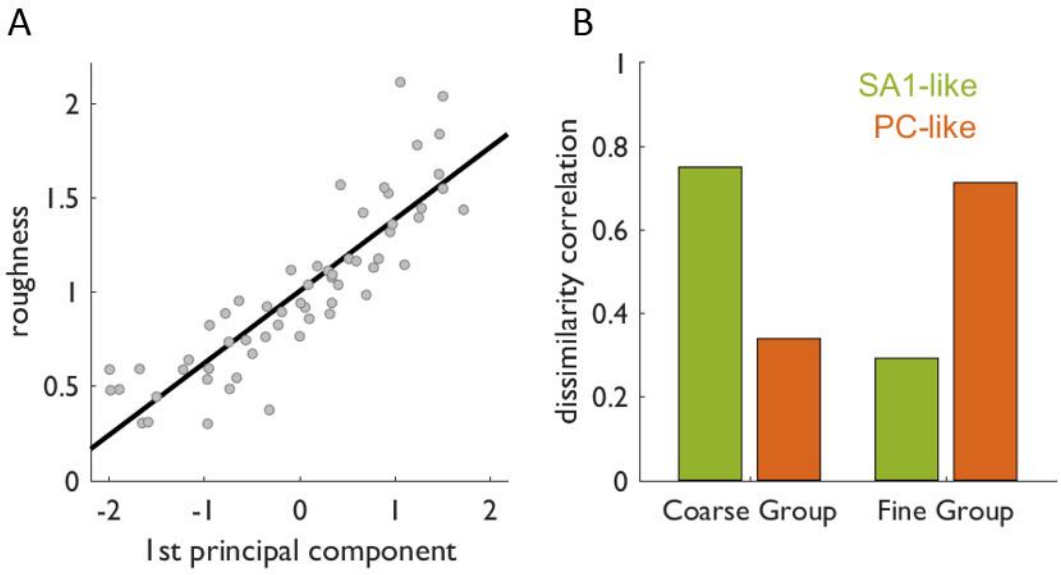

Figure 2.6. **Relating neuronal responses to perceptual judgments of texture**. A| Perceived roughness vs. the first principal component of the population response (*r*=0.88). B| Prediction of the perceived dissimilarity based on the firing rates of SA1-like neurons (green, SA1 coefficient > 0.5, N=53) and PC-like neurons (orange, SA1 coefficient > 0.5, N=23) for two different groups of textures. SA1-like cells predict differences in coarse spatial structure, while PC-like cells predict differences in fine structure.

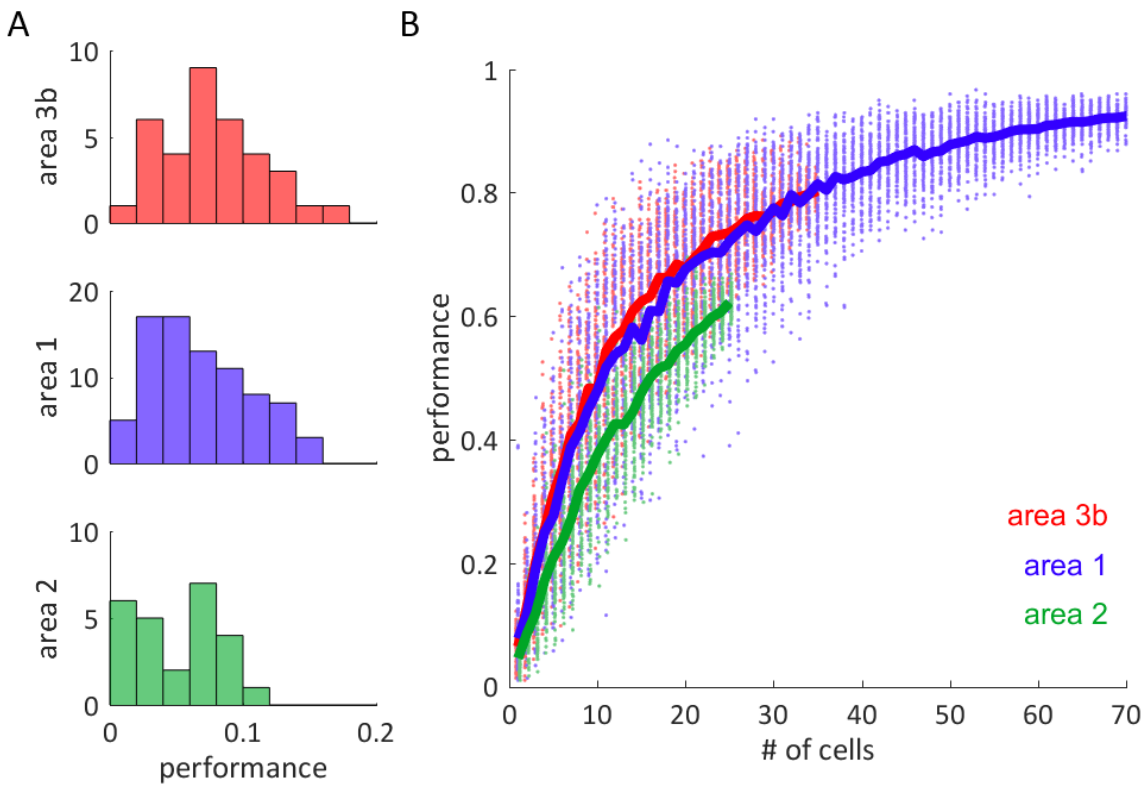

Figure 2.S1. **Classification performance by cortical area.** A| Classification performance based on the responses of individual neurons in areas 3b, 1, and 2. B| Texture classification performance of groups of neurons in each area as a function of group size (as in Figure 2). Each dot denotes a random sample, the line denotes the mean at each size. Classification performance is largely similar across areas.

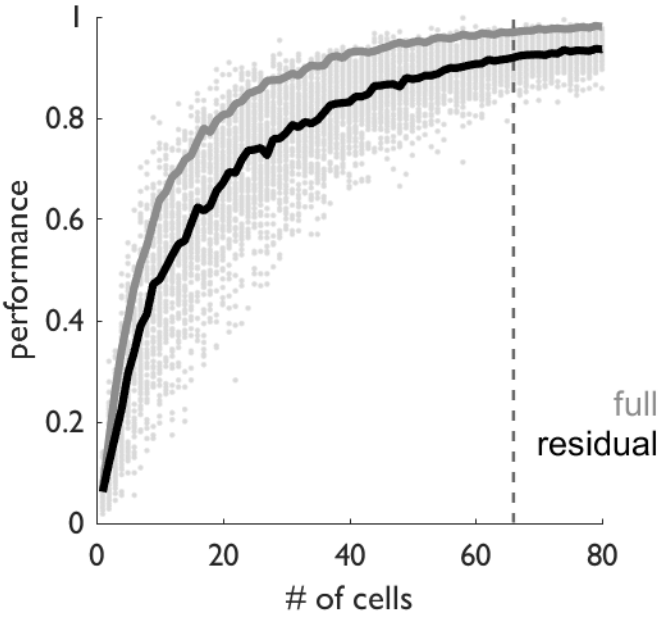

Figure 2.S2. **Classification performance with the mean firing rate removed.** We performed a texture classification (as in Figure 2) using only the residuals of the regression of each neuron's response on the mean population response (see Methods). The black line shows the performance of these residuals, the gray line reproduces the performance of the original response. Classification performance is only slightly reduced when the mean population response is removed.

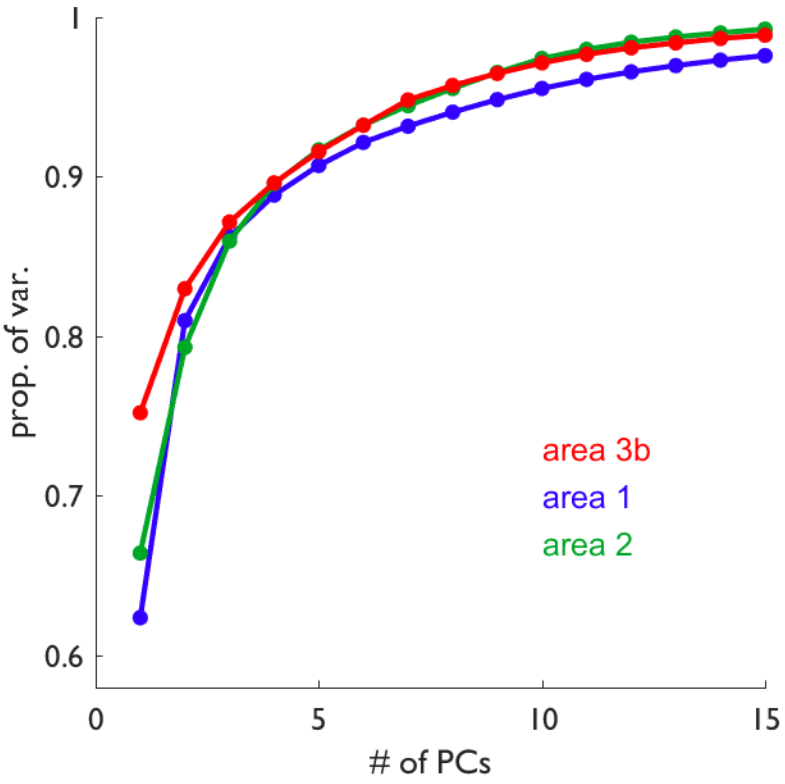

Figure 2.S3. **Principal component analysis of individual cortical areas.** We performed a principal components analysis on the population texture response of each cortical area. The cumulative proportion of variance explained by the first 15 principal components. In all three areas, the majority of response variance is explained by only the first few components.

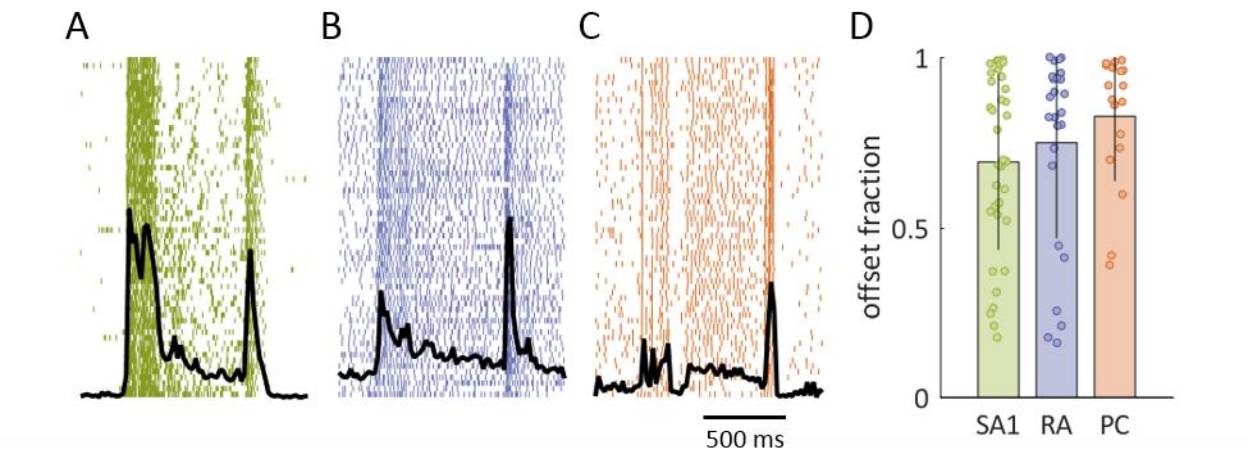

Figure 2.S4. **Responses of cortical neurons to a skin indentation as a gauge of submodality input.** A-C| Spiking responses of 3 different neurons to a probe indented into the skin for 500 ms (60 repetitions). Many neurons which, according to the multiple regression, receive dominant input from SA1 (A), RA (B), or PC (C) fibers still exhibit both a sustained response and an off response, suggesting convergent input from slowly (SA1) and rapidly (RA and/or PC) fibers. D| Fraction of the combined sustained and offset response carried by the offset response for SA1-like (green, N=53), RA-like (blue, N=45), or PC-like (orange, N=23) neurons. Error bars denote the standard deviation of fractions across cells. While SA1 afferents exhibit almost no offset responses[1], most SA1-like neurons exhibit strong offset responses ($p<0.05$ for 93% of SA1-like neurons, paired-sample t-test). Similarly, while RA and PC fibers produce essentially no sustained response[1], many RA-like and PC-like neurons produce robust sustained responses ($p<0.05$ 83%, and 68% of RA-like and PC-like neurons, paired-sample t-test). Overall, 65/94 (69%) of neurons exhibited significant modulation in both their offset and sustained responses, and, of the remaining 29, ten yielded two or more significant weights in the multiple regression (F-test, as in the main text). Thus, in total, 75/94 (80%) neurons displayed submodality convergence by one or both of these measures.

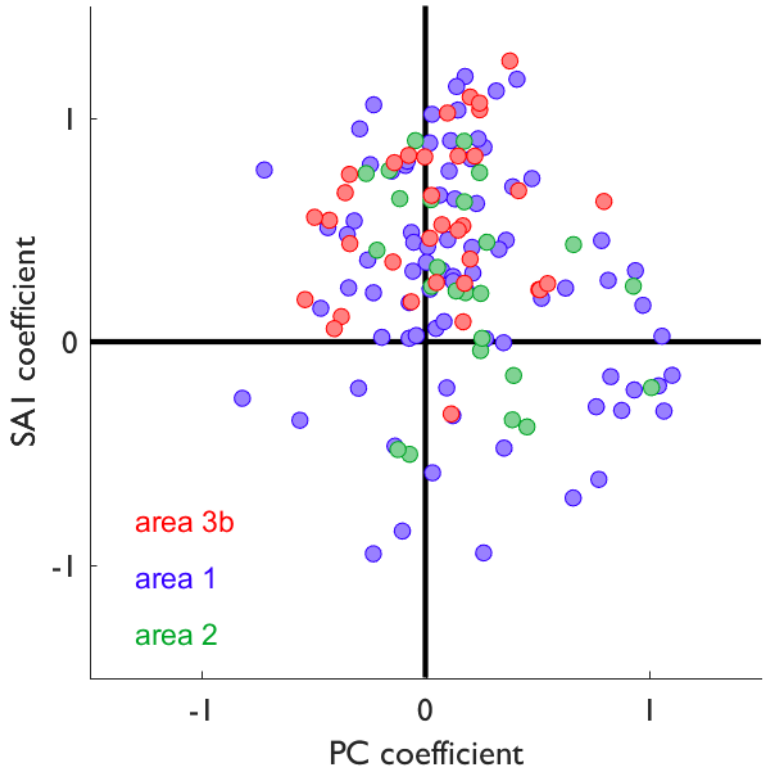

Figure 2.S5. **Weights of SA1 and PC input in determining cortical firing rates.** We performed a multiple regression of the firing rates evoked in tactile fibers (SA1, RA, and PC afferents) onto the firing rates of cortical neurons to the same set of textures. Here, we plot the normalized SA1 and PC regression coefficients for each neuron in areas 3b (red), 1 (blue), and 2 (green). Note that the most strongly PC-like neurons are in areas 1 and 2.

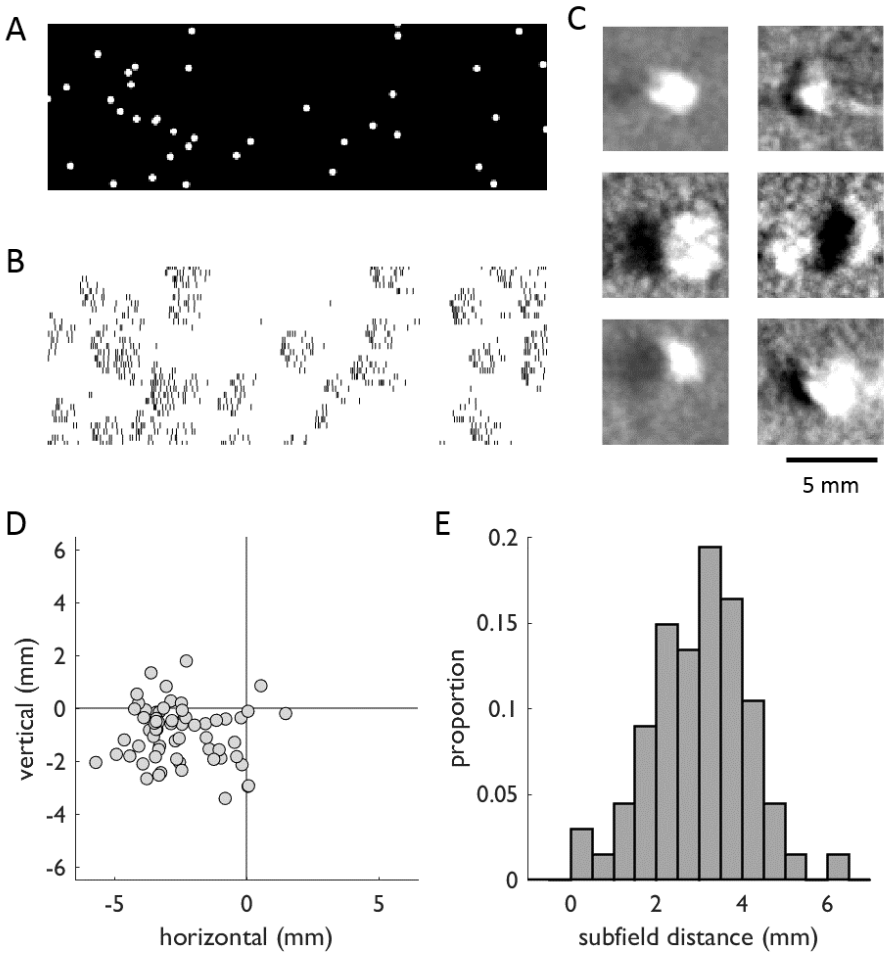

Figure 2.S6. **Receptive fields of somatosensory neurons.** A| Patch of the random dot pattern used to obtain spatial receptive fields. B| Spiking response to the stimulus patch. C| Receptive fields from 6 example neurons (top left RF was obtained from neuron whose response is shown in panel B). White regions are excitatory, black regions are inhibitory. D| Location of the inhibitory center relative to the excitatory center. Inhibitory subfields were spatially offset from excitatory subfields. Most inhibition was located behind the excitatory subfield horizontally (temporally lagged). E| Histogram of excitatory-inhibitory subfield distance across all measured cells. Inhibition was 2-4 mm behind excitation.

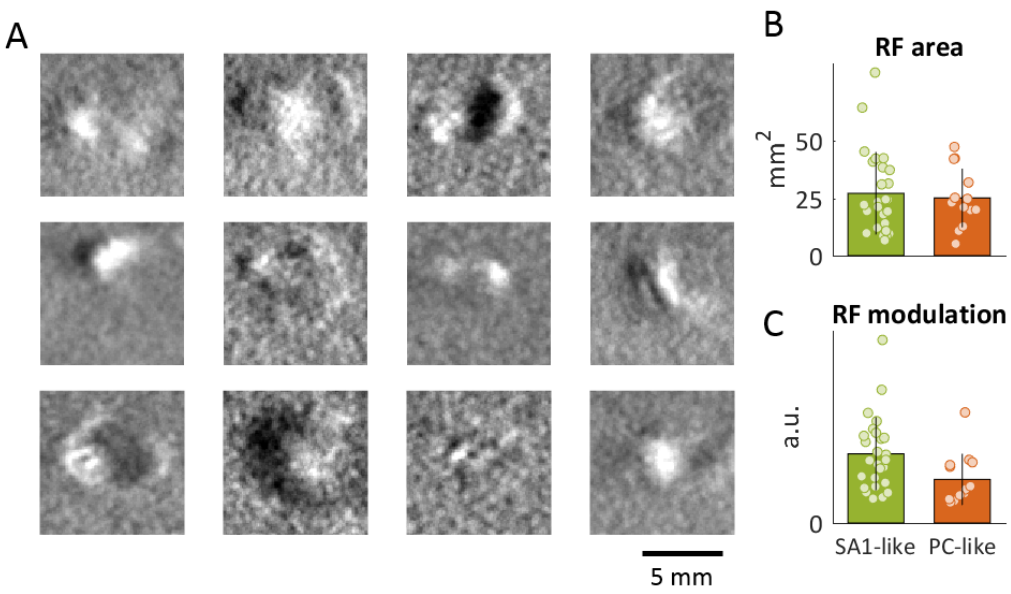

Figure 2.S7. **Receptive fields of PC-Like neurons.** A| Receptive fields of 12 PC-like neurons (PC regression coefficient > 0.5). White regions are excitatory, black regions are inhibitory. B| Combined excitatory and inhibitory area of cortical neurons is similar between the two populations (p=0.71, two-sided t-test). C| Modulation depth (distance between the max and min values of the RF). SA1-like cells show a more strongly modulated response to spatial structure than do PC-like cells (p<0.05, two-sided t-test), which is consistent with the greater sensitivity of SA1-like neurons to coarse spatial features.

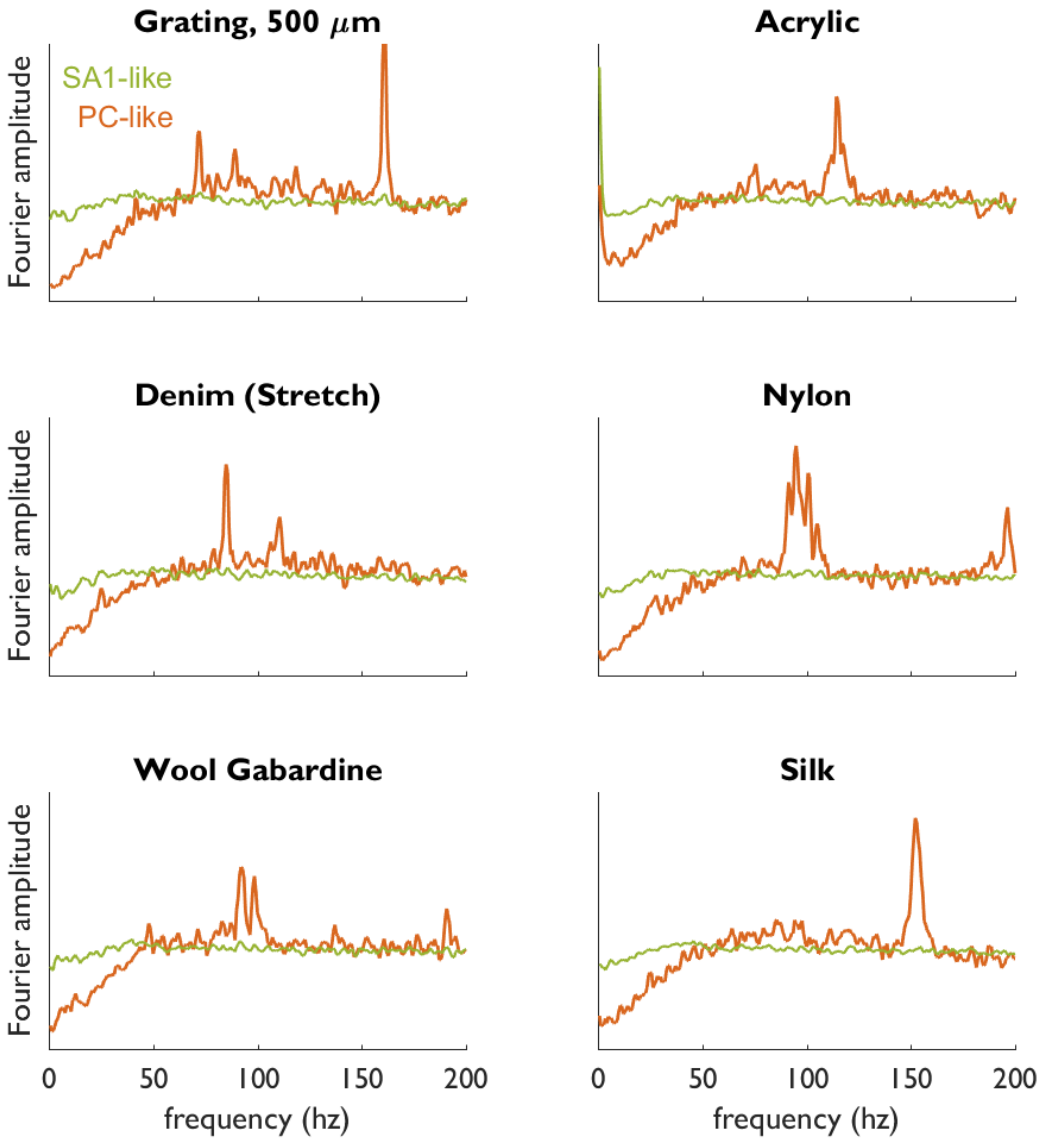

Figure 2.S8. **Amplitude spectra of cortical responses to periodic textures.** The mean absolute value of the Fourier transform of the spiking responses of SA1-like cells (green, cells with SA1 coefficient > 0.5, N=53) and PC-like cells (orange, cells with PC regression coefficient > 0.5, N=23) to six different textures. PC-like cells exhibit texture-evoked phase locking to frequencies between 50-200 Hz.

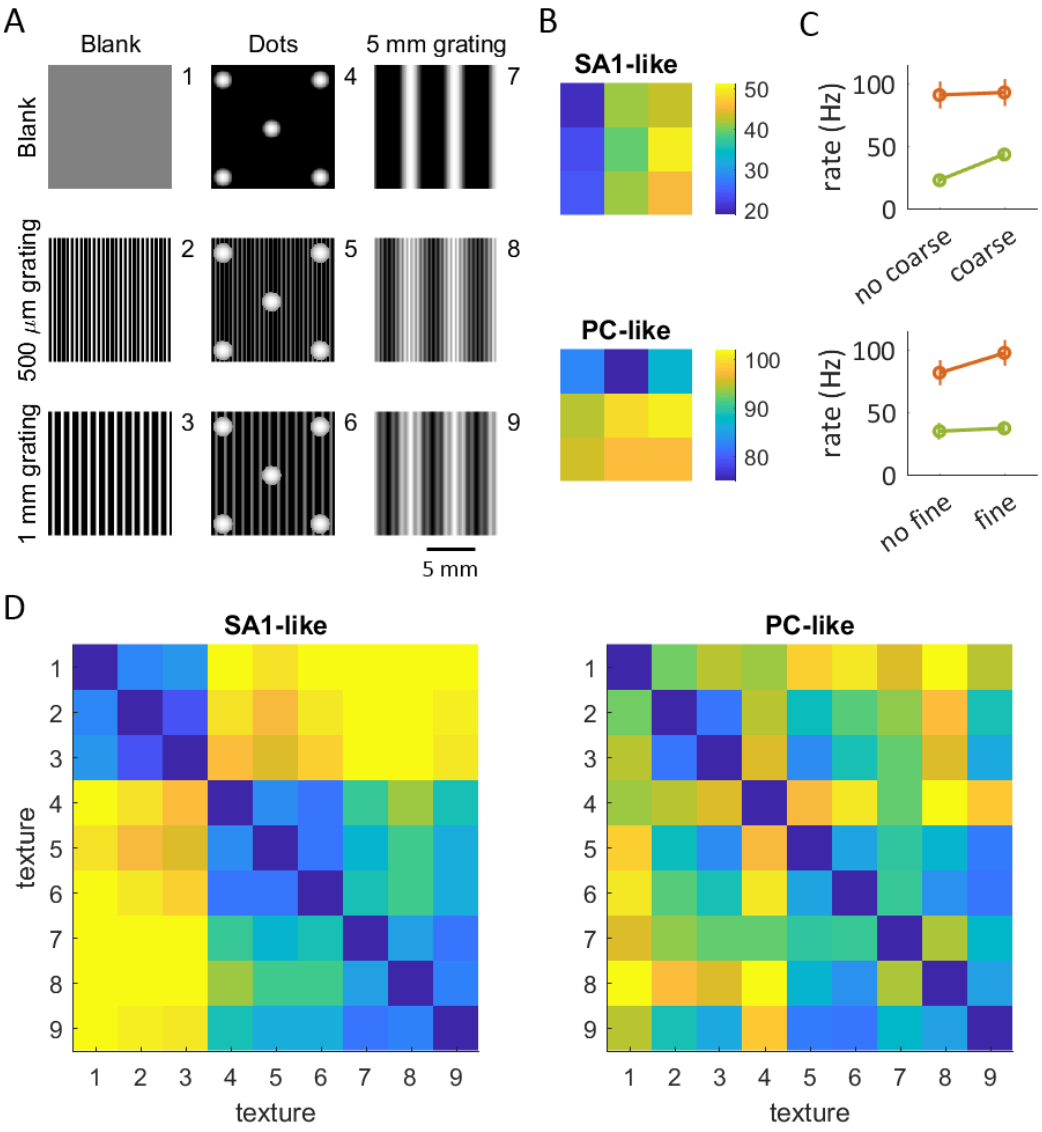

Figure 2.S9. **Encoding of coarse vs. fine texture.** A| Surface profiles of custom-made 3D-printed textures designed to probe the interaction of coarse and fine features. We parametrically combined three coarse textural features (columns left to right: blank, 7 mm dots, 5 mm grating) with three "fine" ones (rows top to bottom: blank, 0.5 mm grating, 1 mm grating). B| Mean firing rate of SA1-like (SA1 regression coefficient > 0.5, N=53) and PC-like (PC regression coefficient > 0.5, N=23) neurons evoked by all nine textures (arranged as in A). C| Mean firing rate of SA1-like (green) and PC-like (orange) neurons evoked

by textures with and without coarse structure (top) and textures with and without fine structure (bottom). Error bars denote the standard errors across cells and textures. SA1-like neurons show increased firing rates when coarse structure is present, while PC-like neurons show increased firing rates when fine structure is present. D| Mean discriminability of firing rate responses for all possible pairings of textures, for SA1-like and PC-like neurons. SA1-like neurons are more sensitive to coarse structure than PC-like neurons, and PC-like neurons are more sensitive to fine structure than SA1-like neurons.

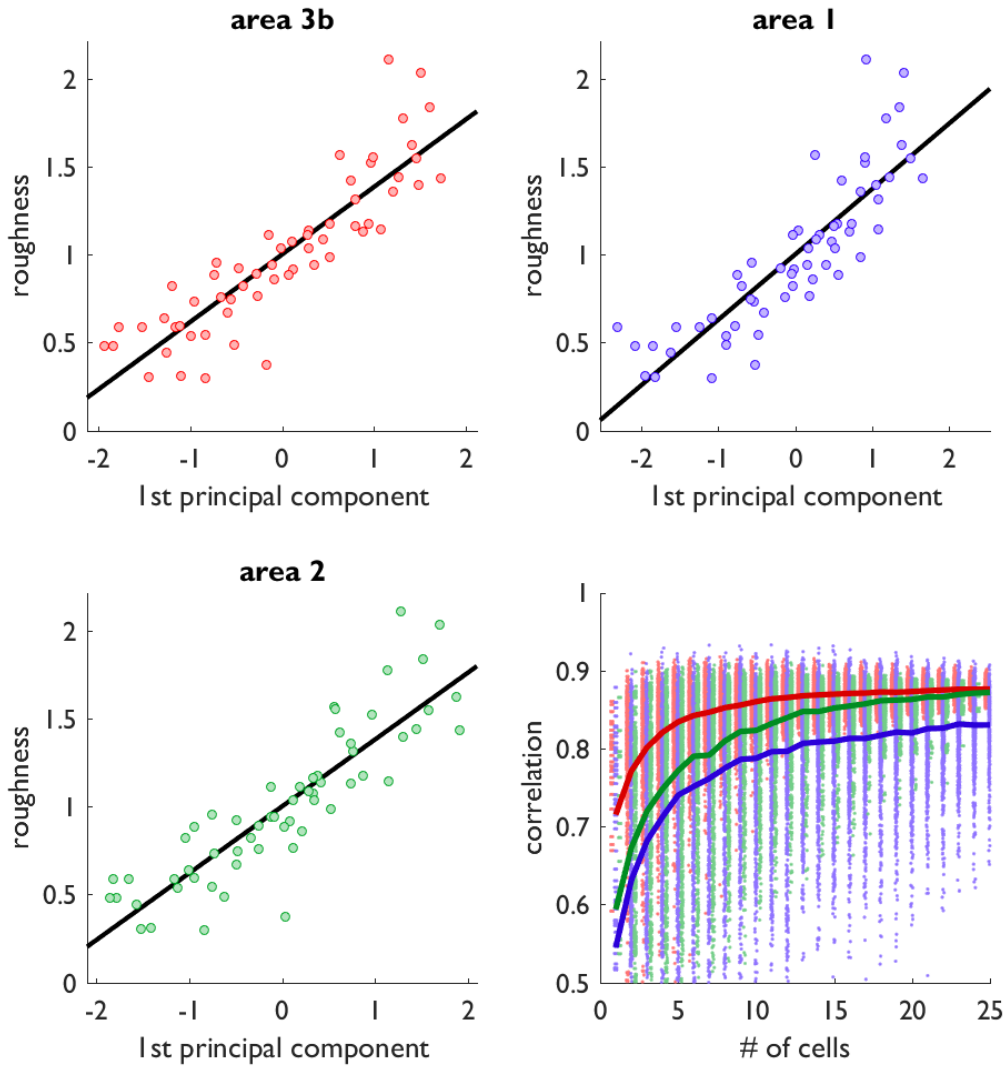

Figure 2.S10. **Relationship between perception and neuronal responses, broken down by area.** Perceived roughness is associated with the first principal axis of cortical responses to texture in A| area 3b (r=0.88), B| area 1 (r=0.86), and C| area 2 (r=0.87). D| The correlation between roughness and the population response increases with the number of cells used to compute the principal component. Dots denote the performance of random samples of neurons, traces denote the mean within each area for each sample size.

Velvet [P]	Silk, metallic (silk/metal) [P]	500 micron grating [*]	Upholstery, yellow [P]	Red fabric dots (backing)
Computer paper	Thin corduroy [P]	Upholstery, onyx	Wool, blend [P]	Embossed dots, 5 mm spacing (plastic) [P†]
Microsuede (polyester) [P†]	Organza [P]	Chiffon [P†]	Dots, 7.7 mm spacing [*]	Upholstery, fuzzy
Satin [P†]	Possum fur	1 mm grating [*]	Upholstery, beach mat	Receptive field mapping dots (2nd half)
Sueded cuddle (polyester) [P]	Foam drapery tape [P]	Upholstery, red grating	Upholstery, tan	Upholstery, green
Rabbit fur, long hair	Thick corduroy [P]	Fabric grating, wide spacing	Leather dot pattern	5 mm grating [*]
Vinyl (20 gauge) [P]	Wool/rayon felt [P]	Stretch denim (cotton/Lycra) [P†]	Wrapping paper (bumpy)	Hucktowel (cotton) [P†]
Careerwear flannel (cotton) [P]	Butcher paper	Faux croc skin	Ruffled fabric	Receptive field mapping dots (1st half)
Parchment paper	Nylon (200 denier) [P†]	Upholstery, gridded	Red fabric dots (front)	Embossed dots, 4 mm spacing (plastic) [P†]
Sting ray skin	Denim (cotton) [P]	Silk, crinkled [P]	Dots, 7.7 mm / 500 micron grating overlay [*]	5 mm grating / 1 mm grating overlay [*]
Snowflake fleece fuzz (polyester) [P]	Rabbit fur, short hair	Upholstery, Sunbrella	Dots, 7.7 mm / 1 mm grating overlay [*]	5 mm grating / 500 micron grating overlay [*]
Acrylic (Blank) [*]	Wool gabardine [P]	Lizard skin	Bumpy polyester	

Table 2.S1. **Texture set.** The 59 textures are ordered by their score along the first principal component (highly predictive of perceived roughness), sorted from low to high by column, then by row. The 24 textures common between the peripheral[2] and cortical experiments are marked with "[P]." Textures

that were 3D printed to disambiguate the effects of coarse and fine structure (pictured in Supplementary Figure 2.S8 and used for Figure 2.5) are marked with "[*]." Textures used to create the spiking rasters in Figure 2.1 are marked with "[†]."

CHAPTER 3: SPEED INVARIANT CODING OF TEXTURE IN SOMATOSENSORY CORTEX

Justin D. Lieber, Katie Long, and Sliman J. Bensmaia

INTRODUCTION

We are endowed with a remarkable ability to identify objects across a wide range of contexts and perspectives. For example, we can visually identify objects in a fraction of a second, even over broad changes in lighting, distance, or viewing angle. Similarly, we can auditorily identify the timbre of voices and musical instruments across a wide range of loudness and pitches (Handel and Erickson, 2001; Marozeau et al., 2003). In both vision and audition, perceptual invariance is achieved despite sensory representations at the periphery (the retina, the cochlea) that are highly dependent on perspective and context (Enroth-Cugell and Robson, 1966; Sachs and Young, 1979; Croner and Kaplan, 1995; Joris et al., 2011). Indeed, a signature of sensory processing is a progression of object representations that become increasingly robust to changes in context (Avidan et al., 2002; Finn et al., 2007; Sadagopan and Wang, 2008; Walker et al., 2011; Cadieu et al., 2014).

In touch, the best known instance of perceptual invariance is for texture: tactile texture perception has been shown to be nearly independent of the force exerted on the surface (Lederman and Taylor, 1972; Lederman, 1981) or the speed at which it is scanned across the skin (Lederman, 1974; Meftah el-M et al., 2000; Boundy-Singer et al., 2017). Remarkably, this perceptual invariance is achieved despite responses in the somatosensory nerves that are strongly modulated by exploratory parameters such as scanning speed (Goodwin and Morley, 1987a; Phillips et al., 1992; DiCarlo and Johnson, 1999) and, to a lesser degree, force (Goodwin and Morley, 1987b; Phillips et al., 1992; Saal et al., 2017). The effect of scanning speed on texture coding in the nerve is particularly pronounced for fine textures, which are encoded in precisely timed, texture-specific spiking sequences which contract or dilate multiplicatively with increases and decreases in speed, respectively (Weber et al., 2013). In this regime, texture

constancy seems to involve similar computations to that of timbre invariance across changes in fundamental frequency (Yau et al., 2009; Saal et al., 2016): in both cases, identity is preserved despite translations of a harmonic stack along the frequency axis with changes in speed or fundamental frequency. Thus, to achieve an invariant percept of texture, texture-specific information must be extracted from peripheral signals that are highly dependent on exploratory parameters, a process about which nothing is known.

While responses to textures scanned at different speeds have been measured in somatosensory cortex (Sinclair and Burton, 1991; Dépeault et al., 2013), the stimuli used in these studies consisted exclusively of embossed dot patterns and gratings, which provide an incomplete picture of texture processing. Indeed, the coding of textures at these large spatial scales (measured in millimeters) is dominated by one population of nerve fibers at the periphery and relies on a spatial mechanism that is insensitive to changes in scanning speed. Fine textural features (smaller than 1 mm) cannot be encoded by a spatial mechanism given the resolution of touch, which is determined by the density of mechanoreceptors in the skin (Johansson and Vallbo, 1979). The perception of these features, instead, relies on the aforementioned temporal code, consisting of millisecond-scale temporal spiking sequences that require movement between skin and surface. For most natural surfaces, texture perception relies on the integration of these two types of codes – spatial for coarse features, temporal for fine ones. While perceptual invariance across speeds has also been observed for a diverse set of natural textures (Boundy-Singer et al., 2017), its neural basis in cortex has yet to been examined.

In the present study, we seek to fill this gap by directly measuring the responses of neurons in somatosensory cortex – including Brodmann's areas 3b, 1, and 2 – to natural textures scanned over the skin at various speeds, spanning the range used in natural texture exploration (Morley et al., 1983; Gamzu and Ahissar, 2001; Libouton et al., 2010; Tanaka et al., 2014; Callier et al., 2015). We then compare the effect of speed in both cortical and peripheral responses. We find that, while the strength

of the response evoked by textures in tactile fibers is highly speed-dependent (as previously shown), responses in somatosensory cortex are largely speed-independent. This speed independence gives rise to a rate-based texture representation in cortex which, unlike its counterpart in the nerve, is robust to changes in scanning speed. We also find that a subset of neurons in cortex exhibit responses to texture that are temporally patterned, much like those in the periphery, and these sequences scale with speed. The role of these temporal signals in cortex remain to be elucidated as the rate-based code is sufficient to account for our ability to perceive textures across changes in scanning speed.

RESULTS

We recorded texture-evoked responses from 20 tactile fibers (9 SA1, 8 RA, and 3 PC fibers) and 49 neurons from somatosensory cortex (14 from area 3b, 26 from area 1, and 9 from area 2) with receptive fields on the distal fingertip. For the peripheral afferents, each of 55 different textures was scanned over the skin at 3 different speeds (40, 80, and 120 mm/s) using a rotating drum stimulator. For the cortical neurons, each of 10 different textures was scanned over the skin at 4 different speeds (60, 80, 100, and 120 mm/s). This range of speeds, from 40 to 120 mm/s, covers the natural range of speeds used to explore tactile textures (Morley et al., 1983; Gamzu and Ahissar, 2001; Libouton et al., 2010; Tanaka et al., 2014; Callier et al., 2015). We sought to determine the effect of scanning speed on the neural representation of texture, and how these representations change between periphery and cortex.

How does speed affect texture-elicited firing rates?

Texture-elicited firing rates at the periphery were highly speed-dependent (Figure 3.1A). Across the full population, firing rates increased by 28.7% per doubling of the speed when measured over the range of speeds tested (median slope across cells), and by 37.1% between 40 and 80 mm/s, where the speed-dependence of the response is most pronounced. These effects were present among all three afferent types, but their strength differed across types (median slope across cells = 23.1%, 31.7%, 47.2%

increase/doubling, for SA1, RA, and PC afferents, respectively), with the speed dependence of RA and PC responses greater than that of SA1 responses (p=0.023 that speed slopes from RAs & PC afferents > speed slopes from SA1 afferents, one-sided two-sample t-test).

In contrast, texture-elicited firing rates in somatosensory cortex were far less modulated by changes in scanning speed (Figure 3.1B). Across the population, cortical firing rates increased by 13.7% per doubling of speed when measured over the range of speed tested, and by 15.2% between 60 and 120 mm/s. Cortical neurons differed over a range in their speed dependence, however: the distribution of speed effects ranged from entirely flat to as strong as 46% per doubling. There was a slight trend towards weaker speed effects in area 3b, and stronger effects in areas 1 and 2 (6.1%, 14.9%, 21.2% increase/doubling in areas 3b, 1, and 2, p=0.045 that cell slopes in 3b < those in 1 & 2, one-sided two-sample t-test). On average, firing rate increases with speed were larger at the periphery than in somatosensory cortex ($p < 10^{-4}$, two-sample t-test across cells) across both textures (Figure 3.1C) and cells (Figure 3.1D). To verify that this speed invariance was not an artifact of the texture set used in the cortical experiments, we separately analyzed these effects on a subset of four textures was used in both cortical and peripheral experiments and found similar results (Figure 3.S1).

To what extent is texture-specific information robust across changes in speed?

Texture responses exhibit less modulation with speed in somatosensory cortex than they do at the periphery. We thus expected that cross-speed decoding of texture identity would be more robust in somatosensory cortex than at the periphery. To test this, we built a simple classifier to assess how well textures could be identified based on the responses they evoked regardless of speed. The cross-speed classifier performed well if the responses to a given texture at a given speed were similar to responses to that same texture at different speeds. On the other hand, if responses to one texture at one speed were similar to responses to different textures at different speeds, performance suffered. High cross-

speed classification implied that a simple decoder could read out texture identity without the need to "correct" for speed.

While afferent responses generally yielded better within-speed classification than cortical responses (36.1% vs. 23.8%, averaged across all speeds), cross-speed performance exhibited a stronger drop-off with speed for peripheral than cortical classifiers (15.0% vs. 5.2% drop-off per doubling in speed). As a result, cross-speed classification performance based on single neuron responses was similar for periphery and cortex when averaged across all conditions (Figure 3.S2, 23.8% and 22.5% for nerve and cortex, respectively). Thus, at the single cell level, the peripheral representation of texture appears to be as robust to changes across speeds as is its cortical counterpart.

Next, we investigated the degree to which texture identity could be decoded from population responses across scanning speeds. As expected, cross-speed classification performance improved as more tactile fibers or cortical neurons were included in the analysis. However, the performance based on afferent responses grew more slowly with sample size than did performance based on cortical responses (Figure 3.2A). Indeed, while similarly sized populations of peripheral and cortical neurons showed similar within-speed classification performance (93.3% and 87.5% for groups of 20 peripheral and cortical neurons, respectively), peripheral performance dropped off with speed much more steeply than did cortical performance (Figure 3.2B, Figure 3.S2, 58.4% and 37.8% drop-off per speed doubling for groups of 20 peripheral and cortical neurons, respectively). As mentioned above, some neurons in cortex exhibit no significant speed-modulation in their responses (41%, 20/49 neurons. For comparison, only 2 afferents do not). When the above analysis was performed on this population alone, the decline in classification performance over changes in speed was minimal (17.0% drop-off per speed doubling for groups of 20 neurons, Figure 3.S3). At the population level, then, the representation of texture in somatosensory cortex is more robust to changes in scanning speed than is its counterpart in the nerve.

How does speed affect the temporal patterning of texture-elicited responses?

Somatosensory neurons have been shown to encode information not only in their response strength (spike count) but also in their response patterning (spike timing). Relevant here are findings that information about the frequency composition of skin vibrations is encoded in the timing of the responses of both tactile fibers (Talbot et al., 1968; Mackevicius et al., 2012) and cortical neurons (Harvey et al., 2013). When textures are scanned over the skin, they produce characteristic vibrations that depend on both texture and scanning speed (Manfredi et al., 2014) and it is these texture-elicited vibrations that shape the temporal spiking sequences evoked in RA and PC afferents (Weber et al., 2013). Decreases or increases in speed result in dilations or contractions of the skin vibrations, respectively, which in turn drive dilations and contractions in the evoked spiking sequences.

We find that the texture responses of cortical neurons are also temporally patterned, a patterning that is particularly evident for periodic textures (Figure 3.3A, Figure 3.S4A). As is the case at the periphery, texture-elicited spiking sequences scale with speed. This scaling effect can be reversed by correcting for speed, which involves rescaling the spiking sequences to a common spatial scale (Figure 3.S4B). Temporal patterning in cortical responses carries texture information and could in principle contribute to texture constancy if sequences are appropriately rescaled (Figure 3.3B-C). Indeed, cross-speed classification performance improves if (scaled) temporal patterning is taken into consideration, in addition to rate (Figure 3.4, Figure 3.S5). Thus, texture information is contained in the timing of cortical responses, but this information can only be decoded when texture scanning speed is taken into account.

DISCUSSION

The mechanisms of speed invariance

The perception of texture is remarkably invariant with respect to scanning speed. Indeed, psychophysical ratings along the three principal perceptual axes of textures – roughness, hardness, and stickiness – are identical across speeds (Boundy-Singer et al., 2017). Furthermore, the perceived dissimilarity of a pair of textures – which probes texture perception across all of its dimensions and attributes – is very similar whether the two textures are scanned at the same speed or at different speeds. What makes this invariance so remarkable is that the response of tactile nerve fibers are highly speed dependent. Indeed, in the nerve, texture elicited firing rates increase with speed, and temporal spiking sequences, which carry critical texture information, also change with speed. The central result of the present study is that the firing rates evoked in cortical neurons when textured surfaces are scanned across the skin are less susceptible to changes in speed than are their peripheral counterparts. This reduction in the speed dependence yields a representation of texture that is much easier to decode, as speed no longer needs to be corrected for.

The computation that underlies the emergence of this invariance remain to be elucidated. The coding of coarse features is predicated on spatial patterns of activation across populations of nerve fibers, and texture-specific patterns are tolerant to changes in scanning speed (Johnson and Lamb, 1981; Phillips et al., 1992). Indeed, at successive time points, the neural image is shifted in the direction of motion, but its configuration does not otherwise change. In contrast, the coding of fine features is predicated upon temporal patterns of activation within individual nerve fibers, and these patterns are highly susceptible to changes in scanning speed (as described above). Perceived roughness depends not only on the spatial image carrying coarse texture information but also on the temporal spiking patterns carrying fine

texture information (Weber et al., 2013; Lieber et al., 2017). Specifically, the spatial variation in SA1 afferent responses and the temporal variation in RA and PC responses accurately predicts the perceived roughness of a surface.

In cortex, firing rates carry enough texture information to yield high classification accuracy and can account both for perceptual judgments of the roughness of textures and for judgments of the perceived dissimilarity of texture pairs (Lieber and Bensmaia, 2018)(in review). Thus, the information about texture that is conveyed in the timing of the responses is converted, at least in part, to a rate-based code in cortex. This conversion involves a computation of the spatial and temporal variation in afferent input. The spatial variation computation is revealed in the spatial RFs of cortical neurons, which comprise excitatory and inhibitory subfields (DiCarlo and Johnson, 2000; Bensmaia et al., 2008). Similarly, cortical responses to vibration suggest that individual neurons act as differencing filters of their time-varying afferent input (Saal et al., 2015). Texture responses across speed suggest that the transformation from periphery to cortex, characterized by a variation computation, yields a cortical representation that is less speed dependent on speed that is its peripheral counterpart. This phenomenon cannot be straightforwardly attributed to the well-established phenomenon of divisive normalization because roughness is also encoded in the population firing rate and so would be eliminated along with speed in the rate code.

A contribution of spike timing?

As mentioned above, a subpopulation of cortical neurons produces responses to vibratory stimuli that can phase lock at frequencies up to 800 Hz (Harvey et al., 2013). These neurons, which receive strong input from PC fibers (Saal et al., 2015), also produce patterned responses to textures, even for textural elements too close together to be resolved spatially. This temporal patterning improves the performance of classifiers when integrated with firing rates. Whether temporal patterning in cortex

plays a role in texture perception remains to be elucidated. Indeed, rate-based signals are not only highly informative about texture but also highly predictive of texture perception. Parsimony might then point to the firing rates as the basis for texture coding in cortex. However, the evidence suggests that temporally coded texture information is converted at least in part into the rates between periphery and somatosensory cortex (Lieber and Bensmaia, 2018). One possibility is that the temporal patterning in the responses of neurons in areas 3b, 1, and 2, is in turn rolled into firing rates downstream along the neuraxis. Indeed, along the auditory neuraxis, temporally coded information is progressively converted to a rate-based code (Saal et al., 2016). The absence of temporal patterning in primary auditory cortex, contrasted with its presence in primary somatosensory cortex, can be attributed to the greater number of synapses interposed between cortex and periphery in hearing than touch. Recordings from cortical structures downstream from areas 3b, 1, and 2 will help elucidate the role in texture processing, if any, of the temporal patterning described here.

METHODS

Experimental Methods

Cortical Texture Responses

The methods for recording the responses evoked in the somatosensory cortex of macaques to textured surfaces scanned across the fingertip have been previously described in detail (Lieber and Bensmaia, 2018). In brief, extracellular recordings were made in the postcentral gyri of three hemispheres of three macaque monkeys (all male, 6-8 yrs old, 8-11 kg). On each recording day, a multielectrode microdrive (NAN Instruments, Nazaret Illit, Israel) was loaded with three electrodes (tungsten, Epoxylite insulated, FHC Inc.), spaced 650 µm apart, which were driven into cortex until they encountered neurons from Brodmann's areas 3b, 1, and 2 of with RFs on the distal fingerpad of digits 2-5. The respective cortical modules were identified based on anatomical landmarks, RF location, and response properties.

Recordings were obtained from neurons that met the following criteria: (1) action potentials were well isolated from the background noise, (2) the finger could be positioned such that the textured surface impinged on the center of the RF, and (3) the neuron was clearly driven by light cutaneous touch. Isolations had to be maintained for at least 30 minutes to complete 5 repetitions of the basic texture protocol. Responses from 49 single units were obtained for the speed protocol: 14 units from area 3b, 26 units from area 1, and 9 units from area 2. In this protocol, ten textures were presented at 4 different speeds: 60, 80, 100, and 120 mm/s (all ± 1.1 mm/s). Four of these textures (satin, chiffon, nylon, and hucktowel) were also used in our recordings of afferent responses (see below) and 6 were not (fabric grating [wide spacing], sunbrella upholstery, fuzzy upholstery, faux croc skin, 7.7 mm dots, 7.7 mm dots / 1 mm grating overlay). The order in which scanning speed was selected was pseudo-random for each texture and each texture was presented 5 times at each speed, for 2.3, 1.7, 1.4, and 1.2 seconds at 60, 80, 100, and 120 mm/s, respectively.

Peripheral Texture Responses

Our methods for recording afferent responses to textured stimuli have been previously described in detail (Weber et al., 2013; Lieber et al., 2017). In brief, we recorded the responses of tactile fibers to 55 textured surfaces scanned over the fingertip, including natural textures such as fabrics, sandpapers, as well as plastic gratings and embossed dots. We analyzed the texture responses of a subset of 20 afferents (9 SA1, 8 RA, and 3 PC fibers) for which we had data at 3 different scanning speeds, namely 40, 80, and 120 mm/s (all ± 0.1 mm/s). Recordings were collected from afferents innervating the distal fingertip in the median and ulnar nerves, using standard methods (Talbot et al., 1968). Anesthesia was maintained using isoflurane.

In these experiments, texture presentation was blocked by speed rather than by texture, as was the case in the cortical experiments. That is, we first recorded the response of afferents to all textures at 80

mm/s, then at 40 mm/s or 120 mm/s, and in the third block at the remaining speed. Our analyses only consider responses during the steady-state contact period for force and speed, which lasted for at 2, 1, and 0.5 seconds, at 40, 80, and 120 mm/s, respectively.

Analysis

Firing rates and speed effects

Firing rates were calculated over the same length of texture, rather than over the same duration of time. Peripheral firing rates were calculated over the full period of 2, 1, and 0.5 seconds, at 40, 80, and 120 mm/s, respectively. Cortical firing rates were calculated over the full period of 2.3, 1.7, 1.4, and 1.2 seconds at 60, 80, 100, and 120 mm/s, respectively.

We report speed effects in units of percentage change per doubling of speed. To calculate these values, we first normalized each cell's response to each texture (across all speeds) by dividing each response (firing rate) by the mean response at 80 mm/s. We then averaged these normalized values across all textures to get a mean normalized response at each speed for each cell. We then calculated each cell's best fit line to (normalized) firing rates vs. $\log_2(speed)$. Our reported speed effects are the slopes of these best fit lines.

Identifying speed-sensitive neurons

Many neurons in somatosensory cortex exhibited almost no modulation with changes in speed. To split neurons into speed-sensitive and speed-insensitive categories, we again performed a regression for each cell, this time using every texture's mean firing rate response at every speed (55x3 conditions at the periphery, 10x4 conditions in cortex). We tested the significance of each slope using an F-test on the regression residuals ($F(1,164)$ for the periphery, $F(1,39)$ for cortex). Cells with $p < 0.05$ were considered significantly speed-sensitive. By this metric, only 29/49 cortical cells showed significant speed sensitivity,

while 18/20 peripheral afferents showed significant speed sensitivity (the 2 that did not were both SA1 afferents).

Classification: peripheral and cortical comparison

To directly compare the ability of the peripheral and cortical populations to encode texture information across speeds, we implemented a nearest neighbor classifier based on firing rates. Specifically, on each iteration, we selected two 250 ms subsets of each neuron's texture response – one from the first half of its response to each texture at one speed, and one from the second half of the response to each texture at another speed. Next, we calculated the mean absolute distance between each pairing of trials from the first half (same speed) and second half response vectors, such that we had a 10x10 distance matrix of each possible pairing of the 10 textures. These distances were then averaged across the neural population, to get a final set of pairwise distances between textures. For each texture, the texture from the second set that yielded the lowest distance was selected; if the textures matched, classification was marked as correct. Performance was averaged across both conditions (training on first half, testing on the second half, and vice versa), all textures, and across 200 random iterations of time windows and texture sets. This procedure was repeated for neuron groups of different sizes. To compare cortical and peripheral classification performance, we randomly selected 10 textures for the peripheral data set (so that it matched its cortical counterpart in size) to carry out this analysis and repeated this procedure with different sets of 10 textures.

Frequency analysis

We sought to characterize the phase-locking properties of cortical neurons. To do so, we first binned spike trains into 0.2 ms bins. Next, we computed the fast Fourier transform of that binned spike train and, from it, its amplitude spectrum. Finally, we computed the mean amplitude spectrum across repeated presentations for each texture, and across the population of neurons.

Timing patterns and classification

We sought to characterize the temporal structure of cortical responses. To this end, we created peri-stimulus time histograms (PSTHs) for each neuron's spiking response. PSTHs were created by convolving each spike train with a Gaussian distribution (σ = 5 ms) and then binning the outcome into 1 ms bins. We noticed that spiking patterns showed spatial, but not temporal, constancy (Figure 3.3). To create spatial PSTHs, we transferred our temporal PSTHs to spatial units (120 μm bin size), interpolating when necessary.

Next, we sought to characterize the extent to which these PSTHs were informative about texture. First, we split each of our PSTHs into two halves – a training set (the first two thirds of a texture's response, 72 mm, corresponding to 1200, 900, 720, 600 ms at 60, 80, 100, 120 mm/s, respectively) and a testing set (the last third of the response, 36 mm, corresponding to 600, 450, 360, 300 ms at 60, 80, 100, 120 mm/s, respectively). Second, we split each neuron's 5 repetitions into two sets: 4 of the 5 repetitions were assigned to the training set (using the first period), and the fifth was assigned to the test set (using the second period). The 4 training repetitions were averaged together for each texture, such that each neuron had 10 averaged training set traces and 10 single-trial test set traces (one for each texture). Third, to maximally align traces from the test set to trace in the training set, we performed a cross-correlation between each test set trace and each training set trace, and found the maximum possible correlation between the two. We averaged these correlation values across all neurons and then, for each texture in the test set, selected the training set texture with the maximum correlation. If the selected training set texture corresponded to the test set texture, classification was correct. Performance was averaged across all textures, all combinations of repetitions, and multiple randomly sampled populations for each sample size. We repeated this procedure for every possible combination of speeds for the training and testing sets, and performed it separately for both temporal PSTHs and spatial PSTHs.

We compared this PSTH classification performance to the classification performance of a firing rate code, implemented using a similar approach. First, we defined a training period (the first 600 ms of the sustained response) and a test period (the 300 ms following that period) for each trial. We tested our results with the firing rates from time periods equivalent to those used during the timing classification, and found comparable results. Second, as with the PSTHs, we split the repetitions into training and testing sets (4 and 1) and computed 1) the firing rate response within 300-ms windows within the training period (1 ms steps, 300 windows total, averaged across repetitions) and 2) the firing rate evoked on each 300-ms test trial. Third, for each texture's test trial, we found the minimum absolute distance between its firing rate and the firing rates across all windows for each training texture, such that we had 10 distance values for each test trial. We averaged these distances over all neurons, and then, for each texture in the test set, selected the training set texture with the minimum distance. Again, if the selected training set texture corresponded to the test set texture, classification was correct. Performance was averaged across all textures, all sets of repetitions, and multiple samples for each sample size, and repeated for every possible combination of speeds for the training and testing sets.

Finally, we assessed whether the combination of rate and timing (in spatial units) would yield better classification performance than each metric separately. To this end, we computed both distance matrices, using the methods described above, for identical populations of neurons. We then looked for the minimum possible distance using a combined distance matrix:

$$D_{both} = D_{rate} - k * D_{PSTH}$$

where *k* was a parameter we could vary to relatively weight the importance of firing rate or the PSTH. We performed classification over a wide range of *k* values (51 logarithmic steps between $k=10^{-6}$ and $k=10^{7}$), which yielded analyses ranging from a pure rate code and a pure temporal code. For each pair of training and testing speeds, we selected value of *k* that resulted in the best performance.

REFERENCES

Avidan G, Harel M, Hendler T, Ben-Bashat D, Zohary E, Malach R (2002) Contrast sensitivity in human visual areas and its relationship to object recognition. J Neurophysiol 87:3102–3116.

Bensmaia SJ, Denchev P V, Dammann JF, Craig JC, Hsiao SS (2008) The representation of stimulus orientation in the early stages of somatosensory processing. J Neurosci 28:776–786.

Boundy-Singer ZM, Saal HP, Bensmaia SJ (2017) Speed Invariance of Tactile Texture Perception. J Neurophysiol 118:jn.00161.2017.

Cadieu CF, Hong H, Yamins DLK, Pinto N, Ardila D, Solomon EA, Majaj NJ, DiCarlo JJ (2014) Deep Neural Networks Rival the Representation of Primate IT Cortex for Core Visual Object Recognition. PLoS Comput Biol 10.

Callier T, Saal HP, Davis-Berg EC, Bensmaia SJ (2015) Kinematics of unconstrained tactile texture exploration. J Neurophysiol:jn.00703.2014.

Croner LJ, Kaplan E (1995) Receptive fields of P and M ganglion cells across the primate retina. Vision Res 35:7–24.

Dépeault A, Meftah E-M, Chapman CE (2013) Neuronal correlates of tactile speed in primary somatosensory cortex. J Neurophysiol 110:1554–1566.

DiCarlo JJ, Johnson KO (1999) Velocity invariance of receptive field structure in somatosensory cortical area 3b of the alert monkey. J Neurosci 19:401–419.

DiCarlo JJ, Johnson KO (2000) Spatial and temporal structure of receptive fields in primate somatosensory area 3b: effects of stimulus scanning direction and orientation. J Neurosci 20:495–510.

Enroth-Cugell C, Robson JG (1966) The contrast sensitivity of retinal ganglion cells of the cat. J Physiol 187:517–552.

Finn IM, Priebe NJ, Ferster D (2007) The Emergence of Contrast-Invariant Orientation Tuning in Simple Cells of Cat Visual Cortex. Neuron 54:137–152.

Gamzu E, Ahissar E (2001) Importance of temporal cues for tactile spatial- frequency discrimination. J Neurosci 21:7416–7427.

Goodwin AW, Morley JW (1987a) Sinusoidal Movement of a Grating Across the Monkey's Fingerpad: Representation of Grating and Movement Features in Afferent Fiber Responses. J Neurosci 7:2168–2180.

Goodwin AW, Morley JW (1987b) Sinusoidal movement of a grating across the monkey's fingerpad: effect of contact angle and force of the grating on afferent fiber responses. J Neurosci 7:2192–2202.

Handel S, Erickson ML (2001) A Rule of Thumb: The Bandwidth for Timbre Invariance Is One Octave. Music Percept 19:121–126.

Harvey MA, Saal HP, Dammann JF, Bensmaia SJ (2013) Multiplexing Stimulus Information through Rate and Temporal Codes in Primate Somatosensory Cortex. PLoS Biol 11.

Johansson R, Vallbo Å (1979) Tactile sensibility in the human hand: relative and absolute densities of four types of mechanoreceptive units in glabrous skin. J Physiol:283–300.

Johnson K, Lamb G (1981) Neural mechanisms of spatial tactile discrimination: neural patterns evoked by braille-like dot patterns in the monkey. J Physiol:117–144.

Joris PX, Bergevin C, Kalluri R, Mc Laughlin M, Michelet P, van der Heijden M, Shera CA (2011) Frequency selectivity in Old-World monkeys corroborates sharp cochlear tuning in humans. Proc Natl Acad Sci 108:17516–17520.

Lederman SJ (1974) Tactile roughness of grooved surfaces: The touching process and effects of macro- and microsurface structure. Percept Psychophys 16:385–395.

Lederman SJ (1981) The perception of surface roughness by active and passive touch. Bull Psychon Soc 18:253–255.

Lederman SJ, Taylor MM (1972) Fingertip force, surface geometry, and the perception of roughness by active touch. Percept Psychophys 12:401–408.

Libouton X, Barbier O, Plaghki L, Thonnard JL (2010) Tactile roughness discrimination threshold is unrelated to tactile spatial acuity. Behav Brain Res 208:473–478.

Lieber JD, Bensmaia SJ (2018) High-Dimensional Representation of Texture in the Somatosensory Cortex of Primates.

Lieber JD, Xia X, Weber AI, Bensmaia SJ (2017) The Neural Code for Tactile Roughness in the Somatosensory Nerves. J Neurophysiol:jn.00374.2017.

Mackevicius EL, Best MD, Saal HP, Bensmaia SJ (2012) Millisecond Precision Spike Timing Shapes Tactile Perception. J Neurosci 32:15309–15317.

Manfredi LR, Saal HP, Brown KJ, Zielinski MC, Dammann JF, Polashock VS, Bensmaia SJ (2014) Natural scenes in tactile texture. J Neurophysiol 111:1792–1802.

Marozeau J, de Cheveigné A, McAdams S, Winsberg S (2003) The dependency of timbre on fundamental frequency. J Acoust Soc Am 114:2946.

Meftah el-M, Belingard L, Chapman CE (2000) Relative effects of the spatial and temporal characteristics of scanned surfaces on human perception of tactile roughness using passive touch. Exp Brain Res 132:351–361.

Morley JW, Goodwin AW, Darian-Smith I (1983) Tactile discrimination of gratings. Exp Brain Res 49:291–299.

Phillips JR, Johansson RS, Johnson KO (1992) Responses of human mechanoreceptive afferents to

embossed dot arrays scanned across fingerpad skin. J Neurosci 12:827–839.

Saal HP, Harvey MA, Bensmaia SJ (2015) Rate and timing of cortical responses driven by separate sensory channels. Elife 4.

Saal HP, Suresh AK, Solorzano LE, Weber AI, Bensmaia SJ (2017) The effect of contact force on the responses of tactile nerve fibers to scanned textures. Neuroscience.

Saal HP, Wang X, Bensmaia SJ (2016) Importance of spike timing in touch: an analogy with hearing? Curr Opin Neurobiol 40:142–149.

Sachs MB, Young ED (1979) Encoding of steady-state vowels in the auditory nerve: Representation in terms of discharge rate. J Acoust Soc Am 66:470.

Sadagopan S, Wang X (2008) Level Invariant Representation of Sounds by Populations of Neurons in Primary Auditory Cortex. J Neurosci 28:3415–3426.

Sinclair RJ, Burton H (1991) Neuronal activity in the primary somatosensory cortex in monkeys (Macaca mulatta) during active touch of textured surface gratings: responses to groove width, applied force, and velocity of motion. J Neurophysiol 66:153–169.

Talbot WH, Darian-Smith I, Kornhuber HH, Mountcastle VB (1968) The Sense of Flutter Vibration Comparison of the Human Capacity With Response Patterns of Mechanoreceptive Afferents From the Monkey Hand. J Neurophysiol 31:301.

Tanaka Y, Bergmann Tiest WM, Kappers AML, Sano A (2014) Contact force and scanning velocity during active roughness perception. PLoS One 9.

Walker KMM, Bizley JK, King AJ, Schnupp JWH (2011) Multiplexed and Robust Representations of Sound Features in Auditory Cortex. J Neurosci 31:14565–14576.

Weber AI, Saal HP, Lieber JD, Cheng J-W, Manfredi LR, Dammann JF, Bensmaia SJ (2013) Spatial and temporal codes mediate the tactile perception of natural textures. Proc Natl Acad Sci U S A 110:17107–17112.

Yau JM, Hollins M, Bensmaia SJ (2009) Textural timbre: The perception of surface microtexture depends in part on multimodal spectral cues. Commun Integr Biol 2:344–346.

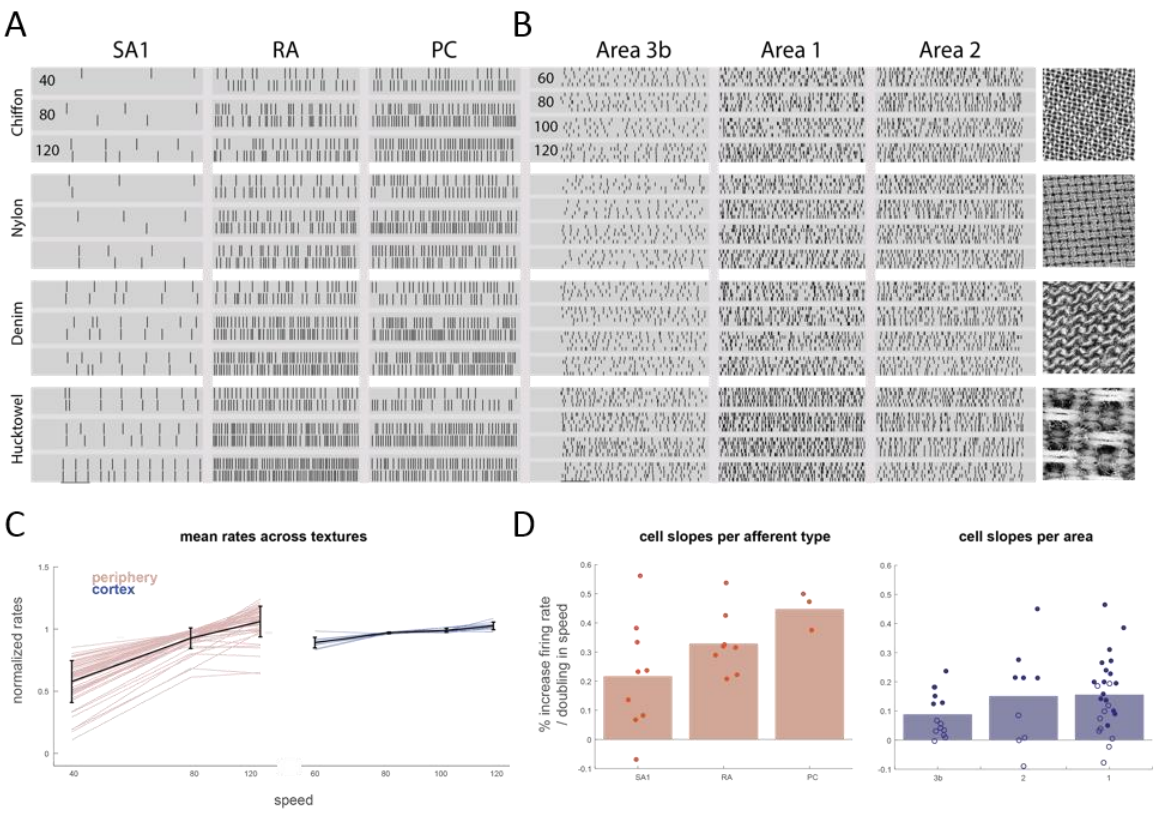

Figure 3.1. **Speed-dependent firing rates at the periphery and in cortex**. A-B| Spiking responses of one afferent of each type and one neuron from each cortical module to four textures scanned across the skin at different speeds. Surface profiles of the 4 example textures are shown to the far right. Texture responses at the periphery are highly-speed dependent, while texture responses in cortex are much less so. C| The mean normalized population response of peripheral (left) and cortical (right) neurons is plotted as a function of speed, for each individual texture (colored lines, red-periphery, blue-cortex) and averaged across all texture (black). D| The slope of the speed effect is plotted for peripheral afferents (split by type) and for cortical neurons (split by cortical area). The slopes of individual neurons are plotted as points. Filled points denote cortical neurons whose slope was significantly greater than zero (i.e. speed-dependent).

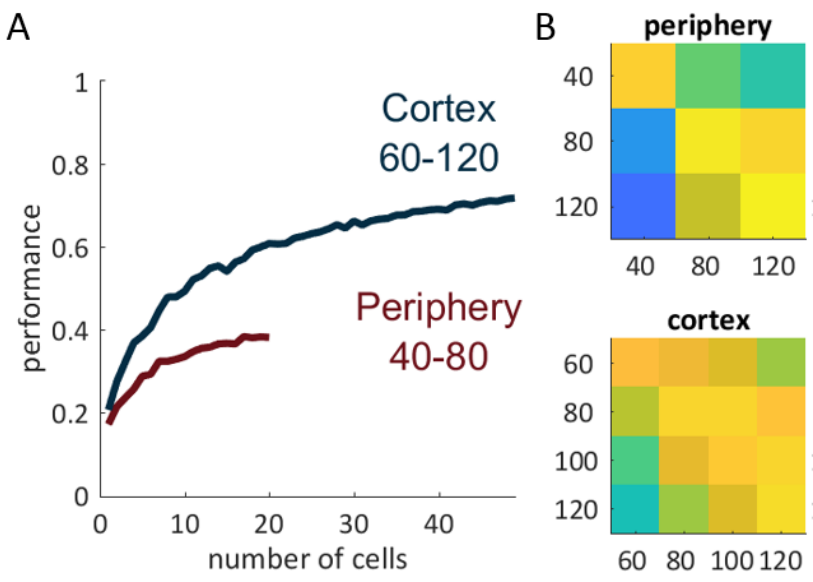

Figure 3.2**. Cross-speed classification performance at the periphery and in cortex.** A| Cross-speed classification performance for groups of tactile fibers (red, between data at 40 and 80 mm/s) and cortical neurons (blue, between data at 60 and 120 mm/s). Peripheral classification was between randomly selected groups of 10 textures. Cortical classification was between the full recorded set of 10 textures. B| Summary of cross-speed classification results for the peripheral population (top) and cortical populations (20 neurons). Populations of cortical neurons carry a texture signal that is more speed tolerant than do their peripheral counterparts.

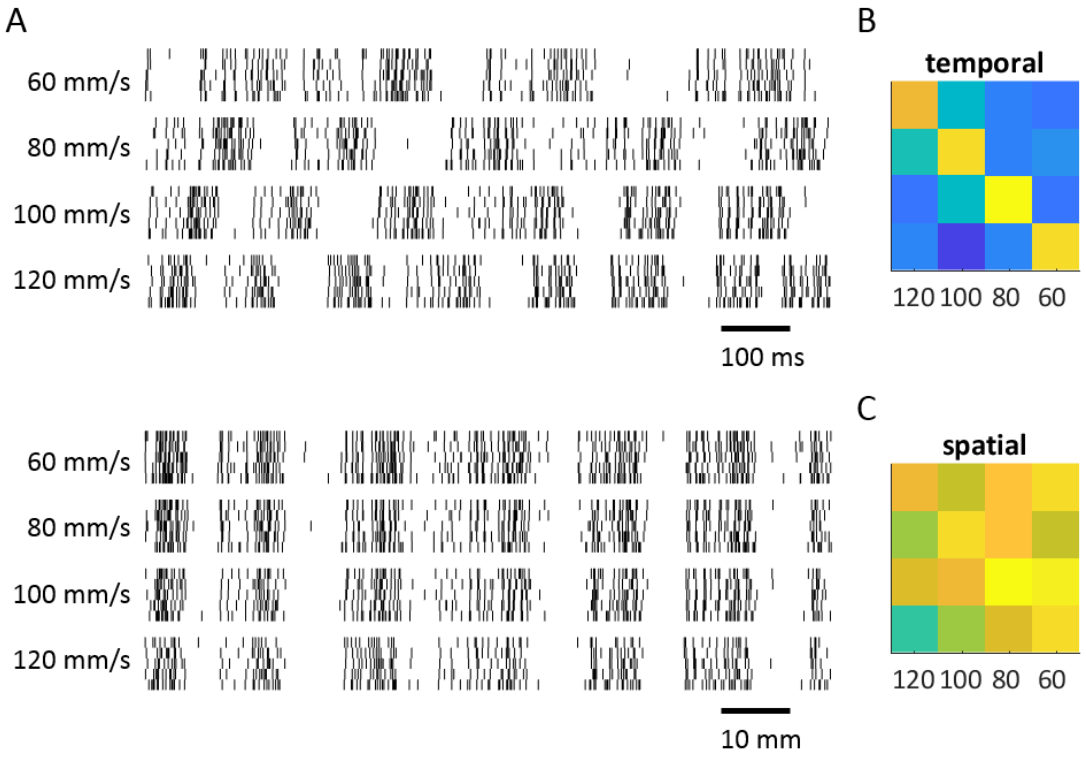

Figure 3.3. **Cortical responses exhibit spatial, but not temporal, constancy across speeds.** A| Spiking responses of an example cortical neuron when a texture (faux croc skin) is scanned over the skin (top) at four different speeds. The spike patterns exhibit constancy when plotted in spatial units (bottom). B| Population classification performance based on matching PSTH shapes within and across speeds. Temporal patterns can only reliably be used for classification within speed. C| Population classification performance based on PSTHs that are warped (proportional to their scanning speed) into spatial units. When using spatial information the PSTHs are informative across speeds.

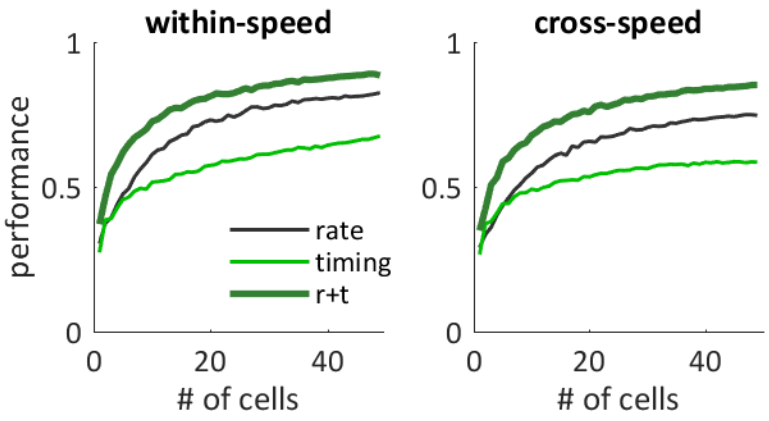

Figure 3.4. **Classification using rate and warped timing.** Classification performance is plotted as a function of cortical group size for comparisons within speed (left) and across speeds (right). Results are plotted for three conditions: rate classification (light green), classification of warped PSTHs (i.e. converted to spatial units, black), and a classification scheme using a combination of both metrics (dark green). Exploiting the structure in the PSTHs leads to improved classification.

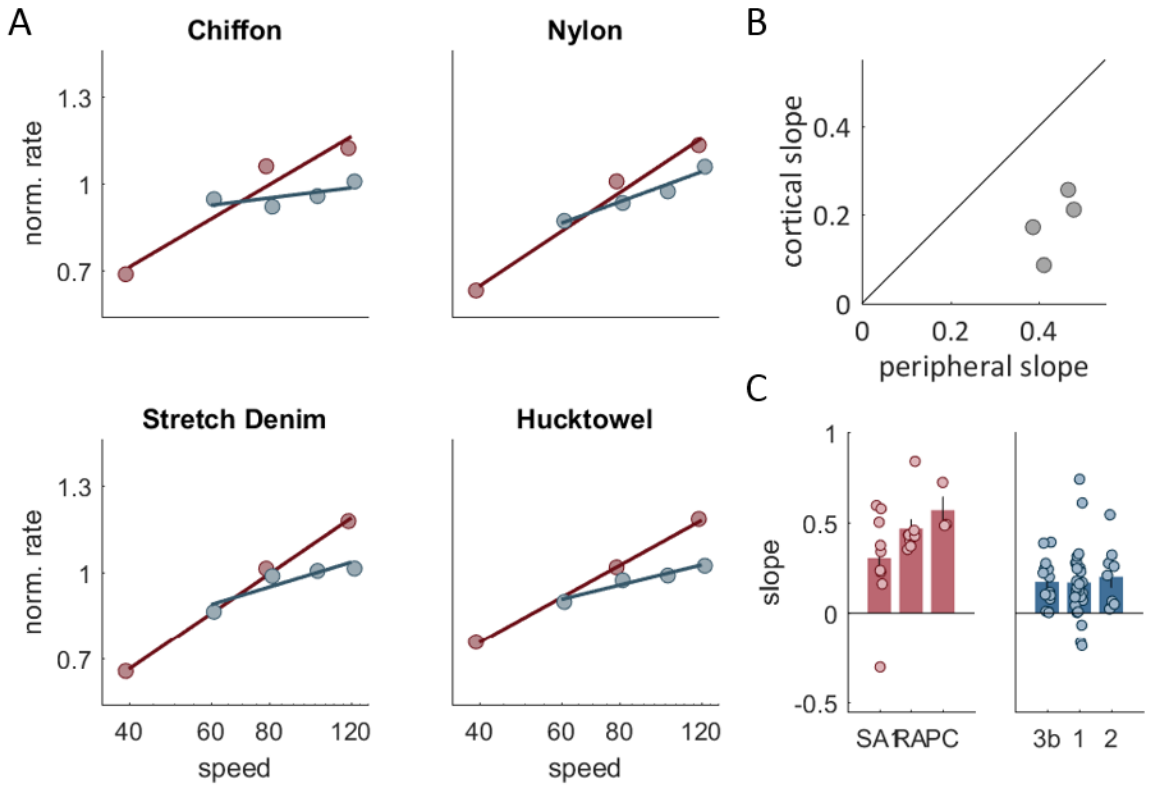

Figure 3.S1. **Effect of speed on stimuli used in the peripheral and cortical data sets.** A| The mean population response of peripheral (red) and cortical (blue) neurons is plotted as a function of speed for four textures shared between the two data sets. Lines represent lines of best fit. B| The slope of the best fit line for cortical neurons is plotted against the slope of the corresponding best fit line for tactile fibers. For each texture, cortical rates increase more slowly than do peripheral rates. C| The mean slope of the speed effect across just these four textures is plotted for peripheral afferents (split by type into SA1, RA, and PC groups) and for cortical neurons (split by cortical area). Slopes of individual neurons are plotted as points. Peripheral slopes are consistently higher than cortical slopes.

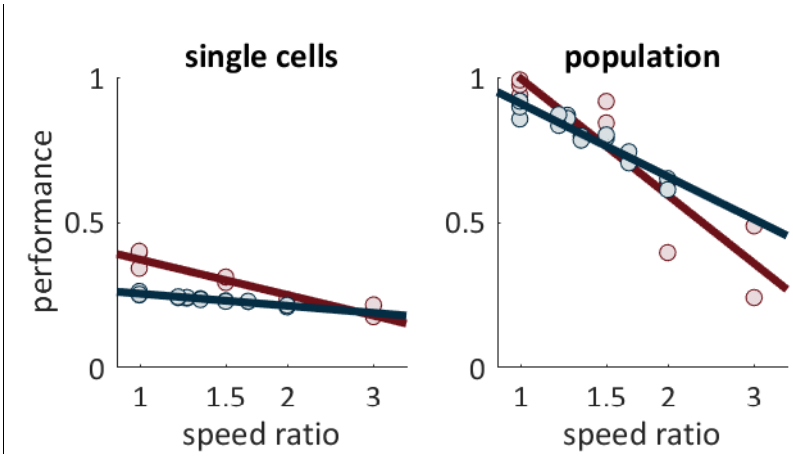

Figure 3.S2. **Classification performance decreases with speed difference.** Classification performance is plotted against the ratio of the speeds used for testing and training the data, for individual neurons (left) and for populations of neurons (right, N=20). A speed ratio of one represents within-speed classification, while a speed ratio of two represents a doubling in speed (e.g training at 80 mm/s and testing at 40 mm/s). Points denote the mean performance across groups of neurons and groups of textures (N=10), plotted for populations of neurons at the periphery (red) and in cortex (blue) neurons. Lines represent lines of best fit. Peripheral classification exhibits a stronger performance drop-off with speed than does cortical classification, especially at the population level.

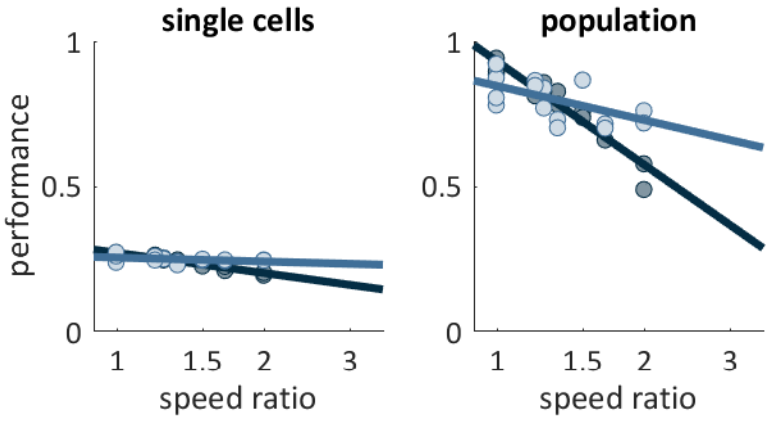

Figure 3.S3. **Classification performance in subgroups of cortical neurons.** Cortical neurons were split into groups that showed significant modulation in response to changes in speed (N=29, dark blue) and those that did not (N=20, light blue). Classification performance is plotted against the ratio of the speeds used for testing and training the data, for individual cells (left) and populations of neurons (right, groups of 20 cells). Points are the mean performance across groups of speed-sensitive and speed-insensitive neurons. Lines represent lines of best fit. Speed-sensitive neurons show a drop-off in performance comparable to peripheral neurons (Figure 3.S2), while speed-insensitive neurons show very little drop-off over large changes in speed.

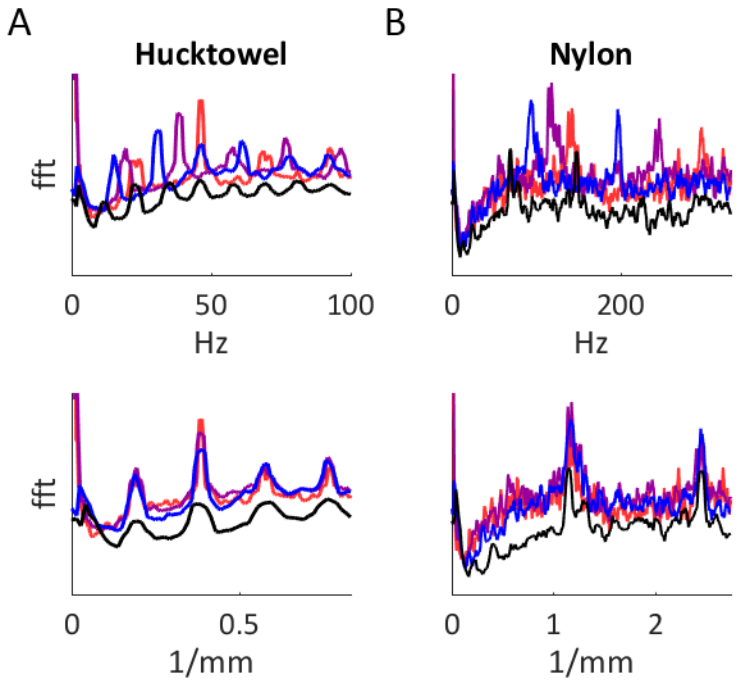

Figure 3.S4. **Amplitude spectra of cortical responses.** A| The temporal (top) and spatial (bottom) frequency composition of the responses of cortical neurons to two textures scanned over the skin. Spectra are averaged across the full population of cortical neurons. Responses show that temporal frequency composition shifts with speed but spatial frequency composition is consistent across speeds. B| For nylon, spectra are averaged over a subset of strongly PC-like neurons (N=5, PC regression weight > 0.8). Amplitude peaks predictably shift even for temporal frequencies in the PC range (100-300 Hz).

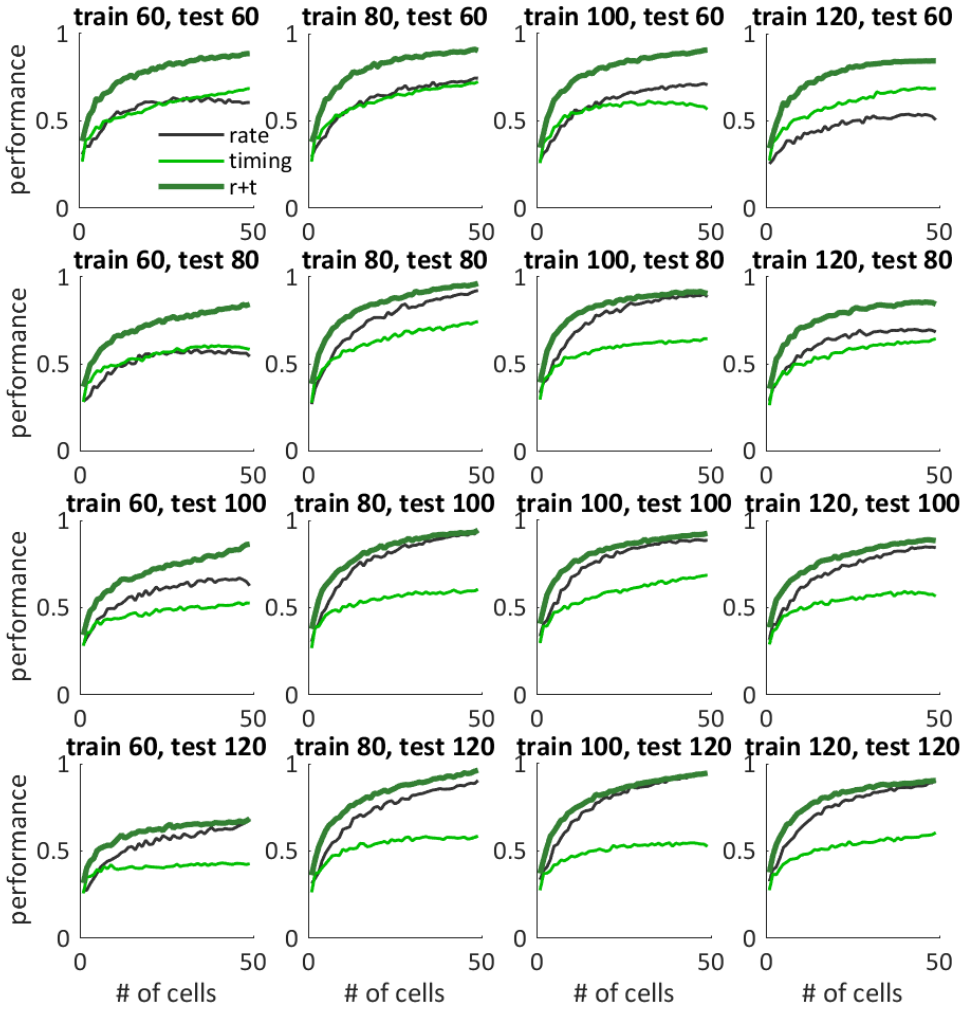

Figure 3.S5. **Breakdown of cortical population classification across all speed conditions.** As in Figure 3.4, classification performance is plotted as a function of cortical group size, for three conditions: rate classification (light green), classification of warped PSTHs (black), and a combination of both metrics (dark green). Each plot shows a different combination of training speed and testing speed (at either 60, 80, 100, or 120 mm/s). For many individual conditions, using PSTH structure for classification provides an advantage over just using rate.

CONCLUSIONS

Summary of results

Over the course of the previous three studies, we sought to explain the peripheral and cortical neural mechanisms that underlie the perception of natural texture. In the first, we show that no single population of peripheral afferents can explain the perception of texture roughness. Rather, texture roughness is built up from a combination of two streams of information: one encoded in the spatial pattern of activity across SA1 afferents, and another in the temporally precise spiking activity of RA and PC afferents.

In the second study, we first show that somatosensory cortex encodes texture information in a high-dimensional representation that is distributed across the full population of active cortical neurons. Next, we demonstrate that differences in the functional role of cortical neurons is predicted by the strength of their submodality input: neurons whose response to texture is most similar to SA1 afferents show a specialization for representing coarse textural features, and neurons whose responses are most similar to PC afferents show a specialization for fine features. Finally, we show that both of these populations are necessary to explain the multidimensional space of texture perception.

In the third study, we show that somatosensory cortex contains a speed-invariant representation of texture. Specifically, we find that, while the firing rate responses of peripheral afferents are highly dependent on the relative scanning speed of a texture, cortical responses were more heterogeneous. While some cortical neurons showed firing rate responses with a similar speed-dependence to peripheral afferents, others were almost entirely speed-independent. Thus, the population representation in somatosensory cortex supports a speed-invariant percept of texture, while the peripheral representation does not.

Spatial and temporal codes for touch

Touch has long been thought to depend on two mechanisms – one based on spatial form, and another based on vibrational cues (Katz, 1925). The early evidence for these two mechanisms was based on a simple fact – that our perception of a surface is radically different depending on whether we indent our finger into it or scan our finger over the surface. It is only with relative motion between the surface and the finger that we gain access to information about the fine microgeometry of the surface (Hollins and Risner, 2000; Hollins et al., 2001).

Our laboratory recently characterized the peripheral neural substrates underlying these complementary perceptual mechanisms (Weber et al., 2013). Spatial form is encoded in the spatial pattern of activation across SA1 and RA afferents, while vibrational cues are carried in the fine timing of RA and PC afferents. Furthermore, in Chapter 2 we directly demonstrate that, in contrast to the conclusions of previous studies (Blake et al., 1997a; Yoshioka et al., 2001), the perception of texture cannot be explained by a purely SA1-mediated spatial code for texture information. Instead, the sensitivity of RA and PC afferents to skin vibrations plays a much larger role than previously appreciated.

The involvement of RA and PC afferents in texture perception helps explain some previously contradictory psychophysical results. First, while spatial patterning is a critical for encoding the perception of embossed dot patterns (Connor and Johnson, 1992), the ability to discriminate sandpapers is uncorrelated with spatial acuity (Libouton et al., 2010). Second, our ability to discriminate texture is significantly impaired by the vibrotactile adaptation of PC afferents (Hollins et al., 2001). Third, while spatial patterns of forces in the skin can predict the roughness of periodic gratings (Taylor and Lederman, 1975), skin vibrations are highly predictive of how rough a surface without obvious spatial features will feel (Hollins et al., 2000b; Bensmaia and Hollins, 2003; Bensmaïa and Hollins, 2005;

Libouton et al., 2012). Thus, neural signals from both the spatial and temporal modes of tactile perception must be combined to fully explain texture perception.

Spatial coding at the somatosensory periphery

Our data support the longstanding theory that the perceived roughness of a texture depends on the variability across the peripheral spatial image, rather than on a simple mean firing rate code (Connor et al., 1990; Connor and Johnson, 1992). However, in contrast to previous results (Blake et al., 1997a), they also emphasize the role of RA afferents in the construction of texture perception. Thus, these data reopen a key question – to what extent do RA afferents contribute to the processing and perception of spatial form? Specifically, our data are consistent with two possibilities: 1) that texture roughness depends on the spatial variability across both the SA1 and RA populations of afferents, or 2) that roughness depends on the spatial variability across *only* the SA1 population of afferents, and that RA afferents contribute primarily through their temporal signals.

A number of results suggest that RA afferents are poor mediators of spatial information for statically indented stimuli. First, RA afferents fire only transiently to statically indented stimuli, and thus have only a limited time to encode spatial information. Second, orientation-selective responses in somatosensory cortex are initially weak, and only reach full selectivity well after RA afferents have stopped firing (Bensmaia et al., 2008). Third, RA afferents can be made to respond tonically to indented stimuli through the use of imposed vibrations. These vibrations preserve spatial patterning in the SA1 population and drive spatial patterning in the RA populations (Bensmaïa et al., 2006b), but degrade the ability of subjects to discriminate these spatial forms (Bensmaïa et al., 2006a). This suggests that tonic RA afferent activation interferes with the ability of the somatosensory system to decode indented spatial form. However, when the finger scans over a surface, RA afferents are robustly activated throughout the extent of the contact period and reliably encode information about spatial form

(Johnson and Lamb, 1981; Connor et al., 1990; Connor and Johnson, 1992; Blake et al., 1997a, 1997b). In other words, while the transient or anomalous activation of RA afferents during static contact may not benefit spatial perception, their naturalistic activation during dynamic contact may still drive the perception of spatial patterns.

Notably, a number of textures in our set robustly activate RA and PC afferents, but not SA1 afferents. This set includes a number of simple gratings that could be reproduced using modern 3D printing techniques. Mirroring the approach of previous studies (Connor et al., 1990; Connor and Johnson, 1992) it would be straightforward to produce "dot patterns," only with inset gratings in the place of raised elements. These stimuli would create spatial patterns of activity that selectively activate RA and PC afferents, without activating SA1 afferents. Furthermore, we could approximate the neural response to these textures, either through reproductions based on previously recorded data, or with new predictions using our lab's model of skin mechanics and afferent transduction (Saal et al., 2017). These data would help us converge on stimuli that produce a maximally divergent prediction between the temporal and spatial variation hypotheses and allow us to test our theory through psychophysical assays.

Spatial coding in somatosensory cortex

Perceptual studies of texture predict that the peripheral representation of spatial features will be subject to spatial differentiation as it ascends the somatosensory neuraxis (Connor and Johnson, 1992). This prediction is borne out in somatosensory cortex, where nearly all neurons show differentiating structure in their receptive fields (Figure D.1A) (DiCarlo and Johnson, 2000; Sripati et al., 2006). In other words, first-order spatial patterns at the periphery are, by the time they reach cortex, transformed into an explicit firing rate code.

This spatial differentiation process draws a strong analog with primary visual cortex (V1), where spatial differentiation has also been well characterized (Figure D.1B) (Hubel and Wiesel, 1962; Jones and Palmer, 1987). Indeed, in both cases, this spatial differentiation endows neurons with selective responsiveness to edge orientation (Hubel and Wiesel, 1968; Bensmaia et al., 2008). Perhaps less obviously, spatial differentiation is also a feature of frequency selectivity in auditory cortex (A1). At the auditory periphery, vibrations in the cochlea undergo spectral decomposition and are transduced into neural signals by a tonotopic array of peripheral receptors. In other words, at the level of the auditory nerve, frequency information is arranged along a spatial axis (a "place code"). In this sense, auditory cortex show response properties that parallel those found in visual and somatosensory cortex, such as flanking inhibition and direction selectivity (Figure D.1C) (Depireux et al., 2001). These broad similarities

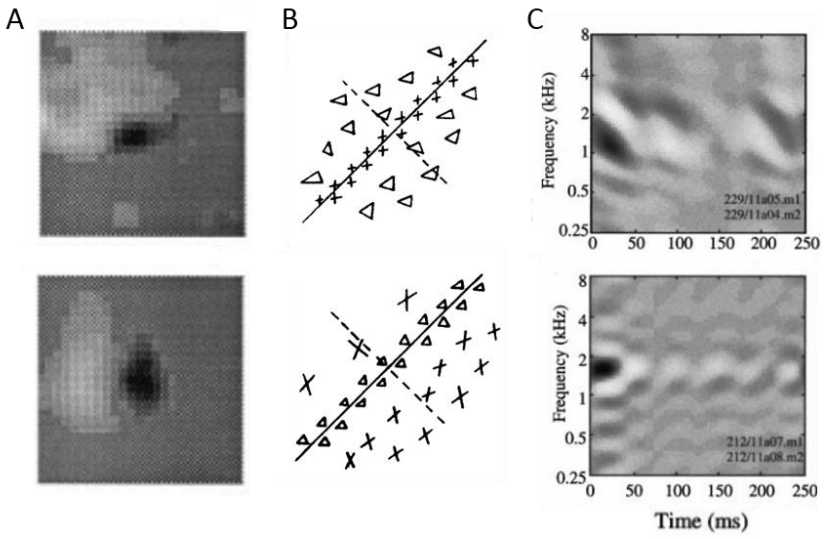

Figure D.1. **Spatial receptive fields in primary sensory areas.** A| Spatial receptive fields from two example neurons in area 3b. Darker colors represent excitatory regions and lighter colors represent inhibitory regions. Adapted from DiCarlo and Johnson 1998. B| Spatial receptive fields from two neurons in primary visual cortex. Excitatory regions are marked with "x", inhibitory regions are marked with a triangle. Adapted from Hubel and Wiesel 1962. C| Spectrotemporal receptive fields from two neurons in primary auditory cortex. Darker colors represent excitatory regions and lighter colors represent inhibitory regions. Adapted from Depireux et. al. 2001. In all three primary sensory areas, neurons show excitatory subregions with flanking inhibition.

suggest that these aspects of spatial processing reflect canonical computations that are preserved across sensory systems.

Our work suggests differences between the neural processing of visual and tactile texture. Like the tactile perception of coarse textures, the perception of visual texture also relies on spatial filters (Portilla and Simoncelli, 2000). However, visual texture perception also relies on higher-order correlations, a processing hypothesized to happen in secondary visual cortex (V2) (Willmore et al., 2010). Indeed, neurons in V2 show a functional selectivity for texture that is not present in V1 (Freeman et al., 2013). In contrast, we did not observe any clear differences between texture responses in primary somatosensory cortex (area 3b) and those of downstream neurons (areas 1 and 2), which have been found to show more complex selectivity for complex spatial features such as pattern motion (Pei et al., 2010, 2011) and curvature (Yau et al., 2013). There are two possible explanations for this seeming discrepancy: 1) texture is processed differently in the visual and somatosensory systems, or 2) higher-order texture selectivity is achieved in a different region of somatosensory processing, such as secondary somatosensory cortex (S2).

A number of neurons in somatosensory cortex exhibit texture responses that are more similar to SA1 afferents than either RA or PC afferents. At the periphery, SA1 afferents are selectively responsive to coarse textural features, showing little modulation across differences in surface microstructure (Weber et al., 2013). In cortex, we show that the most strongly SA1-like neurons also receive convergent input from RA and PC afferents, and thus show robust responses to surface microstructure. However, like SA1 afferents, these SA1-like cortical neurons are characterized by a stronger sensitivity to coarse textural features than fine features. Notably, neurons in area 3b tend to have stronger SA1 input than neurons in area 1 or area 2, as well as receptive fields that are smaller in size (Sur et al., 1985). These properties suggest that area 3b may be a locus of spatial processing within somatosensory cortex.

Temporal coding in the somatosensory system

At the somatosensory periphery, mechnoreceptive afferents encode information about skin vibrations through a multiplexed combination of firing rate and spike timing codes. Specifically, the amplitude of skin vibration is encoded by the mean firing rate across the population of peripheral afferents (Johnson, 1974; Muniak et al., 2007), while the frequency of skin vibration is encoded in finely timed spiking patterns (Talbot et al., 1968; Mackevicius et al., 2012). Importantly, the perception of vibrotactile frequency cannot be explained by a simple rate code; rather, it must rely on the fine timing of these spike patterns (Talbot et al., 1968; LaMotte and Mountcastle, 1975; Mackevicius et al., 2012; Birznieks and Vickery, 2017).

In somatosensory cortex, the nature of these representations is essentially unchanged: individual neurons encode information about vibrational amplitude in their firing rates, and frequency information (above 100 Hz) in the fine timing of their spiking responses (Harvey et al., 2013). Remarkably, this encoding method relies on the preservation of precise PC afferent spike timing (< 2 ms jitter) across three synapses of tactile processing before these signals first enter somatosensory cortex (Saal et al., 2015).

These same temporal signatures are present in the neural response to tactile texture. This is potentially surprising, as texture stimuli are significantly more complex than those from a vibrating probe. As discussed above, textures contain coarse spatial features encoded by the population activity of SA1 and RA afferents. Natural textures also contain surface microgeometry that is too fine to be encoded by these spatial mechanisms; rather, the interaction of this microgeometry with the resonant structure of the fingerprint ridges is what leads to texture-specific skin vibrations (Manfredi et al., 2014). Despite the fact that 1) these textures robustly engaged the spatial encoding mechanism and 2) the skin vibrations were created through natural scanning interactions, rather than an external motor, we still saw

consistent phase locking in both the peripheral (Weber et al., 2013) and cortical responses. Thus, our data suggest that the neural code for vibrotaction is still active and engaged during natural exploratory behaviors.

This vibrotactile code is undoubtedly informative about the frequency content of texture-elicited skin vibrations. However, it is unclear whether this frequency information contributes to the perception of texture identity. Notably, the frequency of these vibrations is highly dependent on the relative speed between the skin and the surface (Manfredi et al., 2014). In contrast, the perception of texture is remarkably invariant to changes in speed (Boundy-Singer et al., 2017). Spectral cues have been shown to predict some aspects of texture perception (Bensmaïa and Hollins, 2005), but only for textures explored at a single speed. In fact, these predictable, speed-dependent shifts in frequency could potentially be a cue for the perception of tactile speed during texture exploration (Dallmann et al., 2015).

If vibrotactile signals contribute to texture perception, it cannot be through a simple code for fundamental frequency, as these shift predictably with speed. Instead, the somatosensory system would need to decode speed-invariant features of the skin vibrations, such as the relative strength of frequencies across the harmonic stack. Notably, this exact problem is solved by the auditory system: we can reliably identify the timbre of a voice or an instrument across large changes in pitch (Handel and Erickson, 2001; Marozeau et al., 2003).

Frequency specific information about skin vibrations is encoded in somatosensory cortex at a precision of less than 2 ms (Harvey et al., 2013). This is remarkably precise for a cortical signal. While the auditory nerve encodes temporally precise information for frequencies as high as 10 kHz (Heinz et al., 2001), spiking in auditory cortex is rarely phase-locked above 50 Hz (Gao et al., 2016). And while specific spiking events in the visual system can be very precise (Bair and Koch, 1996; Reinagel and Reid, 2000; Butts et

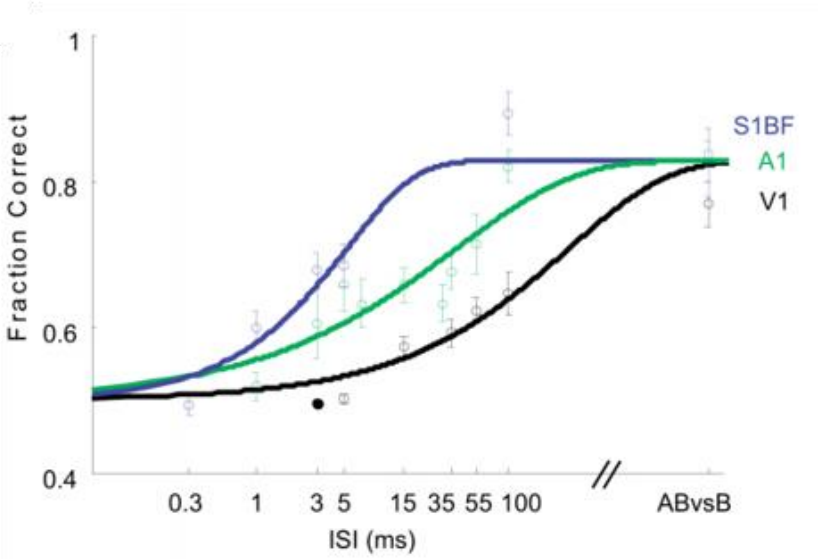

Figure D.2. **Sensitivity of primary cortical areas to finely timed electrical stimulation.** A| Rats were implanted with two nearby stimulating electrodes in one of three cortical areas (the barrel field of somatosensory cortex (S1BF), primary auditory cortex (A1), or primary visual cortex (V1)), and trained to detect patterns of electrical stimulation delivered either simultaneously or at a short relative delay (ISI). The best achieved performance (averaged across animals) is plotted as a function of stimulation ISI. Somatosensory cortex was more sensitive to precisely timed stimulation than either visual or auditory cortex. Adapted from Yang and Zador 2012.

al., 2007; Desbordes et al., 2008), neurons in visual cortex have trouble following temporal frequencies above 10-20 Hz (Movshon et al., 1978). This may be due to the fact that somatosensory cortex is closer to its first order representation (3 synapses) than the auditory (4 synapses) or visual systems (5 synapses). Indeed, somatosensory cortex may be more sensitive to precisely timed electrical stimulation than either visual or auditory cortex (Figure D.2) (Yang and Zador, 2012).

In summary, consistent with previous reports (Paul et al., 1972; Hyvärinen and Poranen, 1978; Merzenich et al., 1978; Hyvärinen et al., 1980), we find a subpopulation of PC-like, temporally precise neurons localized within area 1 of somatosensory cortex. We show that these neurons are critical for the encoding and perception of fine textural features. Thus, these neurons establish, for the first time, a cortical substrate for Katz's 1925 hypothesis that texture perception relies on the perception of skin vibrations.

Combination of spatial and temporal codes

In somatosensory cortex, we see multiple lines of evidence that the spatial and temporal streams of information are combined, often within individual neurons. First, the texture responses of many cortical neurons cannot be explained by inputs from a single afferent type; rather they are best explained by convergent afferent input. Second, as has been previously shown (Pei et al., 2009), many cortical neurons show responses to an indented probe that have both strong sustained components (a signature of SA1 afferents, but not RA and PC afferents) and strong offset responses (a signature of RA and PC afferents, but not SA1 afferents). Finally, while some cortical neurons showed tendencies to be more SA1-like or PC-like, even the most PC-like (temporal) neurons in our set exhibited spatially patterned receptive fields. Overall, we estimate that 80% of cortical neurons show response properties indicative of both the spatial and temporal streams of information.

This combination of spatial and temporal information within individual tactile neurons draws a parallel with neurons in auditory cortex. At the auditory periphery, frequency information is encoded spatially across hairs cells on the basilar membrane. Overlaid with this code, temporal fluctuations of these base frequencies (modulation frequencies) are faithfully encoded in the temporal structure of auditory nerve responses (Wang and Sachs, 1993), and then later explicitly transformed into a firing rate code (Muller-Preuss et al., 1994). As a result, neurons in auditory cortex show selective tuning for both carrier frequencies (Figure D.3A) (Recanzone et al., 2000) and modulation frequencies (Figure D.3B) (Liang et al., 2002; Wang, 2007) – a combination of both spatial and temporal encoding mechanisms (Wang et al., 2008). Furthermore, these two coding mechanisms are both relevant to auditory perception. Carrier and modulation frequencies act as independent perceptual dimensions (Ewert and Dau, 2000), and both features are critical to explaining the perception of natural auditory texture (Figure D.3C) (McDermott and Simoncelli, 2011). Thus, in both the auditory and somatosensory systems, the perception of natural stimuli is encoded by coexisting spatial and temporal neural codes.

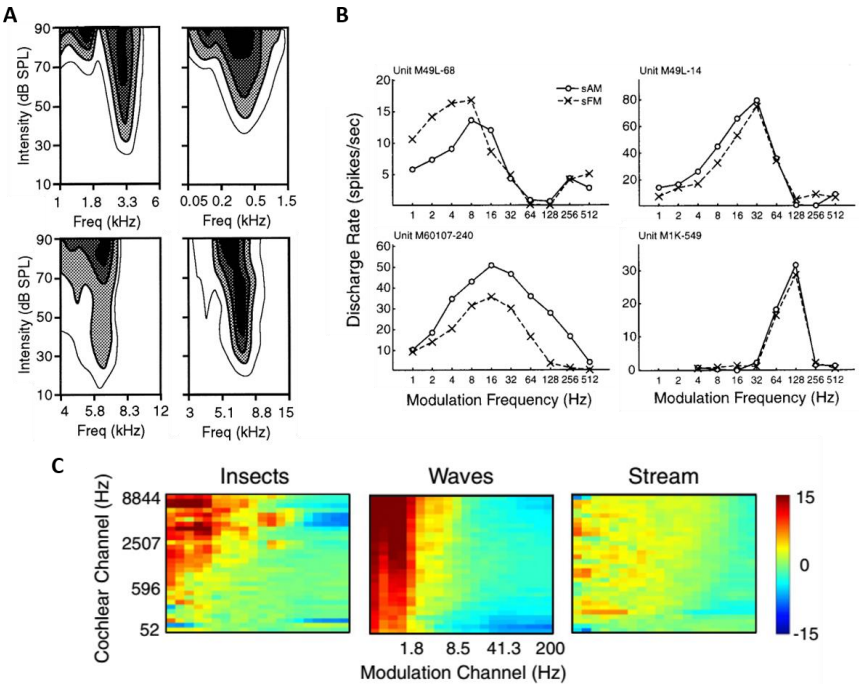

Figure D.3. **Spatial and temporal codes in the auditory system.** A| The firing rate response of four example neurons in primary auditory cortex (A1) when presented pure tones at a range of frequencies and intensities. Darker colors represent higher firing rates. Neurons in A1 show selective responses to specific carrier frequencies, which are encoded by a spatial mechanism. Adapted from Recanzone et. al. 2000. B| The firing rate response of four example neurons in A1 when presented with pure tones that were either sinusoidally amplitude modulated (sAM) or sinusoidally frequency modulated (sFM), across a range of modulation frequencies. Neurons in A1 show selective responses to modulation frequencies, which are encoded by a temporal mechanism. Adapted from Liang et. al. 2002. C| These plots show the frequency content of natural auditory textures. Natural sounds contain a range of carrier frequencies (plotted along the ordinate), and each of these carrier frequencies follows a temporal envelope that can be described by a bank of modulation frequency filters (plotted along the abscissa). The differences in both carrier and modulation frequency content drive differences in auditory texture, and both are necessary to explain auditory perception. Adapted from McDermott and Simoncelli 2011.

The peripheral code for tactile roughness

The dominant perceptual aspect of a surface is how rough it feels (Hollins et al., 2000a). This percept is driven by both the extent to which that surface deforms the skin (Taylor and Lederman, 1975) and by the intensity of the vibrations elicited in the skin (Bensmaia and Hollins, 2003; Bensmaïa and Hollins,

2005). These dual factors correspond to clear neural correlates in peripheral afferents. Spatial deformations of the skin produce spatial patterns of activation across SA1 and RA afferents (Johnson and Lamb, 1981; Phillips and Johnson, 1981), and the variability of these patterns predicts texture roughness (Connor et al., 1990; Connor and Johnson, 1992). Vibrational intensity drives the firing of RA and PC afferents (Talbot et al., 1968), whose activity is critical for explaining the roughness of fine textural features (Lieber et al., 2017). These two streams of information must be combined to create a unified percept; indeed, our experiment confirms that all three afferent classes are necessary to explain the roughness of natural textures.

The cortical code for tactile roughness

The variation signals at the periphery are converted to cortical firing rates by spatial and temporal filters (DiCarlo and Johnson, 2000; Saal et al., 2015). As a result, texture roughness is encoded by the mean firing rate across the full cortical population. Notably, this signal was strongly carried by almost every neuron we recorded activity from, and corresponds to more than half of the texture-driven variance of the cortical population response.

In a sense, this redundancy across cortical neurons is surprising. While the cortical population response is selective for texture identity, that selectivity is largely supported by differences in firing rate that are small compared to this roughness signal. On other words, while the population response across somatosensory cortex can support texture identification, it does not necessarily do so *efficiently*. As mentioned above, the representation of touch in somatosensory cortex is only three synapses removed from that in the nerve, unlike the more elaborated representations in visual cortex (four synapses) or auditory cortex, which each involve at least five synapses. Thus, the relatively "unfiltered" representation of tactile information in primary somatosensory cortex (compared to other systems) may explain its largely homogeneous texture response.

There is evidence that the somatosensory system does eventually work to minimize for this shared signal. In the case vibrations in the flutter frequency range (10-50 Hz), responses in somatosensory cortex tend to increase with both frequency (Salinas et al., 2000) and amplitude (Mountcastle et al., 1969). However, neurons in secondary somatosensory cortex show a wider variety of possible response properties: as frequency is increased, neurons in S2 may show increasing, decreasing, or no changes in firing rate (Figure D.4A). This range of response properties creates a population code for frequency that is resistant to correlated fluctuations in noise (Romo et al., 2003). This same principle suggests that the S2 population response could be invariant to changes in stimulus intensity as well. Indeed, in the context of texture, neurons in S2 show both increasing and decreasing firing rates across increases in grating groove width (Figure D.4B) (Sinclair and Burton, 1993), a physical property of gratings that correlates

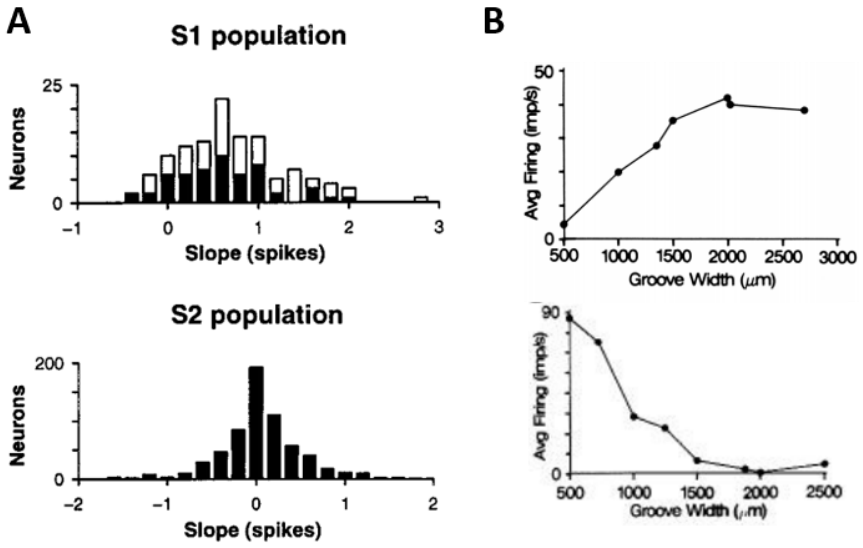

Figure D.4. **Neural coding in secondary somatosensory cortex.** A| Neurons in anterior parietal cortex (S1) generally increase their firing rate in response to vibratory flutter-stimuli (10-50 Hz) of increasing frequency. The top histogram plots the slope of this relationship for neurons in area 3b (white) and area 1 (black). In secondary somatosensory cortex (S2, bottom) there are many more neurons that decrease their firing rate in response to increasing frequency. Adapted from Salinas et. al. 2000. B| The firing rate response of two example neurons in S2 driven when an animal scanned its hand over gratings of different groove widths (where wider groove widths are perceived as rougher). Unlike in anterior parietal cortex, many neurons in S2 decrease their firing rate in response to increasingly rough textures. Adapted from Sinclair and Burton 1993.

with perceived roughness (Sathian et al., 1989). Thus, one synapse downstream of primary somatosensory cortex, the somatosensory system may create a more selective representation of tactile stimuli similar to those seen in the visual or auditory systems.

Implications for neural prosthetics

Our results suggest that two, spatially distinct populations of neurons may encode two separate aspects of texture: SA1-like neurons deep in area 3b may preferentially encode information about coarse textural features, while PC-like neurons located near the surface of area 1 and area 2 may encode fine features. Current methods of intracortical microstimulation (ICMS) of somatosensory cortex can create sensations of precisely timed sensations of spatially localized pressure (Tabot et al., 2013; Flesher et al., 2016), but these percepts often lack the verisimilitude of natural touch. Our results suggest that ICMS approaches could take advantage of these two subpopulations – stimulation of SA1-like cortical neurons could drive sensations reflecting coarse spatial scales, and stimulation of PC-like neurons could drive sensations reflecting fine spatial scales and involving movement. As natural touch relies on the coexistence of these two representations, paired stimulation of SA1-like and PC-like regions with overlapping projective fields could potentially drive a more natural percept for patients using a prosthetic limb (Saal and Bensmaia, 2015).

REFERENCES

Bair W, Koch C (1996) Temporal Precision of Spike Trains in Extrastriate Cortex of the Behaving Macaque Monkey. Neural Comput 8:1185–1202.

Bensmaïa SJ, Craig JC, Johnson KO (2006a) Temporal factors in tactile spatial acuity: evidence for RA interference in fine spatial processing. J Neurophysiol 95:1783–1791.

Bensmaïa SJ, Craig JC, Yoshioka T, Johnson KO (2006b) SA1 and RA afferent responses to static and vibrating gratings. J Neurophysiol 95:1771–1782.

Bensmaia SJ, Denchev P V, Dammann JF, Craig JC, Hsiao SS (2008) The representation of stimulus orientation in the early stages of somatosensory processing. J Neurosci 28:776–786.

Bensmaia SJ, Hollins M (2003) The vibrations of texture. Somatosens Mot Res 20:33–43.

Bensmaïa SJ, Hollins M (2005) Pacinian representations of fine surface texture. Percept Psychophys 67:842–854.

Birznieks I, Vickery RM (2017) Spike Timing Matters in Novel Neuronal Code Involved in Vibrotactile Frequency Perception. Curr Biol 27:1485–1490.e2.

Blake DT, Hsiao SS, Johnson KO (1997a) Neural coding mechanisms in tactile pattern recognition: the relative contributions of slowly and rapidly adapting mechanoreceptors to perceived roughness. J Neurosci 17:7480–7489.

Blake DT, Johnson KO, Hsiao SS (1997b) Monkey cutaneous SAI and RA responses to raised and depressed scanned patterns: effects of width, height, orientation, and a raised surround. J Neurophysiol 78:2503–2517.

Boundy-Singer ZM, Saal HP, Bensmaia SJ (2017) Speed Invariance of Tactile Texture Perception. J Neurophysiol 118:jn.00161.2017.

Butts DA, Weng C, Jin J, Yeh CI, Lesica NA, Alonso JM, Stanley GB (2007) Temporal precision in the neural code and the timescales of natural vision. Nature 449:92–95.

Connor CE, Hsiao SS, Phillips JR, Johnson KO (1990) Tactile roughness: neural codes that account for psychophysical magnitude estimates. J Neurosci 10:3823–3836.

Connor CE, Johnson KO (1992) Neural coding of tactile texture: comparison of spatial and temporal mechanisms for roughness perception. J Neurosci 12:3414–3426.

Dallmann CJ, Ernst MO, Moscatelli A (2015) The role of vibration in tactile speed perception. J Neurophysiol 114:3131–3139.

Depireux DA, Simon JZ, Klein DJ, Shamma SA (2001) Spectro-Temporal Response Field Characterization With Dynamic Ripples in Ferret Primary Auditory Cortex. J Neurophysiol 85:1220–1234.

Desbordes G, Jin J, Weng C, Lesica NA, Stanley GB, Alonso JM (2008) Timing precision in population coding of natural scenes in the early visual system. PLoS Biol 6:2672–2682.

DiCarlo JJ, Johnson KO (2000) Spatial and temporal structure of receptive fields in primate

somatosensory area 3b: effects of stimulus scanning direction and orientation. J Neurosci 20:495–510.

Ewert SD, Dau T (2000) Characterizing frequency selectivity for envelope fluctuations. J Acoust Soc Am 108:1181.

Flesher SN, Collinger JL, Foldes ST, Weiss JM, Downey JE, Tyler-Kabara EC, Bensmaia SJ, Schwartz AB, Boninger ML, Gaunt RA (2016) Intracortical microstimulation of human somatosensory cortex. Sci Transl Med 8.

Freeman J, Ziemba CM, Heeger DJ, Simoncelli EP, Movshon JA (2013) A functional and perceptual signature of the second visual area in primates. Nat Neurosci:1–12.

Gao L, Kostlan K, Wang Y, Wang X (2016) Distinct Subthreshold Mechanisms Underlying Rate-Coding Principles in Primate Auditory Cortex. Neuron 91:905–919.

Handel S, Erickson ML (2001) A Rule of Thumb: The Bandwidth for Timbre Invariance Is One Octave. Music Percept 19:121–126.

Harvey MA, Saal HP, Dammann JF, Bensmaia SJ (2013) Multiplexing Stimulus Information through Rate and Temporal Codes in Primate Somatosensory Cortex. PLoS Biol 11.

Heinz MG, Colburn HS, Carney LH (2001) Evaluating Auditory Performance Limits: I. One-Parameter Discrimination Using a Computational Model for the Auditory Nerve. Neural Comput 13:2273–2316.

Hershler O, Hochstein S (2009) Representation of Angles Embedded within Contour Stimuli in Area V2 of Macaque Monkeys. Attention, Perception, Psychophys 71:1478–1486.

Hollins M, Bensmaia S, Karlof K, Young F (2000a) Individual differences in perceptual space for tactile textures: evidence from multidimensional scaling. Percept Psychophys 62:1534–1544.

Hollins M, Bensmaïa SJ, Washburn S (2001) Vibrotactile adaptation impairs discrimination of fine, but not coarse, textures. Somatosens Mot Res 18:253–262.

Hollins M, Fox A, Bishop C (2000b) Imposed vibration influences perceived tactile smoothness. Perception 29:1455–1465.

Hollins M, Risner SR (2000) Evidence for the duplex theory of tactile texture perception. Percept Psychophys 62:695–705.

Hubel DH, Wiesel TN (1962) Receptive fields, binocular interaction and functional architecture in the cat's visual cortex. J Physiol 160:106–154.

Hubel DH, Wiesel TN (1968) Receptive fields and functional architecture of monkey striate cortex. J Physiol 195:215–243.

Hyvärinen J, Poranen A (1978) Receptive field integration and submodality convergence in the hand area of the post-central gyrus of the alert monkey. J Physiol 283:539–556.

Hyvärinen J, Poranen A, Jokinen Y (1980) Influence of attentive behavior on neuronal responses to

vibration in primary somatosensory cortex of the monkey. J Neurophysiol 43:870–882.

Johnson K, Lamb G (1981) Neural mechanisms of spatial tactile discrimination: neural patterns evoked by braille-like dot patterns in the monkey. J Physiol:117–144.

Johnson KO (1974) Reconstruction of population response to a vibratory stimulus in quickly adapting mechanoreceptive afferent fiber population innervating glabrous skin of the monkey. J Neurophysiol 37:48–72.

Jones JP, Palmer LA (1987) The two-dimensional spatial structure of simple receptive fields in cat striate cortex. J Neurophysiol 58:1187–1211.

Katz D (1925) The World of Touch (Krueger LE, ed).

LaMotte RH, Mountcastle VB (1975) Capacities of humans and monkeys to discriminate vibratory stimuli of different frequency and amplitude: a correlation between neural events and psychological measurements. J Neurophysiol 38:539–559.

Liang L, Lu T, Wang X (2002) Neural representations of sinusoidal amplitude and frequency modulations in the primary auditory cortex of awake primates. J Neurophysiol 87:2237–2261.

Libouton X, Barbier O, Berger Y, Plaghki L, Thonnard JL (2012) Tactile roughness discrimination of the finger pad relies primarily on vibration sensitive afferents not necessarily located in the hand. Behav Brain Res 229:273–279.

Libouton X, Barbier O, Plaghki L, Thonnard JL (2010) Tactile roughness discrimination threshold is unrelated to tactile spatial acuity. Behav Brain Res 208:473–478.

Lieber JD, Xia X, Weber AI, Bensmaia SJ (2017) The Neural Code for Tactile Roughness in the Somatosensory Nerves. J Neurophysiol:jn.00374.2017.

Mackevicius EL, Best MD, Saal HP, Bensmaia SJ (2012) Millisecond Precision Spike Timing Shapes Tactile Perception. J Neurosci 32:15309–15317.

Manfredi LR, Saal HP, Brown KJ, Zielinski MC, Dammann JF, Polashock VS, Bensmaia SJ (2014) Natural scenes in tactile texture. J Neurophysiol 111:1792–1802.

Marozeau J, de Cheveigné A, McAdams S, Winsberg S (2003) The dependency of timbre on fundamental frequency. J Acoust Soc Am 114:2946.

McDermott JH, Simoncelli EP (2011) Sound texture perception via statistics of the auditory periphery: evidence from sound synthesis. Neuron 71:926–940.

Merzenich MM, Kaas JH, Sur M, Lin C-S (1978) Double representation of the body surface within cytoarchitectonic area 3b and 1 in “S1” in the owl monkey (Aotus Trivirgatus). J Comp Neurol 181:41–73.

Mountcastle VB, Talbot WH, Sakata H, Hyvärinen J (1969) Cortical neuronal mechanisms in flutter-vibration studied in unanesthetized monkeys. Neuronal periodicity and frequency discrimination. J Neurophysiol 32:452–484.

Movshon JA, Thompson ID, Tolhurst DJ (1978) Spatial and temporal contrast sensitivity of neurones in areas 17 and 18 of the cat's visual cortex. J Physiol 283:101–120.

Muller-Preuss P, Flachskamm C, Bieser A (1994) Neural encoding of amplitude modulation within the auditory midbrain of squirrel monkeys. Hear Res 80:197–208.

Muniak MA, Ray S, Hsiao SS, Dammann JF, Bensmaia SJ (2007) The neural coding of stimulus intensity: linking the population response of mechanoreceptive afferents with psychophysical behavior. J Neurosci 27:11687–11699.

Paul RL, Merzenich M, Goodman H (1972) Representation of slowly and rapidly adapting cutaneous mechanoreceptors of the hand in Brodmann's areas 3 and 1 of Macaca Mulatta. Brain Res 36:229–249.

Pei Y-C, Denchev P V, Hsiao SS, Craig JC, Bensmaia SJ (2009) Convergence of submodality-specific input onto neurons in primary somatosensory cortex. J Neurophysiol 102:1843–1853.

Pei YC, Hsiao SS, Craig JC, Bensmaia SJ (2010) Shape invariant coding of motion direction in somatosensory cortex. PLoS Biol 8.

Pei YC, Hsiao SS, Craig JC, Bensmaia SJ (2011) Neural Mechanisms of Tactile Motion Integration in Somatosensory Cortex. Neuron 69:536–547.

Phillips J, Johnson K (1981) Tactile spatial resolution. II. Neural representation of bars, edges, and gratings in monkey primary afferents. J Neurophysiol:1192–1203.

Pons TP, Garraghty PE, Cusick CG, Kaas JH (1985) The somatotopic organization of area 2 in macaque monkeys. J Comp Neurol 241:445–466.

Portilla J, Simoncelli EP (2000) A Parametric Texture Model Based on Joint Statistics of Complex Wavelet Coefficients. Int J Comput Vis 40:49–71.

Recanzone GH, Guard DC, Phan ML (2000) Frequency and intensity response properties of single neurons in the auditory cortex of the behaving macaque monkey. J Neurophysiol 83:2315–2331.

Reinagel P, Reid RC (2000) Temporal coding of visual information in the thalamus. J Neurosci 20:5392–5400.

Romo R, Hernández A, Zainos A, Salinas E (2003) Correlated neuronal discharges that increase coding efficiency during perceptual discrimination. Neuron 38:649–657.

Saal HP, Bensmaia SJ (2015) Biomimetic approaches to bionic touch through a peripheral nerve interface. Neuropsychologia 79:344–353.

Saal HP, Delhaye BP, Rayhaun BC, Bensmaia SJ (2017) Simulating tactile signals from the whole hand with millisecond precision. Proc Natl Acad Sci.

Saal HP, Harvey MA, Bensmaia SJ (2015) Rate and timing of cortical responses driven by separate sensory channels. Elife 4.

Salinas E, Hernandez A, Zainos A, Romo R (2000) Periodicity and firing rate as candidate neural codes for

the frequency of vibrotactile stimuli. J Neurosci 20:5503–5515.

Sathian K, Goodwin a W, John KT, Darian-Smith I (1989) Perceived roughness of a grating: correlation with responses of mechanoreceptive afferents innervating the monkey's fingerpad. J Neurosci 9:1273–1279.

Sinclair RJ, Burton H (1993) Neuronal activity in the second somatosensory cortex of monkeys (Macaca mulatta) during active touch of gratings. J Neurophysiol 70:331–350.

Sripati AP, Yoshioka T, Denchev P, Hsiao SS, Johnson KO (2006) Spatiotemporal receptive fields of peripheral afferents and cortical area 3b and 1 neurons in the primate somatosensory system. J Neurosci 26:2101–2114.

Sur M, Garraghty PE, Bruce CJ (1985) Somatosensory cortex in macaque monkeys: laminar differences in receptive field size in areas 3b and 1. Brain Res 342:391–395.

Tabot GA, Dammann JF, Berg JA, Tenore F V., Boback JL, Vogelstein RJ, Bensmaia SJ (2013) Restoring the sense of touch with a prosthetic hand through a brain interface. Proc Natl Acad Sci 110:18279–18284.

Talbot WH, Darian-Smith I, Kornhuber HH, Mountcastle VB (1968) The Sense of Flutter Vibration Comparison of the Human Capacity With Response Patterns of Mechanoreceptive Afferents From the Monkey Hand. J Neurophysiol 31:301.

Taylor MM, Lederman SJ (1975) Tactile roughness of grooved surfaces: A model and the effect of friction. Percept Psychophys 17:23–36.

Wang X (2007) Neural coding strategies in auditory cortex. Hear Res 229:81–93.

Wang X, Lu T, Bendor D, Bartlett E (2008) Neural coding of temporal information in auditory thalamus and cortex. Neuroscience 157:484–493.

Wang X, Sachs MB (1993) Neural encoding of single-formant stimuli in the cat. I. Responses of auditory nerve fibers. J Neurophysiol 70:1054–1075.

Weber AI, Saal HP, Lieber JD, Cheng J-W, Manfredi LR, Dammann JF, Bensmaia SJ (2013) Spatial and temporal codes mediate the tactile perception of natural textures. Proc Natl Acad Sci U S A 110:17107–17112.

Willmore BDB, Prenger RJ, Gallant JL (2010) Neural representation of natural images in visual area V2. J Neurosci 30:2102–2114.

Yang Y, Zador AM (2012) Differences in Sensitivity to Neural Timing among Cortical Areas. J Neurosci 32:15142–15147.

Yau JM, Connor CE, Hsiao SS (2013) Representation of tactile curvature in macaque somatosensory area 2. J Neurophysiol 109:2999–3012.

Yoshioka T, Gibb B, Dorsch a K, Hsiao SS, Johnson KO (2001) Neural coding mechanisms underlying perceived roughness of finely textured surfaces. J Neurosci 21:6905–6916.